ΠΑΝΕΠΙΣΤΗΜΙΟ ΙΩΑΝΝΙΝΩΝ
ΤΜΗΜΑ ΜΑΘΗΜΑΤΙΚΩΝ

Παναγιώτης Λιναρδόπουλος

ΑΝΑΛΥΤΙΚΕΣ ΚΑΙ ΑΡΙΘΜΗΤΙΚΕΣ ΛΥΣΕΙΣ ΤΗΣ ΡΟΗΣ ΤΟΥ ΑΙΜΑΤΟΣ ΜΕ ΕΦΑΡΜΟΓΕΣ ΣΤΗΝ ΑΘΛΗΤΙΚΗ ΦΥΣΙΟΛΟΓΙΑ/ΠΑΘΟΦΥΣΙΟΛΟΓΙΑ ΜΕΣΩ ΜΟΝΤΕΛΩΝ ΥΠΟΛΟΓΙΣΤΙΚΗΣ ΡΕΥΣΤΟΔΥΝΑΜΙΚΗΣ

ΜΕΤΑΠΤΥΧΙΑΚΗ ΔΙΑΤΡΙΒΗ

Ιωάννινα, 2024

UNIVERSITY OF IOANNINA
Department of Mathematics

Panagiotis Linardopoulos

ANALYTICAL AND NUMERICAL SOLUTIONS OF BLOOD FLOW WITH APPLICATIONS IN ATHLETIC PHYSIOLOGY/PATHOPHYSIOLOGY USING COMPUTATIONAL FLUID DYNAMICS

Master's Thesis

Ioannina, 2024

Η παρούσα διατριβή αφιερώνεται στους γονείς μου Δημήτρη και Αλεξάνδρα και στην γιαγιά μου Μαρία.

Η παρούσα Μεταπτυχιακή Διατριβή εκπονήθηκε στο πλαίσιο των σπουδών για την απόκτηση του Μεταπτυχιακού Διπλώματος Ειδίκευσης στα Εφαρμοσμένα Μαθηματικά και Πληροφορική που απονέμει το Τμήμα Μαθηματικών του Πανεπιστημίου Ιωαννίνων.

Εγκρίθηκε την 27/06/2024 από την εξεταστική επιτροπή:

Ονοματεπώνυμο	**Βαθμίδα**
Μιχαήλ Ξένος	Καθηγητής
Θεόδωρος Χωρίκης	Καθηγητής
Ευστράτιος Τζιρτζιλάκης	Καθηγητής

ΥΠΕΥΘΥΝΗ ΔΗΛΩΣΗ

"Δηλώνω υπεύθυνα ότι η παρούσα διατριβή εκπονήθηκε κάτω από τους διεθνείς ηθικούς και ακαδημαϊκούς κανόνες δεοντολογίας και προστασίας της πνευματικής ιδιοκτησίας. Σύμφωνα με τους κανόνες αυτούς, δεν έχω προβεί σε ιδιοποίηση ξένου επιστημονικού έργου και έχω πλήρως αναφέρει τις πηγές που χρησιμοποίησα στην εργασία αυτή."

Παναγιώτης Λιναρδόπουλος

Ευχαριστιες

Η παρούσα μεταπτυχιακή διατριβή εκπονήθηκε στα πλαίσια της ολοκλήρωσης του Μεταπτυχιακού Διπλώματος Ειδίκευσης "Εφαρμοσμένων Μαθηματικών και Πληροφορικής" του τμήματος Μαθηματικών, Πανεπιστημίου Ιωαννίνων.

Αρχικά, θα ήθελα να ευχαριστήσω τον κ. Θεόδωρο Χωρίκη, Καθηγητή του τμήματος Μαθηματικών του Πανεπιστημίου Ιωαννίνων και τον κ. Ευστράτιο Τζιρτζιλάκη, Καθηγητή του Τμήματος Μηχανολόγων Μηχανικών του Πανεπιστημίου Πελοποννήσου για την διαθεσιμότητα τους και την συμμετοχή τους στην εξεταστική τριμελή επιτροπή μου καθώς και για τις επισημάνσεις και διορθώσεις που μου παρείχαν, το εκτιμώ βαθύτατα.

Θα ήθελα να ευχαριστήσω μέσα από την καρδία μου τον επιβλέποντα της μεταπτυχιακής μου διατριβής, κ. Μιχαήλ Ξένο, καθηγητή του τμήματος Μαθηματικών του Πανεπιστημίου Ιωαννίνων. Στάθηκε αρωγός στο εγχείρημα της εκπόνησης μιας διπλωματικής της οποίας το θέμα πρότεινα εγώ και απ'την πρώτη στιγμή με ενθάρρυνε, μου έδωσε κουράγιο και στάθηκε δίπλα μου σε ό,τι και αν χρειάστηκα έτσι ώστε να φέρουμε εις πέρας τον στόχο μας. Θα ήθελα να γνωρίζει πώς νιώθω τιμή που επέλεξε να συνεργαστεί μαζί μου και πώς τον εκτιμώ και θαυμάζω τόσο σαν επιστήμονα αλλά και σαν άνθρωπο.

Τέλος, χρωστάω το μεγαλύτερο ευχαριστώ στους γονείς μου Δημήτριο και Αλεξάνδρα που θυσίασαν τόσα πολλά για εμένα ώστε να μπορέσω να "ταΐσω" την φιλοδοξία μου, να ακολουθήσω το όνειρο μου, και που μου έδωσαν την δυνατότητα να χτίσω ένα καλύτερο μέλλον για εμένα. Τους χρωστάω τα πάντα και ελπίζω αυτή η διατριβή να τους έκανε να αισθανθούν περήφανοι. Ένα τελευταίο ευχαριστώ στην γιαγιά μου Μαρία, που με κόπο και ζήλο ήταν δίπλα μου σε πολλά από τα σχολικά μου βήματα και φρόντισε να μου καλλιεργήσει την περιέργεια και την όρεξη να ψάχνω σε βάθος ό,τι κάνω στην ζωή μου.

Ιωάννινα 2024,
Παναγιώτης Λιναρδόπουλος

Περιληψη

Η μελέτη της αιματικής ροής αποτελεί αντικείμενο μείζονος ενδιαφέροντος τόσο για την ιατρική κοινότητα όσο και για τις υπόλοιπες, βιο-ιατρικώς εμπλεκόμενες επιστήμες. Η επιστήμη των Μαθηματικών και το σύνολο των εργαλείων που την απαρτίζει, την καθιστά μοναδική στην δυνατότητα της μοντελοποίησης του καρδιαγγειακού συστήματος ενώ ταυτόχρονα, ανοίγει νέους δρόμους για την κατασκευή μαθηματικών μοντέλων που προβλέπουν την επίδραση της ροής στο καρδιαγγειακό σύστημα μέσω διάφορων μεταβολών της ροής, της πίεσης και της διατομής των αρτηριών. Μέσω απλουστευμένων μαθηματικών μοντέλων, όπως αυτό των Hagen-Poiseulle, περιγράφουμε με αναλυτικό τρόπο την ροή μέσα σ' ένα αγγείο και παρέχονται χρήσιμες πληροφορίες για το πώς διαφορετικοί παράγοντες την επηρεάζουν.

Μελετάται η ροή Womersley, η οποία αποτελεί επέκταση της ροής Poiseulle όταν στην προηγούμενη, συμπεριλαμβάνεται το φαινόμενο της παλμικότητας. Μοντελοποιεί την αιματική ροή στις αρτηρίες και περιγράφει τόσο την ροή όσο και την πίεση μέσω κυματομορφών. Εισάγεται ο αριθμός Womersley και μελετάται η μεταβολή του προφίλ της ταχύτητας

Μέσω της μηδενικής-διάστασης μοντέλου Windkessel, μελετούμε την ροή και την πιέση στις αρτηρίες και ειδικότερα σε συγκεκριμένα τμήματα της αορτής. Το μοντέλο Windkessel είναι ενα ολιστικό, αφαιρετικό μοντέλο και αποτελεί μία προσεγγιστικά-άρτια αναπαράσταση φόρτου που εν γένει δέχεται η καρδιά κατά την διάρκεια του καρδιακού κύκλου. Η δομή του σαν μοντέλο αυτό καθ' αυτό χαρακτηρίζει την αρτηριακή συμμόρφωση, την αντίσταση των βαλβίδων και την ορμή της αιματικής ροής και την αντίσταση της ροής η οποία μεταβαίνει απο αγγεία μεγαλύτερης διατομής(αρτηρίες) σε μικρότερης (τριχοειδή). Στην διατριβή αυτή, μελετάται το μοντέλο Windkessel των 3-στοιχείων το οποίο τοποθετείται στα τερματικά των μεγάλων αρτηριών και γίνεται μία σύζευξη του με το μονοδιάστατο μοντέλο στ΄οποίο περιγράφονται οι εξισώσεις συνέχειας, ορμής και διατασιμότητας του τοιχώματος. Το μονοδιάστατο μαθηματικό μοντέλο είναι ένα ευέλικτο μαθηματικό εργαλείο καθώς με κατάλληλες μεταβολές στις αρχικές, τις συνοριακές

συνθήκες και στις συνθήκες των διακλαδώσεων του αρτηριακού δέντρου, μπορεί να αναπαράξει ακριβή ποιοτικά και ποσοτικά αποτελέσματα σε διάφορες αιμοδυναμικές συνθήκες. Μέσω του μονοδιάστατου μοντέλου κατασκευάζουμε ένα μοντέλο που μας παρέχει κυματομορφές ροής και πίεσης σε ολόκληρο το αρτηριαρακό δέντρο, με την δυνατότητα να απομονώσουμε τις επιμέρους κυματομορφές σε οποιοδήποτε τμήμα του δέντρου.

Μέσω της ανάπτυξης και χρήσης λογισμικών υπολογιστικής ρευστοδυναμικής (CFD) κατασκευάζουμε εξατομικευμένα καρδιαγγειακά μοντέλα. Αρχικά, λαμβάνουμε ιατρικές εικόνες (MRI/ CT scans) και έπειτα, μέσω **προηγμένων** λογισμικών, ανακατασκευάζουμε μια 3D γεωμετρία στην οποία κατασκευάζουμε κατάλληλο υπολογιστικό πλέγμα και ορίζουμε κατάλληλες συνοριακές συνθήκες. Τέλος, χρησιμοποιούμε κατάλληλους αλγορίθμους, έτσι ώστε να επιλύσουν τις διέπουσες εξισώσεις (Εξισώσεις Navier-Stokes) για να προσομοιώσουμε την αιματική ροή, λαμβάνοντας υπόψιν την αλληλεπίδραση ρευστού-στερεού και μέσω μετά-επεξεργασίας (post-processing), λαμβάνεται το επιθυμητό μοντέλο προσομοίωσης.

Με την επιβολή κατάλληλων συνοριακών συνθηκών, τιμών σε ταχύτητα και πίεση, τροποποίησης της δεδομένης γεωμετρίας, και κατά συνέπεια τροποποίησης των υπολογιστικών μοντέλων, προσομοιώνουμε: **1)**Περιβάλλον άθλησης ενός υγιούς ατόμου και μελετούμε πώς μεταβάλλεται η αιματική ροή υπό την επίδραση των διαφορετικών εντάσεων άθλησης και **2)**Την επίδραση της άθλησης στην αιματική ροή παρουσία μίας καρδιαγγειακής ασθένειας όπως αυτή του ανευρύσματος της κοιλιακής αορτής.

Συμπερασματικά, στην παρούσα διατριβή κατασκευάζουμε μονοδιάστατα μαθηματικά μοντέλα (όπου τα συζεύγουμε με μηδενικής διάστασης μοντέλα Windkessel) τα οποία στην συνέχεια χρησιμοποιούνται για την κατασκευή τρισδιάστατων μοντέλων συγκεκριμένων αρτηριακών τμημάτων, μέσω προηγμένων υπολογιστικών προγραμμάτων και μέσω κατάλληλης μαθηματικής μοντελοποίησης, αναπαράγουμε επιθυμητά περιβάλλοντα όπως αυτά της άθλησης και έπειτα των ιατρικών παθήσεων και μελετούμε πώς μεταβάλλεται η ροή, η πίεση του αίματος καθώς και οι διάφορες αιμοδυναμικές παράμετροι στην εκάστοτε περίπτωση.

Abstract

The study of blood flow and the field of hemodynamics is an important field, either from a medical point of view or a bioengineering one. The field of mathematics and the conglomeration of its tools enables scientists to create accurate models of the cardiovascular system while simultaneously creating new modelling techniques which are able to predict how the flow is effected through changes in velocity, pressure and in the cross-sectional areas of the arteries. Through simplified mathematical models such as the Hagen-Poiseuille, we are able to describe, in an analytical way, how blood flows through a vessel and how different parameters can affect that.

Then, Womersley flow is introduced as an extension of Poiseuille's flow in order to include the phenomenon of pulsatility. This flow provides a more accurate description of blood flow through velocity and pressure waveforms. Lastly, Womersley number is introduced and the change of the velocity profile is studied as well.

Through the zero-dimensional Windkessel model, we study the flow and the pressure in specific segments of the aorta. The Windkessel model is a holistic model and constitutes an accurate representation of the cardiac load during cardiac cycle. It describes the arterial compliance, the resistance of the valves and the momentum of the blood flow (and its resistance) while blood flows from larger blood vessels (arteries) to smaller blood vessels (trichoids/capillaries). In this thesis the 3-element Windkessel that is studied, is placed in the terminating points of large arteries and is coupled with the one-dimensional model which consists of the Equations of Continuity, Momentum and Wall Distensibility, creating a hyperbolic system of PDEs. The one-dimensional mathematical model is a flexible mathematical tool due to the fact that with appropriate modifications in initial, boundary conditions and in bifurcating conditions in the arterial tree, it is able to reproduce accurate qualitative and quantitative results in various hemodynamic conditions.

From the development and utilization of CFD softwares, we construct patient-

specific cardiovascular models. Images originating from MRI/CT scans are segmented and used to reconstruct a 3D geometry model of a specific arterial segment and then, after constructing a computational mesh and extracting suitable boundary conditions in the form of waveforms from the one-dimensional model that was developed earlier, an appropriate solver is deployed to solve the three-dimensional fluid flow problem. Through adjustments of the geometry of the model, parameters of interest (such as cross-sectional area, distensibility modulus) and through the enforcement of specific boundary conditions and flow/pressure waveforms, we are able to study the phenomenon of blood flow in the simulating environment of exercise in different intensities and in the presence of a cardiovascular disease such as an abdominal aortic aneurysm.

In conclusion, in this thesis we construct one-dimensional models which are coupled with the zero-dimensional Windkessel models and are later used to construct three-dimensional models of a specific arterial segment. Via CFD and accurate mathematical modelling, we are able to simulate different environments, such as the gradual exercise increase and the existence of a cardiovascular disease such as an aneurysm and study the alteration of flow, pressure and other hemodynamic indices in each state, in a patient-based fashion.

Contents

Περίληψη **i**

Abstract **ii**

1 Introduction **3**

1.1 Function of blood vessels 4

1.2 Governing equations of blood flow in arteries 6

1.3 Mechanism of blood flow: Poiseuille's Law 8

1.3.1 Aftermath of Poiseuille's Law 10

1.3.2 Failure of Poiseuille's Law 13

1.4 Bernoulli's principle in blood flow applications 14

1.5 Biomechanical characteristics of blood vessels 19

1.5.1 Young's Modulus 20

1.5.2 Laplace's Law of Wall Tension 20

2 Analytical solutions of pulsatile blood flow **23**

2.1 Derivation of the Womersley solution 24

2.1.1 Derivation of dimensionless Womersley equation 28

2.2 Derivation of Greenfield-Fry solution 33

3 Mathematical modeling of blood flow in the cardiovascular system **37**

3.1 Zero-dimensional models 38

3.2 One-dimensional models 42
3.2.1 Coupling of 1D and 0D models 43
3.3 Formulation of equations of the 1D model 44
3.3.1 Inflow, Bifurcating and Outflow Conditions 46
3.4 Spatial Discretization of the system using FVM 50
3.4.1 Solver of the non-linear algebraic systems 52
3.4.2 CFL Condition 53
3.5 Time Discretization using Explicit Euler and θ-scheme 55

4 1D Results in the Abdominal Aortic model 57
4.1 Direct effects of exercise in the cardiovascular system 57
4.2 Results: Flow and Pressure waveforms in the 1D model 59

5 The three-dimensional model of the Lower abdominal aorta 69
5.1 3D Results and hemodynamic indices 73
5.2 Limitations of the 1D and 3D models in the thesis 84
5.3 A glimpse of a future step: Effect of exercise in AAA 85
5.4 Conclusions 90

CHAPTER 1

Introduction

Mathematical modelling is defined as the process of describing a system using mathematics as tools and as a language. It is of great importance to be able to construct a model of practically everything, since one might be able to provide a deeper explanation of how this particular system operates, study the effects of different factors that are taken into consideration and make predictions regarding the behaviour of the given system. Blood flow is described as the steady motion of blood inside the cardiovascular system, which is a system that consists of three components: blood [1] , heart and blood vessels[2].

The study of mathematical and numerical modelling of the cardiovascular-arterial system and their processes is a subject of research that has garnered significant attention from the mathematical community due to its inherent mathematical complexity and the escalating impact of cardiovascular diseases globally. Recent research indicates that cardiovascular diseases are the leading cause of death worldwide, responsible for over 17.3 million deaths annually. This alarming figure is expected to exceed 23.6 million by 2030. In Europe, cardiovascular diseases currently account for nearly half (47%) of all deaths [67].

Mathematical modeling presents significant challenges due to the intricate complexity of the cardiocirculatory system, the multiscale nature of physiological processes and the requirement of the development of computational techniques that are stable, dependable and efficient and are also in agreement with experimental and clinical data.

With the continuous emergence of new diagnostic tools, the advancements

[1] In this thesis, blood is considered as a Neutonian fluid for simplification reasons. However, in large arteries such as the aorta, blood behaves almost Neutonian.

[2] Blood vessels are modelled as non-rigid tubes.

in medical imaging and the technological advancements that keep on happening, the rise of patient-specific computational fluid dynamics (CFD) models has ushered in a new era of computer-aided diagnostics [95]. The goals of this thesis are to create an accurate 1D model and ultimately a 3D model to simulate the blood flow in specific large systemic arteries and in the lower part of the abdominal aorta (including the iliac bifurcation) respectively, while reenacting certain conditions: A resting state, two different levels of exercising and a case of a person who suffers from a cardiovascular disease such as the presence of an aneurysm in the region of the abdominal aorta, or, atherosclerosis, which is a phenomenon that potentially leads to coronary artery diseases (CAD). In order to achieve this, a one-dimensional model and its coupling with a zero-dimensional, 3-element Windkessel model is used in order to reproduce accurate flow and pressure waveforms in the arterial system, representing each simulation environment [6].

From the coupled model used above, suitable boundary conditions are extracted, depending on which environment (Gradual increase of exercising intensities or the pathological case of an aneurysm) is simulated and then are inserted on a Computational Software such as SimVascular in order to provide the 3D model with crucial information and create an accurate model.

In this introductory chapter, we briefly define important concepts that are required from a mathematical perspective such as: the mathematical formulation, the development of the cardiovascular system, the Navier-Stokes equations in cartesian and cylindrical coordinates and more. Reader should bear in mind that this thesis is firstly providing an analytical approach towards the equations that can be used to model blood flow. Such equations are the **Hagen-Poiseuille (Poiseuille's Law)**, the **Bernoulli principle** and the **Womersley** flow.

1.1 Function of blood vessels

Blood circulates through body tissues in blood vessels via bulk flow, meaning that all components move together in a single direction. Blood vessels can be categorized as three major types: arteries, veins and capillaries.

- Arteries transport blood from the heart to all other regions of the body.
- Veins carry blood back toward the heart through the establishment of a low-pressure collection system designed to transport oxygen-depleted

blood back to the heart.

- Capillaries, which are the smallest blood vessels, connect arteries and veins.

A high amount of blood vessel branching exists throughout the human body, ensuring that nearly every cell is in close proximity to at least one of the smallest branches of this system, known as capillaries. Nutrients and other substances, mostly byproducts, move between the capillaries and the surrounding cells through the interstitial fluid via diffusion and mediated transport. However, blood flow through all organs is primarily passive, driven by the maintenance of higher arterial pressure compared to venous pressure, which is achieved through the pumping action of the heart [36].

During periods of rest, approximately 5% of the total circulating blood is located within capillaries in the body. Remarkably, despite this relatively small volume, these capillaries fulfill the crucial functions of the entire cardiovascular system, particularly in supplying nutrients and removing metabolic waste products [40].

The cardiovascular system operates as a closed-loop system, where blood is pumped out of the heart through arteries and then returns to the heart via veins. This system can be further understood as comprising two closed-loop systems, both of which begin and end at the heart: the pulmonary circulation and the systemic circulation.

The pulmonary circulation consists of the right heart pump and the lungs. The systemic circulation involves the left heart pump, which distributes blood to the organs throughout the body. The right and left heart pumps operate in a series arrangement, meaning that both pumps circulate the same volume of blood in a given minute. In medical terms, cardiac output is typically measured in liters per minute.

In the systemic circulation, blood is propelled out of the left ventricle through a singular large artery known as the **aorta**. All arteries within the systemic circulation originate from the aorta, which is recognized as the body's largest artery with a diameter ranging from 2 to 3 centimeters, and then branch into smaller vessels successively. The aorta comprises four main divisions: the ascending aorta, which commences at the aortic valve and serves as the origin for the two coronary artery branches, the aortic arch, the thoracic aorta, and the abdominal aorta. Eventually, the smallest arteries further divide into arterioles.

The arterioles branch into a extremely large number of the smallest diameter vessels, namely, the capillaries (with an estimation over 10 billion averagely in the human body). Then, blood leaves the capillaries and returns to the heart via the venules [36].

1.2 Governing equations of blood flow in arteries

In order to develop a mathematical model that describes the velocity and the pressure of blood flow, one has provide some assumptions, i.e cylindrical shape of the vessels, deformable components with circular cross-sections and an alteration of areas as blood flows through them. As mentioned earlier, blood is considered as a Neutonian fluid, which is governed by the **Navier-Stokes** equations. In addition, one supposes that the flow is incompressible and that the viscosity remains constant.

Let the velocity components in x, y, z directions be u, v, w, respectively. Let ρ be the density of blood, p be the blood pressure and μ be the dynamic viscosity of blood. Then, the Navier-Stokes in cartesian coordinates with gravitational forces are :

$$\rho\left(\frac{\partial u}{\partial t}+u\frac{\partial u}{\partial x}+v\frac{\partial u}{\partial y}+w\frac{\partial u}{\partial z}\right)=-\frac{\partial p}{\partial x}+\mu\left(\frac{\partial^2 u}{\partial x^2}+\frac{\partial^2 u}{\partial y^2}+\frac{\partial^2 u}{\partial z^2}\right)+\rho g_u, \quad (1.1)$$

$$\rho\left(\frac{\partial v}{\partial t}+u\frac{\partial v}{\partial x}+v\frac{\partial v}{\partial y}+w\frac{\partial v}{\partial z}\right)=-\frac{\partial p}{\partial y}+\mu\left(\frac{\partial^2 v}{\partial x^2}+\frac{\partial^2 v}{\partial y^2}+\frac{\partial^2 v}{\partial z^2}\right)+\rho g_v, \quad (1.2)$$

$$\rho\left(\frac{\partial w}{\partial t}+u\frac{\partial w}{\partial x}+v\frac{\partial w}{\partial y}+w\frac{\partial w}{\partial z}\right)=-\frac{\partial p}{\partial z}+\mu\left(\frac{\partial^2 w}{\partial x^2}+\frac{\partial^2 w}{\partial y^2}+\frac{\partial^2 w}{\partial z^2}\right)+\rho g_w \quad (1.3)$$

And the continuity equation is expressed as:

$$\frac{\partial \rho}{\partial t}+\rho\left(\frac{\partial u}{\partial x}+\frac{\partial v}{\partial y}+\frac{\partial w}{\partial z}\right)=0. \quad (1.4)$$

Under the assumption that the force of gravity inside the body can be neglected, the Navier-Stokes equations can be written as :

$$\rho\left(\frac{\partial u}{\partial t}+u\frac{\partial u}{\partial x}+v\frac{\partial u}{\partial y}+w\frac{\partial u}{\partial z}\right)=-\frac{\partial p}{\partial x}+\mu\left(\frac{\partial^2 u}{\partial x^2}+\frac{\partial^2 u}{\partial y^2}+\frac{\partial^2 u}{\partial z^2}\right) \tag{1.5}$$

$$\rho\left(\frac{\partial v}{\partial t}+u\frac{\partial v}{\partial x}+v\frac{\partial v}{\partial y}+w\frac{\partial v}{\partial z}\right)=-\frac{\partial p}{\partial y}+\mu\left(\frac{\partial^2 v}{\partial x^2}+\frac{\partial^2 v}{\partial y^2}+\frac{\partial^2 v}{\partial z^2}\right) \tag{1.6}$$

$$\rho\left(\frac{\partial w}{\partial t}+u\frac{\partial w}{\partial x}+v\frac{\partial w}{\partial y}+w\frac{\partial w}{\partial z}\right)=-\frac{\partial p}{\partial z}+\mu\left(\frac{\partial^2 w}{\partial x^2}+\frac{\partial^2 w}{\partial y^2}+\frac{\partial^2 w}{\partial z^2}\right) \tag{1.7}$$

Equations (1.5) – (1.7) are the **Navier-Stokes** equations in Cartesian Coordinates.

Depending on the nature of the problem, the Navier-Stokes equations can be rearranged to match the geometry of the model, depending on the problem of interest.

In blood flow, it has been assumed that blood vessels i.e arteries, veins e.t.c. are in the shape of cylinders, thus, it is helpful to rewrite the Navier-Stokes equations in cylindrical coordinates (r, θ, z) in order to take advantage of the symmetry of the problem, as a frequent instance is **the axisymmetric flow** under the assumption of no tangential velocity ($v/u_\theta = 0$). Thus, the remaining quantities are independent of θ .

The classic transformation of cartesian coordinates to cylindrical coordinates is the following

$$\begin{cases} x = r\cos\theta, \\ y = r\sin\theta, \\ z = z. \end{cases}$$

Thus, the continuity equation in cylindrical coordinates, in the axisymmetric case is:

$$\frac{1}{r}\frac{\partial\left(ru_r\right)}{\partial r}+\frac{\partial u_z}{\partial z}=0. \tag{1.8}$$

The equations, in the axisymmetric case, for the two remaning velocity components from the momentum equations of Navier-Stokes are written as:

$$\frac{\partial u_r}{\partial t} + u_r \frac{\partial u_r}{\partial r} + u_z \frac{\partial u_r}{\partial z} = -\frac{1}{\rho}\frac{\partial p}{\partial r} + \frac{\mu}{\rho}\left(-\frac{u_r}{r^2} + \frac{1}{r}\frac{\partial}{\partial r}\left(r\frac{\partial u_r}{\partial r}\right) + \frac{\partial^2 u_r}{\partial z^2}\right), \quad (1.9)$$

$$\frac{\partial u_z}{\partial t} + u_r \frac{\partial u_z}{\partial r} + u_z \frac{\partial u_z}{\partial z} = -\frac{1}{\rho}\frac{\partial p}{\partial z} + \frac{\mu}{\rho}\left(\frac{1}{r}\frac{\partial}{\partial r}\left(r\frac{\partial u_z}{\partial r}\right) + \frac{\partial^2 u_z}{\partial z^2}\right). \quad (1.10)$$

1.3 Mechanism of blood flow: Poiseuille's Law

In order to maintain an adequate interstitial homeostasis, our bodies have to ensure that blood flows uninterruptedly through the millions of capillaries in the body. Regarding the flow through a given blood vessel, there are several parameters that affect it. All bloods vessels possess certain physiological characteristics such as lengths L and internal radii r through which blood flows when a pressure difference at the inlet and outlet exists (p_0 and p_1 respectively). Between the vessel ends, there is pressure difference ΔP, which supplies the driving force for flow [36, 42].

Due to the development of friction between blood flow and the rigid vessels walls, this fluid movement is characterized by a resistance (vascular), which is a way of measurement of difficulty that blood encounters in order to flow through a vessel. Thus, it is possible to provide a relative relationship between vascular flow, the pressure difference, and resistance as:

$$\text{Flow}(Q) = \frac{\text{Pressure Difference}}{\text{Resistances}} = \frac{\Delta P}{R}. \quad (1.11)$$

Where Q = flow rate (volume/time), ΔP = pressure difference and R = resistance to flow (mm Hg $\cdot$ time/volume)

The above equation can be applied not only to a single vessel but can also describe the flow through a network of vessels such as the vascular bed of an organ or the even the entire systemic circulatory system. It's acknowledged that the resistance to flow through a cylindrical tube or vessel is influenced by multiple factors [36].

Those factors where originally described from Jean Léonard Marie Poiseuille, a famous French scientist, who discovered a simple yet fruitful relationship between the laminar flow rate in a capillary tube (with constant cross-section) and the geometry of the tube, the dynamic viscosity and the pressure gradient of the system. Namely, those factors are :

1. Radius of the artery.
2. Length of the artery.
3. Viscosity of the fluid (Pathophysiology of the system, blood).
4. Inherent resistance to flow.

The equation that combines the aforementioned factors can be written as:

$$R = \frac{8L\mu}{\pi r^4} \tag{1.12}$$

where r = inside radius of the vessel, L = length of the vessel and μ =blood viscosity.

It is crucial to observe that a slight change in the radius of the vessel would lead to a significant effect in the resistance to the flow (since radius is in 4th power). In perspective, if one would decrease the vessel diameter by 50% then the resistance to the flow would increase by 16 times.

Now, combining the equations (1.11) and (1.12), an equation known as Poiseuille's Law occurs which is used to better approximate the factors that influence the flow though a cylindrical vessel and is the following:

$$Q = \frac{\Delta P \pi r^4}{8L\mu} = \frac{\pi r^4}{8L\mu}\Delta P \tag{1.13}$$

The above description of the (volumetric) flow rate is derived under certain conditions:

- **Steady flow:** Poiseuille's law is applied only to laminar flows, meaning that the the fluid velocity profile and the material properties do not change in time.
- Flow is **incompressible** thus, ρ = constant.

- All dominant forces acting on the fluid particles, besides viscosity terms and pressure are assumed to be zero or negligibly small.

1.3.1 Aftermath of Poiseuille's Law

Poiseuille's Law is frequently used in the field of haemodynamics due to the fact that volumetric flow rate is extremely sensitive to changes in cross-sectional area. Hence the reason why constricted capillaries lead to higher blood pressure, constricted veins reduce blood flow rate while the heart overtires to increase the blood pressure and keep blood flow constant.

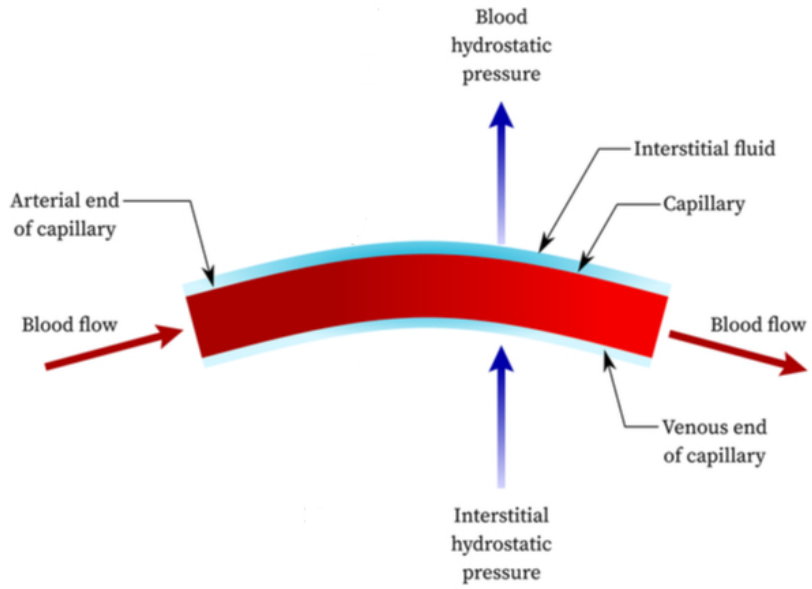

Figure 1.1: Enacting forces on blood capillary [60].

In general, flow (and in accordance, blood flow) exists due to pressure difference. This explains why arterial blood pressure is arguably the most tightly regulated cardiovascular parameter in the human body. Regulation is primarily achieved by controlling the diameters of vessels, such as arterioles, within specific tissue or organ systems. While factors like vessel length and blood viscosity influence vascular resistance, they are not easily modifiable.

Nevertheless, the heart's fundamental role is to maintain pressure within arteries higher than that within veins, thus establishing a pressure gradient to

drive flow. Typically, the average pressure in systemic arteries is around 100 mmHg, gradually decreasing to nearly 0 mmHg in the superior vena cava and inferior vena cava.

The volume of blood that flows through any tissue in a given period of time (normally expressed as l/min) is called local blood flow. The velocity of blood flow (expressed as cm^3/s or ml/s) can generally be considered to be inversely related to the vascular cross-sectional area [36, 67].

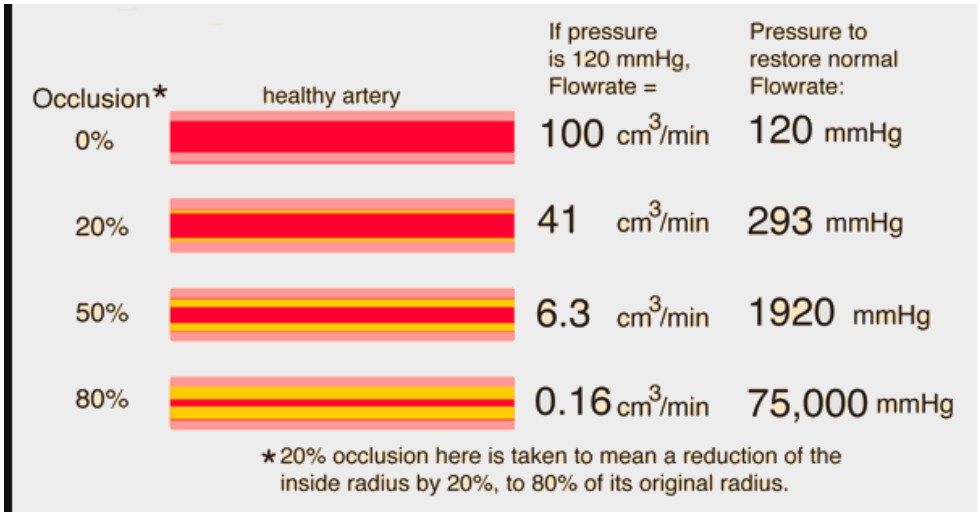

Figure 1.2: Effect of small arterial occlusion [57].

Remark: As shown in Figure (1.2), an amount of only 19% occlusion is enough to decrease the flow flow rate in half. Poiseuille's Law provides a systemic approach to predictions of blood flow rate and provides an insight of the complexity of that task that regulating blood flow is, to different regions of the human body.

From Eq. (1.13), it occurs that the flow resistance depends upon the fourth power to the radius of a vessel. The processes described in Figure (1.3) below are the vasodilation and vasoconstriction respectively and are mechanisms of immense value and functionality in regards of blood flow inside arteries.

It becomes evident that small blood vessels play a significant role in impeding flow. Even minor blockages, namely occlusions, in arteries can result in considerable hemodynamic impacts. Thus, the control of flow is managed

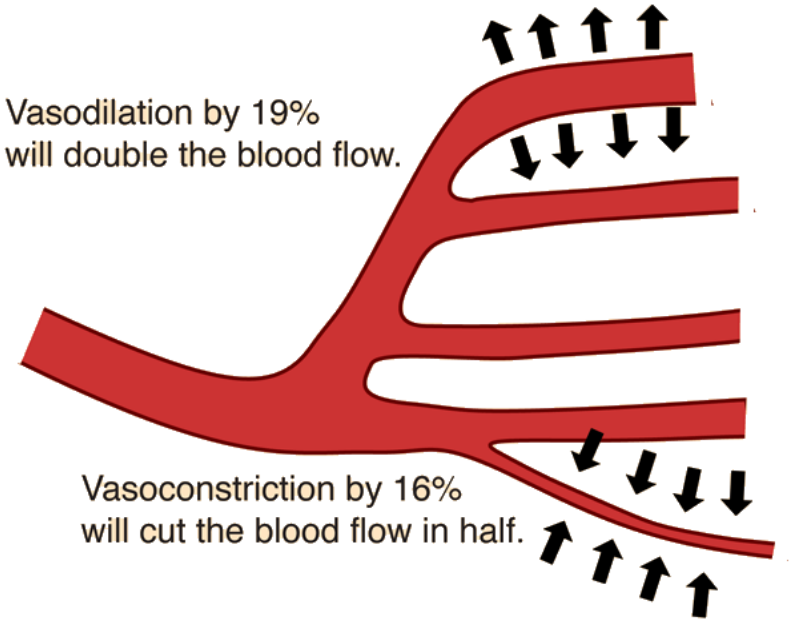

Figure 1.3: Effect of Vasodilation and Vasoconstriction mechanisms [57].

through the dilation or constriction of the arterioles [32]. The delicate balance of arterial dilation and constriction serves as a subtly tuned mechanism for regulating blood flow, ensuring adequate perfusion to tissues and organs under diverse physiological conditions, such as during different levels of physical activity.

In order to understand the magnitude of importance of what a small change in the diameter of a vessel can have and in terms of visualization of what is described, we consider the Figure (1.4) below where:

Given the parameters provided in Figure (1.4) below, if a vessel with a length of 100 cm and a diameter of 5 mm experiences a reduction in diameter to 1 mm over a 1 cm segment, the resistance in this narrowed section would be approximately 6.25 times greater than that of the entire length of the larger vessel. This observation reaffirms the earlier conclusion that even a small constriction within a blood vessel can significantly increase the resistance to flow. Such phenomena have profound medical implications, as numerous pathological conditions directly impact the radius of blood vessels, highlighting the importance of understanding vascular dynamics in diseased vessels.

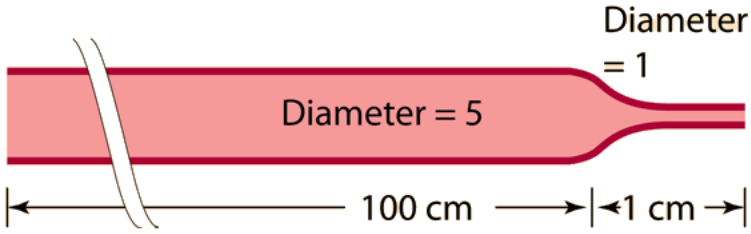

Figure 1.4: Change in diameter of the vessel . Adopted from[57].

1.3.2 Failure of Poiseuille's Law

Poiseuille's law, to this day, is a powerful mathematical tool that describes the blood flow rate and the blood pressure and played a pioneering role in the early days of haemodynamic studies. Poiseuille's law underlines the significant effect of vessel diameter uppon the resistance and flow and therefore provides a pathway to comprehend how physiological (e.g., vascular tone) and pathological (e.g., vascular stenosis) changes in vessel diameter affect pressure and flow. However, it seems to be limiting as a mathematical formulation in terms an inability to model every real-world scenario in the field of haemodynamics. Nevertheless, it remains a widely-accepted mathematical approach and is vastly utilized in numerical simulations of blood flow.

Some of the reasons that Poiseuille's Law seems insufficient and cannot be adopted as the solely hemodynamic model are:

1. As it is going to be discussed in the next chapter of this thesis, blood flow in the circulatory system is **pulsatile** and is driven by the rhythmic contraction and relaxation of the heart. Poiseuille's law assumes that the flow is steady-state, which means that the fluid velocity and the pressure remain unchanged as time passes by, which is not a realistic assumption as the blood flow and pressure vary dynamically during the entire cardiac cycle, making Poiseuille's law unsuitable for capturing and describing a pulsatile flow [66].

2. Poiseuille's law is suitable only for **Neutonian fluids**. Blood is a non-Neutonian fluid, which means that it does not obey Newton's viscosity law as the rate of strain is not proportional to the stress and thus, its viscosity changes with shear rate varies depending on the flow conditions [56].

3. Poiseuille's law assumes a straight, constant-diameter cylindrical tube. In reality, blood vessels have more complex geometries, including tapering, branching, and curving, which affect the flow . Poiseuille's law does not apply to these complex geometries.

4. In reality, blood vessels are not rigid tubes, but rather compliant and elastic structures that can expand and contract in response to changes in blood pressure. Poiseuille's law assumes rigid vessels and does not consider the effects of vessel compliance on flow dynamics.

5. While Poiseuille's law is valid for laminar flow, blood flow in larger arteries and regions with high flow rates can exhibit turbulence, which cannot be captured.

6. Lastly, Poiseuille's law assumes fully developed flow at the inlet and outlet of the pipe. However, blood flow in arteries and veins experiences transitional flow phases and developing flow conditions as blood either moves away from or towards the heart.

1.4 Bernoulli's principle in blood flow applications

The fundamental equations governing fluid flow are commonly associated with the names of Daniel Bernoulli and J. L. M. Poiseuille, where the latter one was introduced in the previous chapter.

Bernoulli considered a type of fluids that are nonviscous or frictionless (so-called "**ideal**" fluids) in which pressure can originate from two viable sources: 1) pressure due to the action of gravity on the fluid column (weight of fluid) and 2) the pressure related to changes in the velocity of the fluid (inertial forces).

The Bernoulli equation is derived from the conservation equations and illustrates the relationship between velocity, elevation, and pressure in a nonviscous fluid. For frictionless ($\tau = 0$) and steady flow behavior ($\frac{\partial V}{\partial t} = 0$), the equation of linear momentum is reduced to,

$$\rho V \nabla \cdot V = -\nabla P + \rho g \tag{1.14}$$

Where ρ is the fluid density, V is the fluid velocity, P the accelerative or decelerative pressure of fluid if there is a change in velocity and/or is due to

gravity if there is an elevation from a given reference plane, g is the gravitational acceleration ($9.8m/s^2$).

Integrating equation (1.14) yields :

$$P + \rho gh + \frac{1}{2}\rho \bar{V}^2 = \text{constant}. \tag{1.15}$$

Where h is the height of the fluid from a given reference plane or namely, elevation and $\bar{V}$ = is the mean velocity fluid in a tube system ($\bar{V}$ volume flow rate/cross sectional area of tube)

Between two points along a streamline, equation (1.15) can be written as :

$$\frac{P_2 - P_1}{\rho} + \frac{1}{2}(V_2^2 - V_1^2) + g(h_2 - h_1) = 0 \tag{1.16}$$

In the Bernoulli equation, all three terms are interconvertible. Acceleration of fluid converts the lateral pressure P to $\rho\bar{V}^2$, which is the reason that P falls. This is known as the **Bernoulli principle**. In this equation, an increase in fluid velocity within a region results in a decrease in pressure at that region. Conversely, deceleration transforms the kinetic energy term $\rho\frac{\bar{V}^2}{2}$ into lateral pressure.

The essence of the aforementioned equation lies in its application to incompressible fluids flowing through pipes of varying sizes where the velocity changes. This change creates an acceleration in the system resulting in different forces and pressures on the pipe's cross-sectional area. It is of significant importance to bear in mind that that Bernoulli's equation applies to flows that are steady (not pulsatile) and laminar (or streamline) in which the incompressible fluid moves as a series of layers. In fully developed flow, molecules adjacent to the wall remain stationary, while those in the center move at the highest velocity, resulting in a parabolic velocity profile [10].

Due to the fact that flowing blood has mass and velocity, it has kinetic energy as well. From the equations (1.15) and (1.16), it occurs that this kinetic energy is proportionate to mean velocity, squared (as it is known that Kinetic Energy = $\frac{1}{2}mV^2$).

As the blood flows inside a vessel, pressure is exerted laterally against the walls of the vessel. This pressure represents the potential energy.

Thus, for the total energy of the blood flowing within the vessel :

$$\textbf{Total Energy} = \textbf{Kinetic Energy} + \textbf{Potential Energy} \tag{1.17}$$

Thus, when Bernoulli's equation is applied to hemodynamics, it asserts that the total energy per unit volume, comprising pressure, kinetic energy, and potential energy, remains constant at any point along a blood vessel. Consequently, variations in flow velocity or elevation induce corresponding changes in pressure. Specifically, an increase in flow speed leads to a decrease in pressure when height remains constant, whereas an increase in height results in reduced pressure when flow speed remains constant. A leveraging of this relationship can yield crucial insights of blood flow dynamics and apply Bernoulli's principle to conditions such as inside the regions of aneurysms or in pre or post-stenosic regions.

The former, implies that blood flow occurs due to difference in total energy between two points in the vessel. Despite the fact that pressure is normally considered as the driving force for blood flow (as it was earlier shown in the Poiseuille's Law chapter), it is the total energy (KE + PE) that drives flow between two points (e.g., longitudinally along a blood vessel or across a heart valve). In the greater part of the cardiovascular system, kinetic energy is relatively low. Therefore, for practical purposes, it's often emphasized that the pressure energy difference, or potential energy, primarily propels flow. However, in situations where kinetic energy is high, the augmentation of kinetic energy onto pre-existing potential energy elevates the total energy of the system. An illustration of this phenomenon can be observed in the flow dynamics across the aortic valve during cardiac ejection [42].

The latter, implies that kinetic and potential energy can be inter-converted so that total energy remains unchanged, which was earlier defined as Bernoulli's principle. Under the assumption that a blood vessel is narrowed and then returns to its normal diameter, in the narrowed area (stenosis) the velocity increases as the diameter decreases.

Quantitatively, V is proportional to $\frac{1}{D^2}$ (where D is the diameter) as flow is the product of mean velocity times the vessel cross-sectional area and this area A is related directly to diameter (or the radius r) squared (following the type $A = \pi r^2$). When the diameter of a blood vessel is halved in the region of stenosis, the velocity of blood flow increases by a factor of four. Due to the fact that **KE** is proportional to V^2, the kinetic energy iincreases by a factor of sixteen. Under the assumption of the conservation of total energy within the stenosis, E decreases because of impendance, as shown in the Figure (1.5).

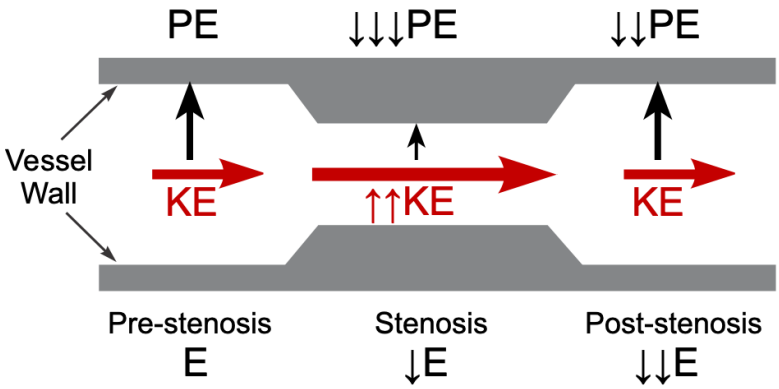

Figure 1.5: Aftermath of stenosis and the effects of it on the kinetic, potential and total energy inside a blood vessel [42].

Consequently, the 16-fold increase in **KE** necessitates a decrease in PE. his decline in PE signifies a reduction in lateral pressure exerted against the vessel walls. Hence, an elevation in velocity corresponds to a reduction in lateral pressure, a phenomenon rooted in the Venturi effect [36, 42]. Once the blood traverses the narrowed segment, **KE** returns to its pre-stenosis value, as the post-stenosis diameter matches the pre-stenosis diameter, thereby conserving flow and by extension, velocity.

Remark: Eq.(1.15) is an approximation, as it does not attribute the loss of energy due to shearing friction that is exhibited between the flowing blood and the walls of the artery. Despite the fact that Bernouli's equation is not a realistic and accurate approach due to the frictionless notion and the overlook of the viscosity of the fluids, it provides a sufficient understanding of the governing physics that are showcased in the arterial and venous system. For instance, when the blood pressure of a person is calculated, a medical expert places a sleeve or an external cuff around the upper arm. This phenomenon occurs because the upper arm is positioned roughly at the same level as the heart, ensuring that pressure remains unaffected by any disparities in height. To measure the systolic pressure, the cuff pressure is elevated until blood flow ceases completely, as described in Eq. (1.15), marking the "cut-off" pressure, which represents the maximum pressure in the artery. Subsequently, the pressure within the external cuff is gradually reduced until blood flow reaches its peak. At this juncture, pressure is at its minimum, indicating the diastolic pressure within the artery.

Another application of Bernouli's principle can be observed when blood

pressure measurements are taken from within the ascending aorta [3]. During ventricular ejection, the velocity and hence the kinetic energy of the flowing blood are very high. The instantaneous blood pressure that is measured within the aorta will be significantly different depending on how the pressure is measured. Usually, the measurement of pressure is acquired through Doppler Echocardiography, which relies on the velocity gradient that is calculated and so, this method of pressure acquisition can be characterized as an indirect approach. Thus, the procedure of catheterization is a useful tool that provides a direct calculation of the pressure. Normally, a catheter is put with two attached sensors, as seen in Figure (1.6). One is an end-port sensor that is facing the flowing stream of blood and the other is a a side-port sensor which is attached to the wall of the aorta (or the specific arterial segment that the catheter has been attached to [89].

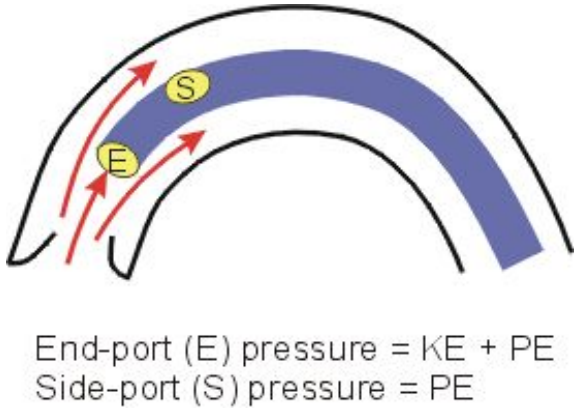

Figure 1.6: Catheter with two attached sensors [42].

[3]The ascending aorta is the first segment of the aorta, which is the largest blood vessel in the human body. It is the first extension of the heart and plays an essential role.

In observation, it is noted that the end-port sensor on a catheter will detect a pressure notably higher than what is measured by a side-port sensor located on the same catheter. This happens due to the fact that the end-port sensor measures the conglomeration of the energy of the blood flow. As the flow reaches the terminating area of the catheter, the kinetic energy converts to potential (or pressure) energy, and is added to the potential energy and as a result, the pressure energy surges. The side-port is not met by the flow, so the kinetic energy is not converted to pressure energy. The side-port sensor, therefore, measures the pressure [4] energy exclusively. The difference between those two pressure measurements can vary between few mmHg up to 20 mmHg, depending on the peak velocity of the flowing blood within the vessel [42].

1.5 Biomechanical characteristics of blood vessels

Looking at blood vessel walls from a biomaterial perspective, they can be conceptualized as composite materials comprising various components like elastin, collagen, and smooth muscle cells, each with distinct yet important mechanical properties.

The structure of the blood vessel wall is designed to endure and propagate the forces exerted by blood flow and pressure, as well as those from the surrounding tissues. They are exposed to various mechanical stresses *in vivo*. The walls of blood vessels are described as viscoelastic and are capable of altering their size or shape in response to application of different kinds of forces uppon them. These forces encompass both the pressures and shear stresses applied by the blood, and the constraints imposed by surrounding tissue. In the case of an artery wall, its intraluminal surface is subjected to mean pressure of 100 mmHg and pulse pressure of 40 mmHg. Arterial walls usually undergo a longitudinal stretching of 30–50 % as evidenced by arterial contraction in the longitudinal direction post-excision. The intraluminal surface experiences wall shear stress of a few Pascals due to blood flow and this shear stress oscillates throughout the cardiac cycle. These mechanical stresses cause the artery diameter to change by approximately 10% and its length to undergo a slight variation during the cardiac cycle. [33, 35].

[4] Which is translated as a lateral pressure acting on the walls of the aorta/vessel.

1.5.1 Young's Modulus

The Young's modulus (or elastic modulus), E, is a fundamental mechanical property that describes the stiffness or rigidity and **not** the elasticity of a material. Its units are force per area and thus are the same units as for stress and pressure, N/m^2 = Pa or mmHg. It is frequently used as a quantifying measurement of how a material responds to an applied force or stress in terms of its deformation or strain by relating the ratio of stress σ to strain ϵ and thus, E is defined as $\frac{\sigma}{\epsilon}$. Specifically, σ is the stress applied to the material and ϵ is the resulting strain, which is the proportional change in length or volume of the material. When one plots the stress-strain relation, then Young's modulus is the slope of the line of that plot.

In more detail, Young's modulus is considered to be a measure of a material's resistance to deformation when subjected to either axial or tensile forces. A higher Young's Modulus indicates a stiffer material that experiences less deformation for given stress, while a lower Young's Modulus indicates a more flexible or compliant material. In linear elastic materials, the slope remains constant over over a significant range of stress/strain and thus, the mechanical properties of the material can be described as a single value of E, known as Young's Modulus. In non-linear materials such as soft biological tissues, the value of E is dependent on the strain and for such materials, there exists a specific modulus, named incremental elastic modulus, which is defined as $E_{inc} = \frac{\Delta\sigma}{\Delta\epsilon}$ that is, the change in stress over the change in strain over a small section of the stress–strain curve [35].

Regarding blood vessels, Young's Modulus is a crucial parameter and is used to characterize their rigidity and how they respond to changes in pressure. Blood vessels, particularly arteries, are not purely elastic but also exhibit viscoelastic behavior, as was mentioned earlier. This means that their mechanical response depends not only on the immediate stress but also on the rate of deformation and the time-dependent properties of the vessel wall. High vascular stiffness, indicated by a higher Young's Modulus, is associated with cardiovascular conditions like hypertension and atherosclerosis and indicates a high risk factor for cardiovascular diseases [23, 35, 42].

1.5.2 Laplace's Law of Wall Tension

Laplace's law establishes a relationship between the tension in the wall of an arterial or venous vessel and the pressure applied by the elastic tube on

the material inside of it. The pressure inside blood vessel walls, denoted as P, exceeds that outside, $P_{external}$ by a pressure difference $\Delta P = P - P_{external}$. We consider a tube (in our occasion, a blood vessel and specifically an artery, which can be modeled as a hollow cylinder as depicted in Figure 1.7) with inner radius R, length L, thickness of the arterial wall W and T is the tensional (or namely, circumferential) stress within the wall of the vessel, where the tensional stress points are tangentially oriented to the vessel wall, in a parallel direction to its surface.

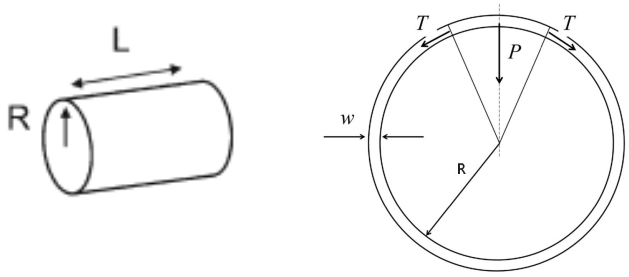

(a) Hollow cylinder (b) Cross section of an artery

Figure 1.7: Laplace's Law of wall tension. Figure was adopted from [33].

The outward force on a section of an area of the cylinder and under the assumption that this section is at an angle $\theta \ll 1$ can be expressed as the pressure difference ΔP times the area, $(R\theta)L$ as shown as well in Figure (1.8).

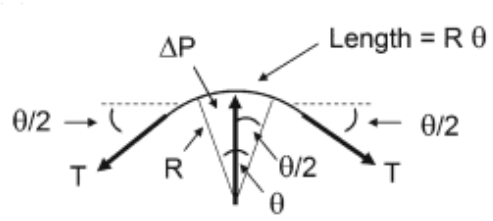

Figure 1.8: Derivation of Laplace's Wall Law for a cylinder, including a force diagram for a section of the cylinder. Figure was adopted from [33].

Thus, the circumferential tension T is the force per unit length (along the tube length) and the film tension (namely, surface tension) σ is equal to $\frac{T}{w}$ (where $w \ll R$). Those tension forces are enacting inside a blood vessel wall at

any given time and while the horizontal components of the surface tension on the right and left respectively cancel each other out, the vertical components of the surface tension (inwards) are equal to $T\sin\left(\frac{\theta}{2}\right) \simeq T\left(\frac{\theta}{2}\right)$ for small angles [28, 33, 42].

When both of these tension components are multiplied by L, it provides the following

$$P = \frac{w}{R}T. \tag{1.18}$$

Which is known as Laplace's Law of Wall tension.
Laplace's law stipulates that the inward pressure applied by the vessel wall on the blood is directly related to the tensional stress in the arterial-venous wall and inversely proportional to the radius of the vessel. Consequently, smaller vessels can apply greater pressure on the blood. Large, thin-walled vessels are typically low-pressure vessels. Elevated pressure causes vessel distension and increases in vessel volume, a characteristic feature of veins. To sustain pressure, arteries require more dense, thicker walls, hence large veins tend to be thin-walled while arteries are thick-walled [33].

Consequently, the artery would act like a bulge-structure where it would keep on inflating and thus creating a pathology, e.g, an aneurysm. Despite the fact that *in vivo*, arteries are multi-layered structures and present different mechanical properties, it is not necessary to implement the elastic moduli of each different layer as, for simplifications reasons in both modelling of the problem and in the construction of computational fluid dynamics softwares, it is oftenly assumed that the wall thickness and elastic composition remain consistent across different positions around the vessels of reference [33, 42].

CHAPTER 2

Analytical solutions of pulsatile blood flow

As was mentioned earlier in this thesis, Poiseuille's Law was able to provide analytical solutions to the flow problem in a tube under certain conditions. Such were: the simplification of the geometry of the tube, its rigidity, its diameter, the existence of laminar flow, stable pressure gradient e.t.c. However, biological problems in general, cannot be solved easily and the blood flow in vessels (and consequently, the arterial system) is not an exception.

The reasoning behind the complexity of those problems is: **1)** the existence of non-linearity in Navier-Stokes **2)** The characteristics of the flow such as velocity and pressure, at the inlet and the outlet of the system which are of critical interest but the clinical data regarding the physiological charasteristics at the outlet cannot be accurately calculated and provided, since the ending of the arterial system is in millions of trichoid vessels where the pressure and velocity differ dramatically.

In vivo, blood flow and pressure in the vasculature are unsteady due to the pulsatile flow conditions in the arteries. The pressure and the volumetric flow rate of the blood vary with time over the period of heart relaxation and contraction and are expressed as waveforms. The theory of pulsatile blood flow was initially proposed by Leonhard Euler in 1775 and further developed by Thomas Young in 1808. Subsequently, numerous efforts have been dedicated to the study of pulsatile blood flow in the vascular system. That is where the pioneering work of Womersley and his colleagues essentially laid the foundation of modern hemodynamics [37]. Its equation was derived as an exact solution of viscous flow equations through a circular tube subjected to a periodic pressure gradient. Through the development of a time-dependent one-dimensional exact solution of the Navier–Stokes equation, Womersley demonstrated that

blood flow in main arteries can be described by a Fourier decomposition of the cardiac harmonics [31, 93].

We begin by introducing a proposition that played a pioneering role in Womersley's work in haemodynamics, the Fourier series theorem, expressed in the form of a proposition.

Proposition A periodic function $f(t)$ with a period T can be represented by the sum of a constant term, a fundamental of period T, and its harmonics.

The exhibited pulsatility of blood flow means that the partial derivative of velocity with respect to time and the partial derivative of pressure with respect to distance along tube's axis x are **nonzero**.

The pressure waveform is periodic, meaning that it depends on a frequency ω (which is calculated in $rads/s$) and on time t. Thus, we can apply the above proposition and express the pressure gradient as:

$$\frac{\partial p}{\partial x}(t) = A_0 + \sum_{n=1}^{\infty} A_n \cos(\omega n t) + \sum_{n=1}^{\infty} B_n \sin(\omega n t), \tag{2.1}$$

where $\omega = \dfrac{2\pi}{T_0}$, A_i and B_i, i=1,2,...,n are the Fourier coefficients and can be explicitly calculated via integrals [43].

Evoking Euler's identity, the pressure gradient can be expressed as:

$$\frac{\partial p}{\partial x} = \mathrm{Re}\left[\sum_{n=0}^{\infty} a_n e^{i\omega n t}\right], \tag{2.2}$$

where $a_n = A_n - iB_n$, n is the number of harmonics, ω is the frequency and A_0 is the mean pressure gradient(which is not pulsatile) [89].

2.1 Derivation of the Womersley solution

Both Womersley flow and the velocity profile of the pulsatile flow are given through the Womersley equation which describes an unsteady flow in a straight circular tube of length L and radius R, fluid density ρ, dynamic viscosity μ and kinematic viscosity ν under the certain conditions below:

1. The fluid is Neutonian, incompressible and homogeneous.
2. The walls of the tube are rigid and circular.

3. The flow is laminar, axisymmetric and parallel to the tube's axis.
4. No-slip condition near the walls of the tube and central axisymmetry are applied.
5. The pressure gradient is time-varying (periodic).
6. No effect of the gravitational field on the fluid.

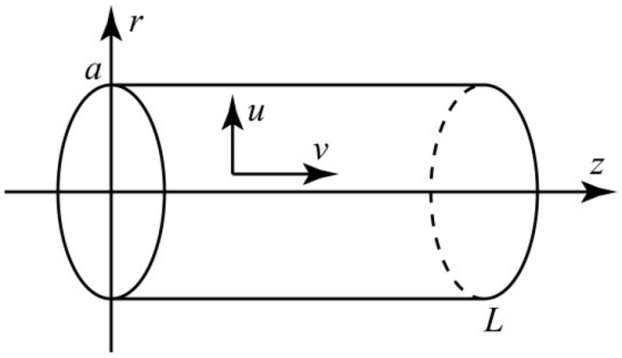

Figure 2.1: Adopted from [20]

Since the flow is axisymmetric there is no swirling flow and no velocity in the transverse or radial directions thus, $\frac{\partial u}{\partial \theta} = v_r = v_\theta = 0$ and given that the flow is uniform there is no alteration in velocity u in x-direction, thus $\frac{\partial u}{\partial x} = 0$. Consequently, the cylindrical Navier-Stokes equations are reduced to the equation,

$$\frac{a_n e^{i\omega nt}}{\rho} = \nu \frac{\partial^2 u}{\partial r^2} + \frac{\nu}{r}\frac{\partial u}{\partial r} - \frac{\partial u}{\partial t} \tag{2.3}$$

As mentioned earlier, the pressure gradient -$\frac{\partial p}{\partial x}$ is described in Eq. (2.2) and thus, for each harmonic n, it is possible to describe each pressure component as a compex exponential,

$$\frac{\partial p}{\partial x}\Big|_n = a_n e^{i\omega nt} := A e^{i\omega nt} \tag{2.4}$$

Now, Eq. (2.3) is a second-order, linear, partial differential equation with a driving function. From the assumptions above plus the fact that the fluid

is incompressible solving this PDE is done by the method of seperation of variables,

$$u(r,t) = \hat{u}(r)e^{i\omega nt} \tag{2.5}$$

where functions $\hat{u} = \hat{u}(r)$ and $e^{i\omega nt}$ is a function of time, t.

Now we need to calculate 3 different derivatives, with respect to t,r and second derivative with respect to r, after replacing Eq. (2.5) in Eq. (2.3),

$$\begin{cases} \dfrac{du}{dr} = \dfrac{d\hat{u}(r)}{dr}e^{i\omega nt} \\ \dfrac{du}{dt} = i\omega n\hat{u}(r)e^{i\omega nt} \\ \dfrac{d^2u}{dr^2} = \dfrac{d^2\hat{u}(r)}{dr^2}e^{i\omega nt} \end{cases}$$

If we replace the derivatives above, Eq. (2.3) is rewritten as,

$$\frac{1}{\rho}Ae^{i\omega nt} = \nu\frac{d^2\hat{u}(r)}{dr^2}e^{i\omega nt} + \frac{\nu}{r}\frac{d\hat{u}(r)}{dr}e^{i\omega nt} - i\omega n\hat{u}(r)e^{i\omega nt} \tag{2.6}$$

And by dividing with $e^{i\omega nt}$, time dependence is dropped and thus,

$$\frac{A}{\rho} = \nu\frac{d^2\hat{u}(r)}{dr^2} + \frac{\nu}{r}\frac{d\hat{u}(r)}{dr} - i\omega n\hat{u}(r) \tag{2.7}$$

Evoking the relationship $\nu = \frac{\mu}{\rho}$, we are able to transform Eq. (2.7) to a zero-order Bessel equation with a driving function,

$$\frac{A}{\mu} = \frac{d^2\hat{u}(r)}{dr^2} + \frac{1}{r}\frac{d\hat{u}(r)}{dr} + i^3\omega n\hat{u}(r)\frac{1}{\nu}. \tag{2.8}$$

Remark: A zero-order Bessel differential equation is written as,

$$\frac{d^2y}{dx^2} + \frac{1}{x}\frac{dy}{dx} + \lambda^2 y = 0. \tag{2.9}$$

The solution of the homogeneous equation of Eq. (2.8), as mentioned in [2, 85], is composed of a Bessel function of first-kind and zero-order. Thus, one possible homogeneous solution is,

$$\hat{u}_{homog}(r) = C_1J_0(\lambda r) + C_2Y_0(\lambda r) \tag{2.10}$$

where C_1, C_2 are constants, J_0 is a zero-order Bessel function of first-kind and Y_0 is a zero-order Bessel function of second-kind (that will vanish, as C_2

constant can be set zero due to the boundary conditions) and lastly, we have set λ^2 to be $i^3\omega n\frac{1}{\nu}$.

However, Eq. (2.8) is inhomogeneous and in order to find a general solution we need to find a particular solution as well. We assume that $\hat{u}_{particular}(r) = C_3$ is a particular solution of the differential equation. It is possible to evoke the boundary condition $\frac{d\hat{u}(r)}{dr} = 0$ and calculate C_3,

$$\frac{A}{\mu} = i^3\omega n\frac{1}{\nu}C_3. \tag{2.11}$$

Thus,

$$C_3 = -\frac{A}{i\rho\omega n}. \tag{2.12}$$

The general solution is,

$$\hat{u}(r) = C_1 J_0(\lambda r) - \frac{A}{i\rho\omega n}. \tag{2.13}$$

Introducing the no-slip condition, we equip ourselves with the boundary condition $u(r = R) = 0$ and thus,

$$C_1 = \frac{A}{i\rho\omega n J_0(\lambda R)}. \tag{2.14}$$

Thus the general solution, for any harmonic n is,

$$\hat{u}(r) = \frac{A}{i\rho\omega n}\left[\frac{J_0(\lambda r)}{J_0(\lambda R)} - 1\right] \tag{2.15}$$

Lastly, if we apply the reverse transform of Eq.(2.5), return to variable u and keep the real, the following is obtained,

$$u(r,t) = \mathrm{Re}\left[\frac{A}{i\rho\omega n}\left\{\frac{J_0(\lambda r)}{J_0(\lambda R)} - 1\right\}e^{i\omega nt}\right], \tag{2.16}$$

where the pressure gradient has been expressed as the real part of $Ae^{i\omega nt}$.

Remark: Eq.(2.16) can provide a descriptive profile of the Womersley flow by summing all of the n harmonic components. A missing reagent is the *Womersley parameter*, which is a key/varying parameter that effects the velocity profile and is introduced in the subsection below.

2.1.1 Derivation of dimensionless Womersley equation

Applying the aforementioned conditions, the Navier-Stokes equations (for fully developed flow) are reduced to :

$$\frac{\partial u}{\partial t} = -\frac{1}{\rho}\frac{\partial p}{\partial x} + \nu\left(\frac{\partial^2 u}{\partial r^2} + \frac{1}{r}\frac{\partial u}{\partial r}\right). \tag{2.17}$$

Now, by introducing characteristic scales for the non-dimensionalized variables $y = \frac{r}{R}$, $z = \frac{x}{R}$, $\tau = t\omega$, $u = \frac{v}{V}$, Eq. (2.17) is converted to the dimensionless form:

$$\frac{R^2\omega}{\nu}\frac{\partial v}{\partial \tau} = -\frac{R}{\rho\nu V}\frac{\partial p}{\partial z} + \frac{\partial^2 v}{\partial y^2} + \frac{1}{y}\frac{\partial v}{\partial y}. \tag{2.18}$$

From Eq. (2.18), a natural scale for pressure occurs:

$$p^* = \frac{Rp}{\rho\nu V} = \frac{Rp}{\mu V} \tag{2.19}$$

Thus, after substitution, the dimensionless, scaled *Womersley equation* is:

$$\alpha^2\frac{\partial v}{\partial \tau} = -\frac{\partial p^*}{\partial z} + \frac{\partial^2 v}{\partial y^2} + \frac{1}{y}\frac{\partial v}{\partial y} \tag{2.20}$$

Where α is a dimensionless quantity, the *Womersley number*(Wo) which is defined as

$$\alpha = R\sqrt{\frac{\omega}{\nu}} \tag{2.21}$$

and suggests a correlation between the frequency of pulse flow and the viscosity in biofluid mechanics.

Specifically, for flows where $a \to \infty$ (or $Wo \gg 1$) they are characterized as inertia-dominated flows, then the viscous forces are negligible compared to the other terms in Eq. (2.20) and the pressure gradient is used for acceleration of the fluid mass. In that case, the velocity profiles deviate from exhibiting a parabolic shape and the flow is out of time phase in relation to the oscillating pressure gradient. This phenomenon is observed in large blood vessels, at high frequency flows. For example, in the aorta, it holds that: $\alpha \geq 20$. For flows where $\alpha \to 0$ (i.e $Wo \ll 1$), they are characterized as friction-dominated flows

and are observed in small blood vessels like capillaries, where $\alpha = 10^{-2}$. In this scenario, the flow is anticipated to conform to the oscillating pressure gradient and the velocity profiles exhibit a parabolic shape such that the fluid oscillating with maximum amplitude is farther from the walls ("almost stable" behavior)[37].

Eq.(2.20) is expressed as,

$$\alpha^2 \frac{\partial v}{\partial t} = -\mathrm{Re}\frac{\partial p}{\partial z} + \frac{1}{r}\frac{\partial}{\partial r}\left(r\frac{\partial v}{\partial r}\right) \tag{2.22}$$

where Re is the Reynolds number $Re := \frac{Rv}{\nu}$ and is introduced as a scaling factor for the pressure gradient.

Now, Eq.(2.22) is linear in regards to v, thus we are able to provide a superposition of the solution for various subharmonics. As introduced earlier, we assume that the pressure gradient is oscillating and can be expressed as a harmonic,

$$\frac{\partial p}{\partial z} = \frac{\partial \hat{p}}{\partial z} e^{i\omega t}. \tag{2.23}$$

It is additionally assumed that velocity v can be written in harmonic form,

$$v(r,t) = \hat{v}(r) e^{i\omega t}. \tag{2.24}$$

As mentioned earlier, there are two asymptotic cases that can be examined for different Womersley parameter values. In the case where Womersley was small (i.e in friction-dominated flow) an equilibrium between the driving pressure gradient and the viscous forces is exhibited. In case where Womersley was large the viscous forces are small compared to instationery inertial forces and thus, an equilibrium in inertia forces and driving pressure gradient is achieved. A detailed analysis of the above is provided below:

Proposition If $\alpha \to 0$, then Eq. (2.22) is reduced to

$$-\frac{1}{\rho}\frac{\partial p}{\partial z} + \frac{\nu}{r}\frac{\partial}{\partial r}\left(r\frac{\partial v}{\partial r}\right) = 0. \tag{2.25}$$

Replacing Eq. (2.23) and Eq. (2.24) in Eq. (2.25) yields,

$$\nu\frac{\partial^2 \hat{v}}{\partial r^2} + \frac{\nu}{r}\frac{\partial \hat{v}}{\partial r} = \frac{1}{\rho}\frac{\partial \hat{p}}{\partial z}, \tag{2.26}$$

Solving for $\hat{v}$,

$$\hat{v}(r) = -\frac{1}{4}\frac{\partial \hat{p}}{\partial z}(1 - r^2). \tag{2.27}$$

Returning back to v yields the solution,

$$v(r,t) = -\frac{1}{4\mu}\frac{\partial \hat{p}}{\partial z}(\alpha^2 - r^2)e^{i\omega t}. \tag{2.28}$$

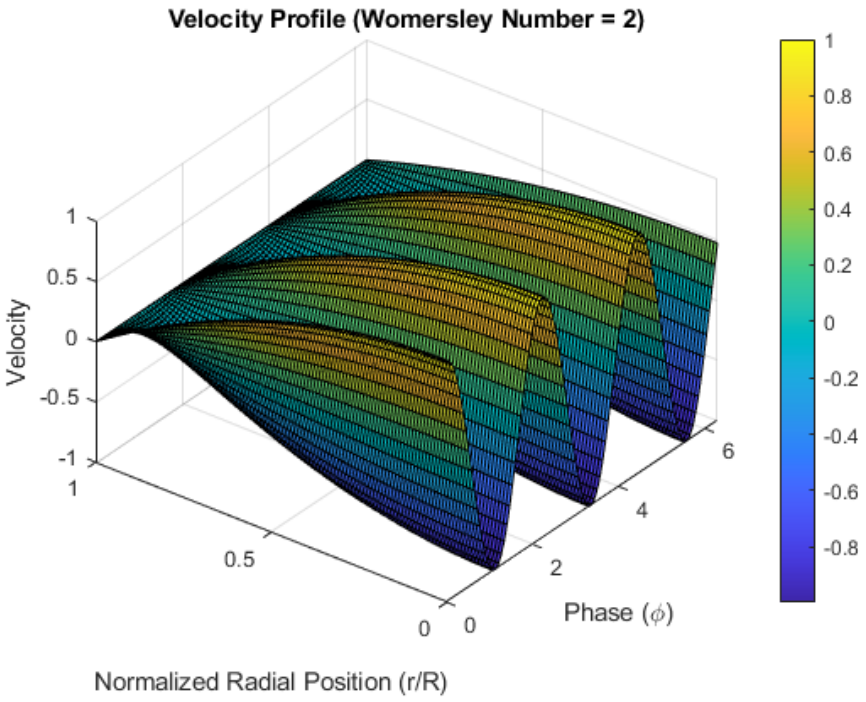

Figure 2.2: Depinction of the 3D pulsatile velocity profile for $Wo(\alpha) = 2$, using MATLAB.

Remark A quasi-static Poiseuille profile is observed in Figure (2.2), which shows that viscous forces dominate over inertia forces. This behavior implies a smooth, predictable nature of flow which is observed in small blood vessels.

If $\alpha \gg 1$, Eq.(2.22) is reduced to,

$$\frac{\partial v}{\partial t} = -\frac{1}{\rho}\frac{\partial p}{\partial z} \tag{2.29}$$

Replacing Eq. (2.23) and Eq. (2.24) in Eq. (2.29) yields,

$$i\omega\hat{v}(r) = -\frac{1}{\rho}\frac{\partial\hat{p}}{\partial z} \tag{2.30}$$

which has the solution,

$$v(r,t) = \frac{i}{\rho\omega}\frac{\partial\hat{p}}{\partial z}e^{i\omega t}. \tag{2.31}$$

Now, the focus is shifted to a parameter of greater significance than velocity.

This key parameter is the rate at which blood flows through a specific cross-sectional area within a blood vessel. Calculating this flow rate is a matter of integrating the velocity function, taking into account the differential area, across the entire cross-section which can be expressed as a function of r, that is, $2\pi r dr$. Thus, the flow is calculated as,

$$Q(t) = \int_0^R u(r,t)2\pi r dr \tag{2.32}$$

To calculate the integral in Eq (2.32), we evoke a known property of Bessel functions,

$$\int xJ_0(x)dx = xJ_1(x), \tag{2.33}$$

where J_1 is a Bessel function of first-kind and of first order.

It occurs that, the flow rate produced by harmonic n, of the pressure gradient is

$$Q_n = \left(\pi R^2\right)\mathrm{Re}\left[\frac{a_n}{i\omega n\rho}\left\{\frac{2J_1(\lambda R)}{\lambda R J_0(\lambda R)} - 1\right\}e^{i\omega nt}\right]. \tag{2.34}$$

Where $Q_0 = a_0\dfrac{8\mu}{\pi R^4}$ is the average flow rate produced from the constant term a_0 that was expressed in the Fourier series that described the pressure gradient.

Thus, the total flow rate is given as

$$Q(t) = Q_0 + \sum_{n=1}^{N} Q_n(t). \tag{2.35}$$

However, in 1955, as Womersley introduced his solution [93], it was at a time when creating a computer model for fluid flow wasn't as straightforward.

Access to Bessel functions [1], which are widely available in today's scientific softwares, was limited. Consequently, he performed velocity term integration, obtained the flow solution , and published the equation [93] that represents the flow response to each of the applied pressure harmonics,

$$Q_n = \frac{\pi R^4}{\mu} M_n \left(\frac{M_{10}}{a^2}\right)_n \sin(\omega n t + \phi_n + \epsilon_{10_n}) \tag{2.36}$$

Where $M_n = \sqrt{A_n^2 + B_n^2}$, is the magnitude of the driving pressure (and A_n, B_n are the coefficients in the Fourier series, or else written as $M_n = |a_n|$ where a_n is the same as the one introduced in Eq.(2.2)), ϕ_n =argument$(-a_n)$, which describes the angle of the phase shift.

In Eq. (2.36), the pressure gradient that is linked with each harmonic is written as:

$$\frac{\partial p}{\partial x}\Big|_n = M_n \cos(\omega n t + \phi_n). \tag{2.37}$$

Repeating the same procedure as before, in order to compute the total flow one needs to use Eq.(2.35).

Now, the quantities that have been mentioned in Eq.(2.36) are defined below:

1. The first term(zeroth) harmonic of the flow sum, Q_0, needs the quantity M_0 which is $M_0 = |J_0(\alpha i^{3/2})| \quad , M_1 = |J_1(\alpha i^{3/2})|$ $M_0 = |J_0(\alpha i^{3/2})| \quad , M_1 = |J_1(\alpha i^{3/2})|$
2. $k = \dfrac{\alpha}{2}\dfrac{M_0}{M_1}$,
3. $\theta_0 =$ argument$(J_0(\alpha i^{3/2}))$, and θ_1 =argument$(J_1(\alpha i^{3/2}))$,
   - Here, α is the Womersley number defined in Eq.(2.21). Those quantities are used in the definition of δ_{10}, a quantity that is defined below.
4. $\delta_{10} = \dfrac{3}{4}\pi - \theta_1 + \theta_0$, which is ultimately used in an alternative definition of the quantity $M_{10} = \dfrac{1}{k}\sqrt{(\sin(\delta_{10}))^2 + (k - \cos(\delta_{10}))^2}$,
5. $\epsilon_{10} = \tan^{-1}\left(\dfrac{\sin(\delta_{10})}{k - \cos(\delta_{10})}\right)$.

2.2 Derivation of Greenfield-Fry solution

In 1965, Fry and Greenfield published an analytical solution of the pulsatile blood flow problem under the same conditions that had been imposed by Womersley, McDonald and many more scientists that were working on the field of haemodynamics. This particular solution that they suggested was comparable to the solution that Womersley had priorly suggested, as they both relate flow rate to pressure gradient in pulsatile flow. Fry and Greenfield's solution provides an analogy of an electric circuit to pulsatile flow behavior. Specifically, this kind of model, known as lumped parameter model or 0-D model , which is discussed in depth in the next chapter of the thesis, utilizes the electro-mechanical resemblance in order to mimic the functions of the human cardiovascular system [18], as it relates the pressure gradient to the electric voltage and the flow rate as electric current so that the calculation of flow rate can be achieved through the pressure gradient. Thus, it is an interesting and insightful modeling technique and is widely used in the development of a pressure-measuring catherer for invasive medical techniques [89].

Under the same observations regarding the Navier-Stokes equations, the cylindrical Navier-Stokes equations(or else, evoking Eq. (2.3) and dividing with ν as well) are reduced to

$$\frac{\partial^2 u}{\partial r^2} + \frac{1}{r}\frac{\partial u}{\partial r} - \frac{1}{\nu}\frac{\partial u}{\partial t} = \frac{1}{\mu}\frac{\partial p}{\partial x}. \tag{2.38}$$

Now, the first two terms of the left-hand side of Eq. (2.38) can be rewritten as,

$$\frac{1}{r}\left[\frac{\partial u}{\partial r} + r\frac{\partial^2 u}{\partial r^2}\right] = \frac{1}{r}\frac{\partial\left(r\dfrac{\partial u}{\partial r}\right)}{\partial r}. \tag{2.39}$$

Using the derivative chain rule, Eq. (2.39) is written as,

$$\frac{1}{r}\frac{\partial\left(r\dfrac{\partial u}{\partial r}\right)}{\partial r} = \frac{1}{\nu}\frac{\partial u}{\partial t} + \frac{1}{\mu}\frac{\partial p}{\partial x}. \tag{2.40}$$

Multiplying the right-hand side and the left-hand side of Eq. (2.40) with $2\pi r dr$ and integrating from $r = 0$ to $r = R$ yields,

$$2\pi \int_0^R \frac{\partial \left(r \frac{\partial u}{\partial r} \right)}{\partial r} dr = \frac{1}{\nu} \int_0^R \left(\frac{\partial u}{\partial t} \right) (2\pi r dr) + \frac{1}{\mu} \frac{\partial p}{\partial x} \int_0^R (2\pi r dr) \tag{2.41}$$

which is equal to

$$2\pi r \frac{\partial u}{\partial r}\Big|_0^R = \frac{1}{\nu} \frac{\partial}{\partial t} \int_0^R u \, (2\pi r dr)) + \frac{1}{\mu} \frac{\partial p}{\partial x} 2\pi \frac{r^2}{2}\Big|_0^R \tag{2.42}$$

The integral term of Eq. (2.42) is the definition of the flow rate.

Thus, the above equation is rewritten as

$$\frac{2}{R} \frac{\partial u}{\partial r}\Big|_R = \frac{1}{\nu \pi R^2} \frac{\partial Q}{\partial t} + \frac{1}{\mu} \frac{\partial p}{\partial x} \tag{2.43}$$

after having replaced the flow rate term and divided with πR^2.

In order to eliminate the term in the left hand side of Eq. (2.43), we evoke Newton's viscosity law, applied on the wall of the rigid tube of interest,

$$\tau_w = -\mu \frac{\partial u}{\partial r}\Big|_R. \tag{2.44}$$

Replacing the above expression in Eq. (2.43) yields

$$-\frac{\partial p}{\partial x} = \frac{\rho}{\pi R^2} \frac{\partial Q}{\partial t} + \frac{2\tau_w}{R}. \tag{2.45}$$

In order to eradicate the τ_{wall} term from Eq. (2.45), one can introduce assumptions regarding what kind of flow there is, to achieve the required goal). Such fair assumption would for example be, the Poiseuille flow which instantly provides an expression for the τ_{wall} term,

$$\tau_{wall} = 4 \frac{\mu Q}{\pi R^3}. \tag{2.46}$$

Which, after replacing it in Eq. (2.45) would yield,

$$-\frac{\partial p}{\partial x} = \frac{\rho}{\pi R^2} \frac{\partial Q}{\partial t} + 8 \frac{\mu Q}{\pi R^4}. \tag{2.47}$$

The above expression of the gradient of pressure is a first-order ordinary differential equation (ODE) where the pressure gradient is linked with the flow rate and its time derivative.

Now, in the case of pulsatile flow, Waite and Fine [89] relate wall shear stress τ_{wall} to the flow rate and its derivative as,

$$2\frac{\tau_{wall}}{R} = R_\nu Q + L_I \frac{dQ}{dt}. \tag{2.48}$$

Where R_ν and L_I are two model parameters that depend on the dynamic viscosity of the fluid, the radius of the vessel and the density of the fluid.

A substitution of those quantities into Eq. (2.48) and a further substitution of Eq. (2.48) into Eq. (2.45) yields

$$-\frac{dp}{dx} = \frac{\rho}{\pi R^2}\frac{dQ}{dt} + \left(R_\nu Q + L_I \frac{dQ}{dt}\right) \tag{2.49}$$

Thus, the Greenfield-Fry mathematical model can be written as,

$$-\frac{dp}{dx}\Big|_n = -Re[a_n e^{i\omega nt}] = L_u \frac{dQ}{dt} + R_\nu Q. \tag{2.50}$$

Where $L_u = L_I + \dfrac{\rho}{\pi R^2}$ and the subscript n, represents every harmonic that was used to express the pulsatile pressure gradient, as was mentioned earlier in this chapter. Finally, Eq. (2.50) is written in such way that reminds of an electrical circuit with an in series inductor with a resist and a source of voltage.

Now, the solution for the flow rate is acquired as a superposition of n-harmonic components plus a steady state solution which can be acquired from the Poiseuille flow rate $Q_0 = a_0 \dfrac{8\mu}{\pi R^4}$.

Thus, the total flow is expressed as follows.

$$Q(t) = Q_0(t) + \sum_{i=1}^{N} Q_n(t). \tag{2.51}$$

Where Q_n is provided by a similar way that Womersley and McDonald did and is more analytically described in the works of Waite and Fine [89], Pedley [65] and Lombardi [47].

CHAPTER 3

Mathematical modeling of blood flow in the cardiovascular system

In order to model blood flow in the cardiovascular system, one needs an "A priori" set of questions, targeted on subjects around the revolving process. In blood flow such questions would be: What are the values of flow and pressure in the arterial system and how would those quantities vary inside different types of blood vessels? How does mild and moderate exercise affect them? How would a pathological condition (such as the presence of an aneurism) would affect them? Is it possible to build a patient-specific model to predict a certain happening of events? The above set of questions are of great importance and are sought out immensely amongst the scientists that are involved in the field of haemodynamics.

However, due to the complex nature of blood flow process the model instantly "inherits" a certain level of complexity because if one wants to be as accurate as possible in the construction of their model, a fair amount of information needs to be provided (A priori), such as the geometry of the blood vessels regarding their diameter, branching or no-branching, compliance of the walls of the blood vessel e.t.c.

In reality, mathematical models are a conglomeration of equations that describe the governing dynamics of the process that is being modelled, with spatial and time variables. Thus, the so-called 0D, 1D, 2D and 3D models describe the amount of spatial dimensions that are included in the developed model respectively. In addition to those equations, to obtain a solution of the problem that is being modeled, one needs a set of input data to "feed" into the model and a set of initial and boundary conditions, which depends on the

nature of the problem and the aspect of the problem that is being studied. The choice of the suitable level of dimensionality for a model, ranging from zero-dimensional (0D) to three-dimensional (3D), is contingent on the aims and the desired level of precision of the study.

3.1 Zero-dimensional models

Zero-dimensional models or namely, *lumped parameter* models presume a uniform distribution of pressure and flow within any specific region of the model(can be a whole vessel or part of vessel) at any particular time. Thus, with a set of ordinary differential equations(with time derivative) one could provide satisfactory system-level interactions between the compartments of the model. In blood flow process, this could be the systolic-diastolic pressure ratios or temporal pressure gradients [35]. 0D models adopt an electric circuit analogue as the processes of blood flow and electric conduction in a circuit present multiple similarities. As discussed previously, the pressure gradient of blood in the circulatory system drives the blood to flow against the hydraulic impedance. The exact analogue exists in electric circuits where the voltage gradient drives current to flow against the electric impedance. Specifically, hydraulic impedance embodies the collective impact of the frictional loss, vessel wall elasticity and blood inertia in blood flow dynamics, whereas electric impedance encapsulates the combination of the resistance, capacitance and inductance in the circuit [77].

The **Windkessel model** is a model that describes a vessel network as a single resistance-compliance-inductance (RLC) combination. It was initially introduced by Stephen Hales in 1733 and was later established by the German physiologist Otto Frank at the end of 19th century. A commonly used Windkessel model is the 2-element, comprising two parallel elements: a capacitor C that represents the storage properties of large arteries and a resistor R that represents the dissipative nature of small peripheral vessels including arterioles and capillaries [77]. It was formulated to capture the fundemental characteristics of the systemic artery network, with the venous system being disregarded and depicted as a far, zero pressure field. Thus, veins were excluded from the modelling of the arterial system. The two-element Windkessel model offers a straightforward and practical approach to capture the pressure decay that is exhibited in the aorta over the period of diastole. for this purpose, even a ba-

sic RC circuit can be used to approximate the total arterial compliance when the peripheral resistance and the aortic pressure pulse waveform are provided [46].

In this thesis, we apply the 3-element Windkessel model (RCR model) to obtain terminal boundary conditions (outlet boundary conditions) at the end of large arteries to model the distal vasculature utilizing a capacitor that emulates the vessel compliance and two resistors emulating the proximal and distal pressure drops respectively [51].

In particular, the 3-Element Windkessel model, initially introduced by Landes and later studied Westerholf and his collleagues [92], is an expansion of the 2-Element model. In this model, a resistor is introduced in series to account for the resistance to blood flow caused by the aortic valve. The additional resistance, r that is added reflects the characteristic impedance of the arterial network, defined as the ratio of oscillatory pressure to oscillatory flow rate in the absence of reflective waves. The sum of the overall resistances $r + R$ depicts total systemic vascular resistance in the previous RC model and the capacitance C represents the elasticity effect of the arterial network.

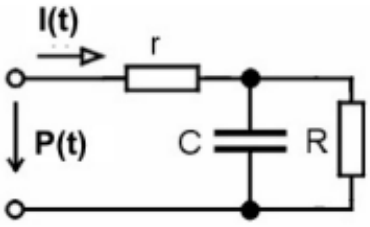

Figure 3.1: The electric analog of a 3-element Windkessel model. $I(t)$ represents the the blood flow from the heart in a correlation to current that flows in an electric circuit and $P(t)$ represents the blood pressure in the aorta in a correlation to a time-varying electric potential.

A different approach to the placement of the resistances in the electric circuit was introduced from Burattini and Natalucci where they placed the second resistance in series with the capacitor C in an attempt to describe the visco-elastic property of the vessel wall [12].

Nevertheless, both configurations of the RCR 3-element Windkessel models

have been found to be equivalent to some degree and present some advantages and disadvantages towards each other. For example, the Westerholf-induced RCR Windkessel model can be used to broadly capture the wave reflection response but cannot be used to capture the wave propagation, notably underestimates peak aortic flow and the mean arterial pressure and it does not generate *realistic* aortic pressure and flow waveforms when compared to a more sophisticated arterial impedance model. Instead, it produces simplified waveforms. [77].

From the mathematical modelling, it occurs that the 2-element Windkessel model is described as,

$$I(t) = \frac{P(t)}{R} + C\frac{dP(t)}{dt} \tag{3.1}$$

and also the 3-element Windkessel model of Fig. (3.1) can be described as,

$$\left(1 + \frac{r}{R}\right) i(t) + CR\frac{di(t)}{dt} = \frac{P(t)}{R} + C\frac{dP(t)}{dt}. \tag{3.2}$$

Now, both models can be explicitly used to simulate the blood flow and blood pressure in the aorta during the systole and the diastole. An interesting work from Marianne Catanho et al.[14] presented a simulation of blood flow and blood pressure in the aorta using only Windkessel models and a comparison between the analytical solution of the 2-element Windkessel model and the numerical solutions of 2-element and 3-element Windkessel models.

Specifically, they modelled blood flow as a sine wave which reaches an amplitude I_0 during the systolic phase and receives the value 0 during the diastolic phase, where the blood flow in the aorta is non-existing. Thus, in ventricular contraction blood flow is written as

$$I(t) = I_0 \sin\left(\pi \frac{mod(t, T_c)}{T_s}\right), \tag{3.3}$$

where T_c represents the period of a cardiac cycle, T_s is the systolic period and it holds that $T_s = \frac{2}{5}T_c$. From the literature provided in [35], they evoked the fact that the blood flow during a single cardiac cycle is 90ml and calculated the amplitude $I_0 = 424.1ml$.

It occured that Eq. (3.1) can be solved in two phases, in the systolic and in the diastolic, which would be homogeneous, as it was mentioned earlier that blood flow $I(t)$ would be equal to zero. In the former phase, the use of

integrating factor $u(t) = e^{\frac{t}{RC}}$ and integration of both sides yields the solution

$$y(t) = c_1 e^{\frac{-t}{RC}} + \frac{-e^{\frac{t}{RC}} T_s I_0 R(C\pi R \cos(\frac{\pi t}{T_s}) - T_s \sin(\frac{\pi t}{T_s}))}{T_s^2 + C^2 R^2 \pi^2} \tag{3.4}$$

and in the latter phase, the homogeneous equation yields the solution

$$P(t) = c_2 e^{\frac{-t}{RC}}, \tag{3.5}$$

where the constants c_1, c_2 are calculated via initial conditions for P(t) in the beginning of the systolic cycle and the diastolic cycle respectively. It is worth mentioning that the processes of systole and diastole preceed each other and as a result, they used an initial input of diastolic pressure at 80mmHg, which is in agreement with the literature results for a healthy person [35].

Plotting the above analytical solutions in MATLAB and using the integrated MATLAB solver ode23 for the numerical solutions yielded them useful yet, expected results, as it can be seen in the Fig. (3.2) below,

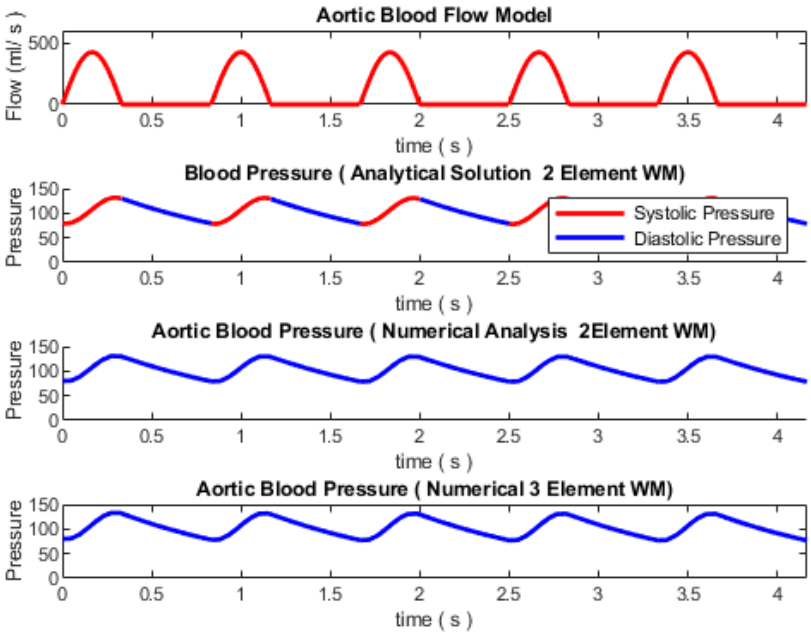

Figure 3.2: Analytical solution of 2-element WK and Numerical solutions of 2-element and 3-element WK models [14].

Thus, their work that is thoroughly provided in [14] showcases the power of modelling that Windkessel models provide in the simulation of both blood flow and blood pressure in the aorta of a healthy individual. It is clear that even in the simplest model, the 2-Element WK model, with only one resistance, the systolic and diastolic blood pressure in five cardiac cycles matched the bibliographic data that is available in the haemodynamic literature with 120/80 mmHg and so did the numerical approximations in both 2-element and 3-element Windkessel models.

Remark: It is crucial to keep in mind that the above modelling is too ideal. Blood flow was modelled as a sine wave where as was shown in Chapter 2 of this thesis, blood flow and pressure waveforms are more accurately described as a Fourier series.

3.2 One-dimensional models

As it was mentioned earlier, zero-dimensional models can provide reasonably accurate estimates for flow, systolic pressure, and diastolic pressure at specific locations within the cardiovascular system, under specific conditions. However, these models do not portray the cardiovascular system as a continuous system but rather as a conglomeration of distinct points. Consequently, they lack the capability to simultaneously provide accurate flow and pressure waveforms across the cardiovascular system and most importantly, cannot include wave propagation effects in the specific blood vessel that they model [61].

One dimensional models are used to study the alteration of flow and pressure waveforms[1] during their propagation in the systemic arteries. This alteration is due to wave reflections that occur in the tapering of blood vessels, from the arterial bed that imposes flow resistance and from bifurcating geometries. Thus, 1D models are used to delineate and define the connection between forward and backward travelling waves in the circulatory system. The 1D equations that are used in 1D models are derived from the incompressible Navier-Stokes equations in polar/cylindrical coordinates, under certain assumptions (such of axisymmetry), the continuity equation and from an equilibrium equation for the elastic/visco-elastic vessel wall. This means that 1D models are

[1]Those two quantities "carry" valuable information regarding the elastic properties of blood vessels, the patho-physiological condition of vital organs, the function of the heart and thus are of significant interest.

composed of fluid-structure interaction equations and from recent studies [13, 62] it occurs that the fundemental variables that are adopted in the 1D models are the cross-sectional area A, pressure p and flow q.

3.2.1 Coupling of 1D and 0D models

Due to the complex structure of the arterial tree, attempting to model the whole cardiovascular system with an implementation of a solely 0D model or 1D model would be impossible and would lead to inaccurate results, from a physiological point of view. Therefore, the introduction of both 0D and 1D models is necessary when it comes to blood flow modelling. Thus, a truncation of the arterial tree is suggested and particularly in two parts: Large arteries, where blood flow is dominated by inertia forces and the tapering of blood vessels is of significant importance, are modelled via a 1D model and small arteries, where the inertia forces are insignificant and viscosity is the dominant force, are modelled[2] via 0D models. In the full-scaled arterial system that is structured, 1D model is coupled at the termination points (as a scope of outflow conditions) of large arteries with the 0D model and thus, this merged system of models provides us a consistent representation of the pulse wave anywhere in the systemic arteries.

Numerous works in the field of haemodynamics [3, 5, 27, 80] have shown that 1D models are just as capable (and in certain cases, more capable) as 3D models when it comes to providing a global assesment of blood flow in the cardiovascular system [3] and to changes in flow and pressure waveforms in large arteries. Thus, besides their initial role to model the arterial system, 1D models can also be successfully used to provide boundary conditions for 3D simulations, which is the ultimate goal of this thesis. In addition, due to the rapid progress that is exhibited in the imaging technology field, with the aid of MRIs, CTs and ultrasounds (and the development of softwares that utilize them to reconstruct 3D geometries), we are able to receive patient-specific information regarding several parameters of interest, such as vessel geometry or even information regarding velocity profiles in specific segments of the blood vessel.

[2]Studies like Olufsen's et.al [61] suggest that modelling of small arteries should be done from a linearized Navier-Stokes equation (due to neglect of nonlinear terms) which leads to a wave equation that can be solved analytically. However, in the thesis we will use the 3-element Windkessel model and we will select specific values for the resistances of the WK model (in a patient-specific fashion) , so that no-artificial reflections or excessive damping of the system occur.

3.3 Formulation of equations of the 1D model

Applying the fundamental laws of conservation of mass and conservation of momentum and a state/equilibrium equation for the fluid-structure (vessel wall) interaction to a 1D impermeable and deformable tubular control volume of an incompressible Newtonian fluid yield,

$$\frac{\partial A}{\partial t} + \frac{\partial q}{\partial x} + \psi = 0, \tag{3.6}$$

$$\frac{\partial q}{\partial t} + \frac{1}{A}\frac{\partial}{\partial x}\left(\frac{q^2}{2}\right) + \frac{A}{\rho}\frac{\partial p}{\partial x} = -\frac{8\pi\mu}{\rho}\frac{q}{A}, \tag{3.7}$$

$$p(x,t) - p_0 = E_\theta \left(\frac{A(x,t)}{A_0(x,t)} - 1\right) \tag{3.8}$$

Where $\mathbf{x}$ is the axial coordinate along the blood vessel, $\mathbf{t}$ is the time, $\mathbf{q}(x,t)$ is is the axial blood flow velocity averaged over the cross-section, $\mathbf{A}(x,t) = \pi R^2$ is the cross sectional area of the lumen and specifically $A(0,t)$ is the inlet area and $A(L,t)$ is the outlet area, $\mathbf{R}$ =$\mathbf{R}(x,t)$ is the radius of the vessel, $\mathbf{p}(x,t)$ is the the blood pressure averaged over the cross-section, $\boldsymbol{\rho}$ is the blood density, which is a constant and equal to 1.06 g/cm^3, $\boldsymbol{\mu}$ is the dynamic viscosity of blood which is a constant and equal to 0.04 dynes/cm^2 s, $\mathbf{E}_\theta$ is Young's modulus in the circumferential direction. A few remarks regarding the above equations,

- Eq. (3.6) is derived from the conservation of mass (volume). This corroborates the physiological fact that the volume of blood entering a vessel during a short period of time, dt, exits either at the end of the vessel or through the vessel wall [61]. Due to the fact that blood is studied at a macroscopic level and thus is a continuous deformable medium, the control volume is fixed in space. This volume category is called Eulerian and is described by the fluid's ability to pass through the volume's boundary. Lastly, ψ term is a sink/source term that is used to describe the flow through the vessel's wall.

- Eq. (3.7) is derived from the conservation of momentum. Navier-Stokes equations are reduced to Eq. (3.7), written in the longitudinal direction (the x-direction). Now, certain assumptions have been imposed:

  1. Axisymmetry of the flow
  2. The velocity profile[3] is assumed to be constant in shape (parabolic) and axisymmetric. Specifically, it is derived from Poiseulle's Law. (Hence the term $-8\pi\mu q$ in the right-hand side of Eq. (3.7)).

  Thus, to receive accurate values of blood flow and pressure along the blood vessel, momentum has to be conserved in the longitudinal direction ($x-$direction). Lastly, the left-hand side of Eq. (3.7) depicts the phenomenon of transport of mass in two mediums, along the vessel and through the wall of the vessel and a pressure term which depicts the pressure that is applied on the vessell wall. The right-hand side of Eq. (3.7) depicts a friction term between the fluid and the wall of the vessel, which generates the no-slip condition.

- Eq. (3.8) is a state equation. In most numerical simulations, the arterial wall is modeled as a thin, circular, incompressible, homogeneous, isotropic, linear elastic membrane. Usually, the viscoelastic nature of the wall is dismissed. The wall is characterized by an elastic modulus E_θ in the circumferential diretion, a Poisson's ratio $\nu = 0.5$ and a thickness h [94]. Under the assumption that the deformation of the arterial wall happens axisymmetrically, the loading happens axisymmetrically, the vessels are modelled as a binded structure in the $x-$direction, a relationship between pressure in the vessel and the cross-sectional area occurs. Evoking the fact that the external forces are applied on the vessel (which are reduced to stresses) in the circumferential direction, as shown in [9] yields,

$$T_\theta = \frac{E_\theta}{1-\nu^2}\frac{r - r_d}{r_d}, \tag{3.9}$$

  where r_d is the radius of the vessel at diastolic pressure.

  Evoking Laplace's Law, the circumferential stress T_θ can be written as,

$$T_\theta = \frac{(P - P_d)r}{h} \tag{3.10}$$

[3] As mentioned in [64], the velocity profiles vary throughout the arterial system. In the aorta it is almost flat and becomes quasi-parabolic in smaller arteries.

and evoking the assumption introduced in [5], that is, $\frac{1}{r_d}$ is a legitimate approximation for the quantity $\frac{1}{r}$, Eq. (3.10) can be rewritten as,

$$p(x,t) - p_0 = \frac{4}{3} Eh \frac{r - r_d}{r_d} = \frac{\beta}{A_d} \left(\sqrt{A} - \sqrt{A_d} \right), \tag{3.11}$$

where $\beta = \frac{4}{3}\sqrt{\pi} Eh$, where A_d is the luminal area at diastolic pressure [94].

Thus, Eq. (3.8) can also be written as,

$$p(x,t) - p_0 = \frac{4}{3} \frac{1}{r_0(x)} Eh \left(1 - \sqrt{\frac{A_0(x)}{A(x,t)}} \right), \tag{3.12}$$

where $A_0(x) = \pi r_0(x)^2$ is the cross-sectional area when $p = p_0$ (namely, *zero transmural* pressure), $r_0(x)$ is the radius when $p = p_0$.

3.3.1 Inflow, Bifurcating and Outflow Conditions

The system of Equations (3.6),(3.7) and (3.8) can be used to compute the blood flow and pressure in a specific vessel. In an attempt to extend this model to a full-scaled arterial tree, one needs to define appropriate initial and boundary conditions in order to tether the blood vessels and receive a full representation of the large arteries in the cardiovascular system. Now, we can characterize the above system. It is a nonlinear, coupled system of partial differential equations and in order to solve this system, one needs to define those boundary conditions. It can be observed, using the method of characheristic curves, that the above system is hyperbolic.

Thus:

- The first boundary condition is at the inlet of "first" (large) artery, which is the ascending aorta and more specifically, at the aortic valve. The inflow (initial) conditions require a specification of the flow and the pressure. As it is shown in [59], the flow wave can be depicted as a periodic extension of a flow waveform such that $q(0,0) = q(0,T)$ where T is the length of the cardiac cycle. As mentioned in Chapter 2 of the thesis, in an analogous way, pressure waveform can be written as a Fourier series with a specific number of harmonics.

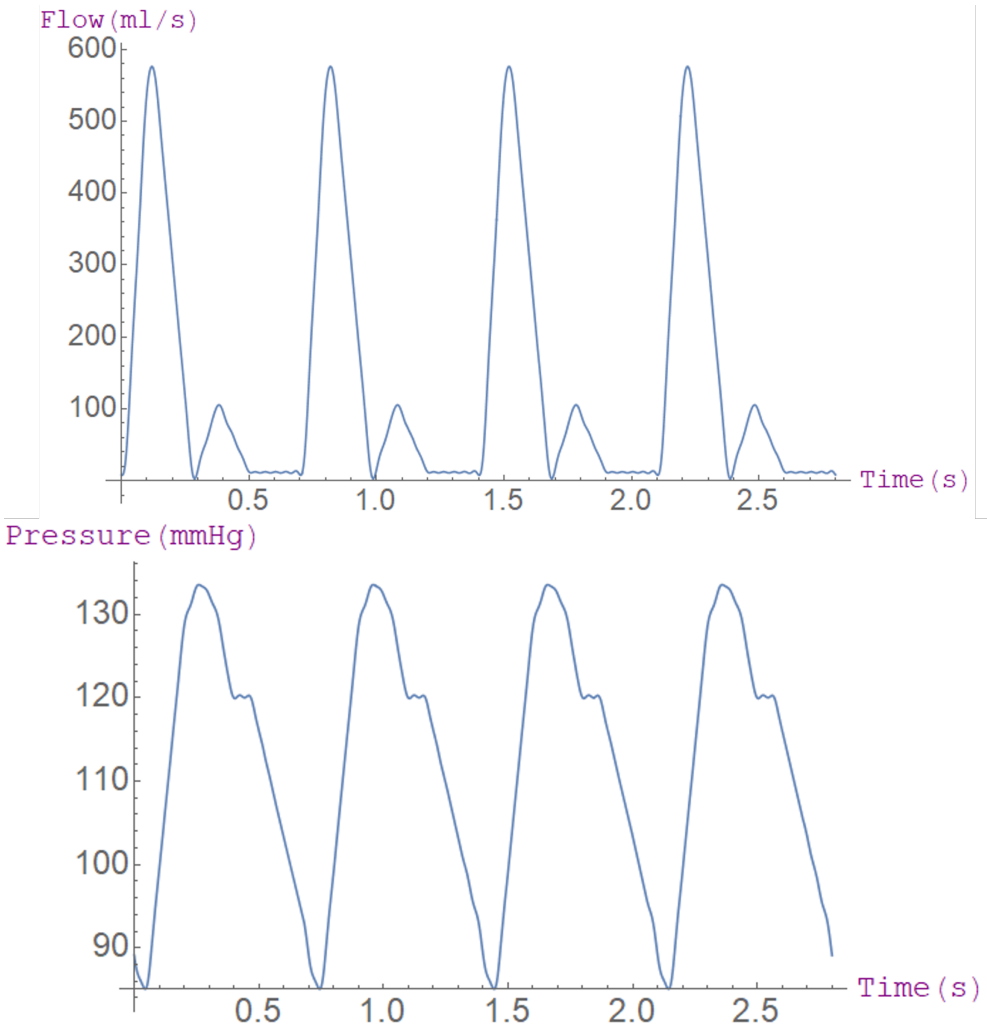

Figure 3.3: Flow and Pressure waveforms of a period $T = 0.7s$, used at the aortic inlet while simulating an environment of mild exercise. Generated in Mathematica with 16 terms in the Fourier series, originally as normalized. (Furtherly discussed in the next chapter)

- Then, right before and after the aortic arch, the aorta has multiple bifurcating points and a "parent-daughter" relationship occurs for each bifurcating occasion. For that kind of structure, Olufsen et. al [61] suggested that three equations are needed: One outflow condition from the parent artery and two inflow conditions to both daughter arteries in

which two of them describe the quantitative changes in flow and the last one describes the pressure relationship between them. In detail, these equations are the following,

$$\mathrm{q}_{parent} = \mathrm{q}_{daughter_1} + \mathrm{q}_{daughter_2}, \tag{3.13}$$

$$\mathrm{p}_{parent} = \mathrm{p}_{daughter_1} = \mathrm{p}_{daughter_2}, \tag{3.14}$$

$$\frac{q_{daughter_1}}{q_{daughter_2}} = \lambda \tag{3.15}$$

Where λ is a quantitative parameter that describes the flow distribution from the parent artery to the daughter arteries.

- Lastly, regarding the outflow boundary condition: Throughout the years of simulations of blood flow in the arterial tree and in arterial segments, multiple kinds of boundary condition specifications have been implemented, such as pure resistance models which are described from a linear algebraic relation between the flow and pressure, characteristic impendance modulis that are mostly derived from experimental data (Relation between flow and pressure that has been calculated with invasive methods, usually a monitoring catheter) and more. Thus, the choice of the most suitable model for outlet/outflow boundary conditions is a matter of concession between accuracy, complexity, computational time and also the extension of the specific study. In this thesis, the outflow boundary conditions that are adopted are the lumped boundary conditions provided from the 3-element Windkessel model (which was introduced earlier in this chapter) that is coupled with the 1D model, at the termination points.

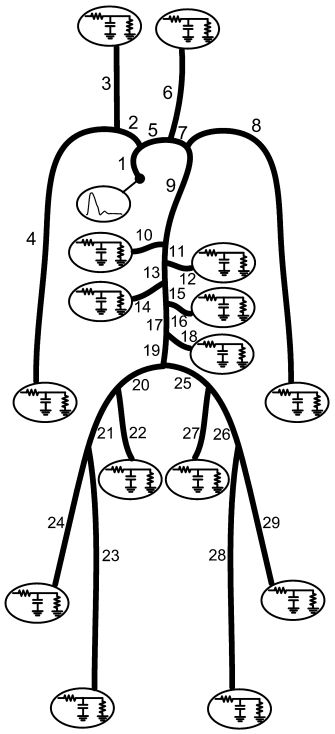

Figure 3.4: The arterial network of basic arteries and the schematic of the lumped parameter (Windkessel) model that is used in the terminating points of arteries [38]. At point 1 in Figure (3.4), a flow waveform is used as inlet.

The Windkessel model imposes a differential relation between flow rate and pressure [26] and is represented by the following equation:

$$\frac{dp}{dt} = R_p \frac{dq}{dt} - \frac{p}{R_d \cdot C} + \frac{q(Rp + R_d)}{R_d \cdot C} \tag{3.16}$$

Where p is the instantaneous pressure at the inlet of the Windkessel model, q is the instantenous flow rate, R_p is th proximal resistance, R_d is the distal resistance and C is the compliance.

Thus, at the terminating point of the large artery where the outflow pressure and flow have been calculated, those quantities are later used as instantenous parameters for calculation of pressure and flow in the Windkessel. In more detail, the specification of those parameters can be acquired from four equations:

$$p(t) - p_1(t) = R_p \cdot q_1(t), \tag{3.17}$$

$$p_1(t) - p_2(t) = R_d \cdot q_2(t), \tag{3.18}$$

$$q_3(t) = C\frac{dp_1}{dt}, \tag{3.19}$$

$$q_3(t) = q_1(t) - q_2(t) \tag{3.20}$$

Here, $p(t)$ and $q_1(t)$ are known and the Windkessel parameters R_p, C, R_d can be acquired from various bibliographic sources [64, 80].

The combination of the above equations yields

$$p_2(t) = R_d \cdot C\frac{dp(t)}{dt} - R_p \cdot R_d \cdot C\frac{dq_1}{dt} + p(t) - (R_p + R_d)q_1(t) \tag{3.21}$$

Thus, an expression for the outflow pressure has been granted and will be later used aswell as a boundary condition in the 3D-simulation of blood flow in specific arterial segments of our interest.

Remark: It should be emphasized that those parameters are patient-specific and can vary from person to person. In addition, those parameters could be modified when one simulates different haemodynamic conditions such as simulating mild and moderate exercise, two environments that will be simulated later in this thesis.

3.4 Spatial Discretization of the system using FVM

Due to the complex nature of the non-linear system of Equations (3.6 - 3.8) and the lack of analytical solutions for the full-scale problem, numerical methods have emerged and have been continuously developing in order to solve the arising problem. As a consequence of the technological advancements, descretization methods have been employed in order to obtain accurate numerical solutions. In the thesis, the spatial descretization method that has been used in the 1D problem is the Finite Volume Method (FVM).

Finite Volume Method is a popular discretization method that was initially introduced from S. Patankar, B. Spalding, R.J. Leverque and more, with the

scope of transmuting partial differential equations (elliptic, parabolic or hyperbolic type) to algebraic ones. It is widely used in the field of Computational Fluid Dynamics in order to discretize the equations of interest (Equation of continuity, Equation(s) of momentum, Equation of energy and in the Fluid-Structure case, the state Equation). This method uses a volume integral formulation via a finite partitioning set of volumes (namely, volumes of reference) and evaluates the variables of interest at discrete locations over each control volume and thus satisfies the law of conservation in both global and local fashion. The process of discretization into control volumes can be carried out through the utilization of 2 approaches usually (regarding the grid, nodes and cell arrangements), the vortex-centered method and cell-centered method. In this thesis, the latter[4] is adopted in our computational model. In this method, the strategy of the grid construction aims to conincide the mesh itself with the control volume and the computational points (namely, the nodes) are positioned in the center of the corresponding control volume and the variables assigned to the nodes are average values over the cells [50].

Then, the equations are integrated over the cell volume ΔV and over a time period T, due to the spatial and the time dependence of the variables. Thus, Equations (3.6 - 3.8) are written as:

$$\int_T \int_{\Delta V} \frac{\partial A}{\partial t} dV dt + \int_T \int_{\Delta V} \frac{\partial q}{\partial x} dV dt = 0$$

$$\int_T \int_{\Delta V} \frac{\partial q}{\partial t} dV dt + \int_T \int_{\Delta V} \frac{1}{A} \frac{\partial}{\partial x} \left(\frac{q^2}{2} \right) dV dt +$$
$$+ \frac{1}{\rho} \int_T \int_{\Delta V} A \frac{\partial p}{\partial x} dV dt + 8 \frac{\pi \mu}{\rho} \int_T \int_{\Delta V} \frac{q}{A} dV dt = 0$$

$$\int_T \int_{\Delta V} p dV dt - \int_T \int_{\Delta V} E_\theta \left(\frac{A}{A_0} - 1 \right) dV dt = 0$$

The integration above yields a non-linear system of algebraic equations where each system of equations contains the total number of unknowns and is equivalent to the number of cells.

[4]Due to the nature of the problem that is modelled, it is important to clarify that **1)** The pressure throughout the control volumes remains stable and **2)** Two cases can be distinguished: In the case where 2 arterial segments are tethered (absence of bifurcating arterial segments), the flow at the outlet is used as inlet flow. In the case of bifurcation, the equations (3.13 - 3.15) are evoked in order to calculate the flow and pressure at each daughter arterial segment.

Regarding the discretization of equations of the 0D Windkessel model that is used at the terminating points of arteries: Due to the solely time-dependance that exists in the equations, the discretization is only in time and thus, Equations (3.17- 3.20) are integrated over a period T.

3.4.1 Solver of the non-linear algebraic systems

In order to solve the non-linear algebraic system that occurs from the discretization of the equations above, we employed Newton's Method which is the default algorithm that MATLAB uses. Newton's method is an iterative algorithm that is used in order to approximate numerical solutions/roots of an equation or a system of equations that cannot be solved analytically.

Let $C^k(D)$ be a set of $k-$ continuously differentiable functions so that $D \to \mathbb{R}^n$, $D \subseteq \mathbb{R}^n$ and suppose that function $\mathbf{F}$ is a vector function which is continuously differentiable in D. Also, let $J_{\mathbf{F}}(x)$ be the Jacobian matrix of $\mathbf{F}$ which is evaluated at $\mathbf{x} = [x_1, x_2..., x_n]^T$, where $\mathbf{x}$ is a vector of $\mathbb{R}^n$. The the Jacobian is defined as:

$$(J_{\mathbf{F}}(\mathbf{x}))_{ij} = \left(\frac{\partial F_i}{\partial x_j}\right)(\mathbf{x}), \quad (i,j) = 1, ..., n. \tag{3.22}$$

Where n is the number of equations [68]. Then, for a given initial value of the vector $\mathbf{x}$, namely $\mathbf{x}_0$, Newton's Method (in a multivariable environment) is expressed as:

$$\mathbf{x}_{n+1} = \mathbf{x}_n - J_{\mathbf{F}}(\mathbf{x}_n)^{-1} F(\mathbf{x}_n) \tag{3.23}$$

Where $J_{\mathbf{F}}(\mathbf{x}_n)^{-1}$ is the inverse Jacobian matrix. A more detailed explanation of the steps of Newton's Method are summarized in the Figure below.

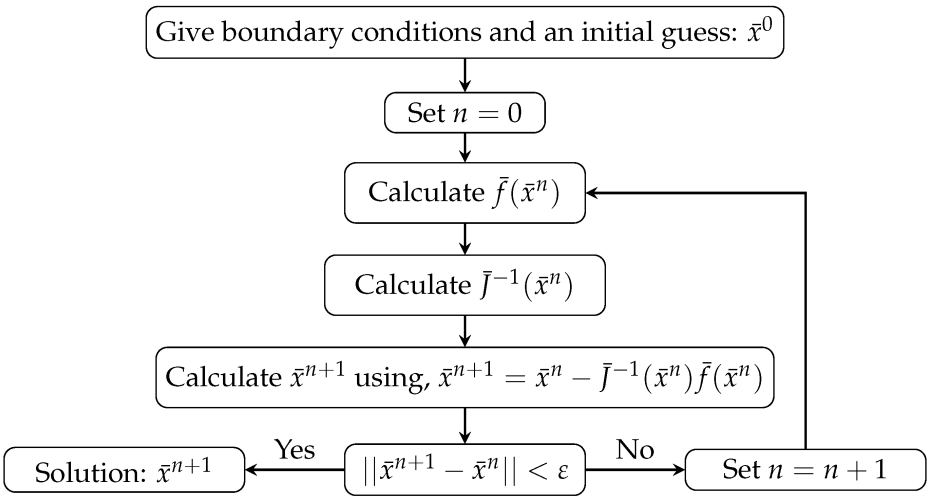

Figure 3.5: Newton's method step by step[17].

Remark. The norm used in the last step of the Figure (3.6) is defined as:

$$||\mathbf{x}^n - \mathbf{x}^{n-1}|| = \sqrt{\left(x_1^{(n)} - x_1^{(n-1)}\right)^2 + \ldots + \left(x_n^{(n)} - x_n^{(n+1)}\right)^2} \tag{3.24}$$

The numerical scheme converges if the norm defined above reaches a certain threshold close to zero, known as tolerance parameter ϵ. This tolerance threshold is provided a priori in the solver and if it is not reached, another iteration occurs. Thus, the correct selection of the threshold parameter is a task of paramount importance, yet, it is not straightforward.

3.4.2 CFL Condition

The Courant-Friedrichs-Lewy (CFL) condition is a criterion that is widely used in Computational Fluid Dynamics which indicates the stability[5] and the convergence towards successfully solving the hyperbolic system of PDEs, if it is satisfied. It involves the temporal discretization (time step), the spatial discretization (spacing of the grid of the geometry of interest) and the inlet velocity and is defined as:

[5]CFL condition is a necessity for stability but is not a solely criterion.

$$C = v\frac{\Delta t}{\Delta x} \tag{3.25}$$

C is a non-dimensional quantity and is called Courant number which is upper bounded, depending on the imposed numerical scheme [8]. In a computational fluid dynamics simulation, the Courant number signifies the rate at which information propagates through a single computational grid cell over a specific time interval. The purpose of tracking and calculating this quantity is of paramount importance as Courant number quantifies and links the amplifications between the time step and the discretized spatial grid and sets up a tolerance threshold between those two simulation parameters. Usually, the upper bound for Courant number, namely C_{max}, is around one but ultimately depends on the type of time integration scheme [19]. For the explicit schemes, C_{max}'s bound is used for stability purposes.

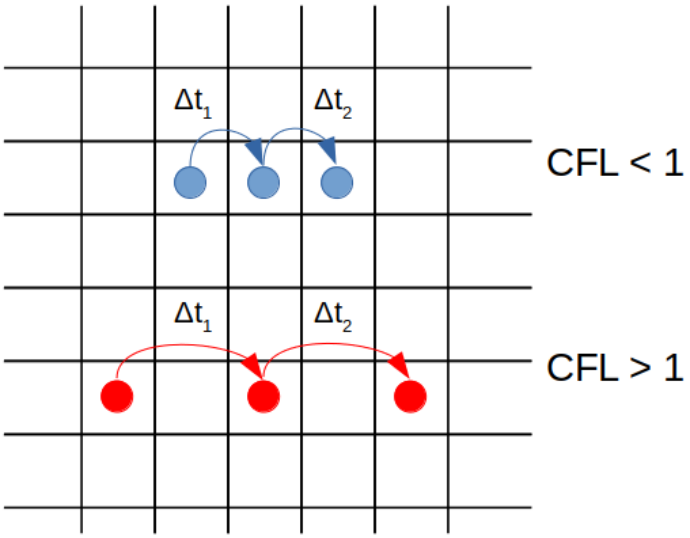

Figure 3.6: The result of surpassing the CFL upper bound [70].

However, for semi-implicit or implicit schemes such as Crank-Nicolson and θ-method, the upper bound of Courant number can be greated than one and does not provide a stability purpose rather than accuracy in the simulation.

The information above holds for the one-dimensional case. For the three-dimensional case, a modifed [70] definition of the Courant number is:

$$C = \frac{1}{2}\frac{\Delta t}{\Delta x}\sum |\vec{U_f} \cdot \vec{\mathbf{n}}| \tag{3.26}$$

Where $\vec{\mathbf{n}}$ is the unit vector pointing towards the centroid of the cell (e.g. tetrahedrons), $\vec{U_f}$ is the velocity inserting from a specific face of the cell.

In the thesis, two time discretization schemes have been imposed and are introduced in the next subsection of this chapter.

3.5 Time Discretization using Explicit Euler and θ-scheme

The hyperbolic system of PDEs (3.6)-(3.9) was spatially discretized earlier by the Finite Volume Method. Then, the system is seperately discretized in time using two schemes:

1. Explicit Euler, which is an explicit method of first-order convergence that has low computation cost.

2. A variation of a Crank-Nicholson scheme, namely θ-scheme, which is of second-order convergence.

At the initial step in the computational code, a steady-state solution is acquired. Then, for the rest of the steps a uniform[6] time mesh is created. The first-order explicit time integration scheme is employed for the discretization of the time derivative terms as first-order forward difference approximations (in the continuity and momentum equations respectively) as:

$$\frac{x(n) - x_0(n)}{\Delta t}, \quad n = 1, \ldots, N \tag{3.27}$$

Where $N, \Delta t$ are the total spatial steps and the temporal step, which are set a-priori of the simulation. The selection of Δt is ultimately dictated by the CFL criterion, as mentioned in the subsection above and x are the equivalent flows for a specific arterial segment depending on n. For our computational model, the values $x(i)$ and $x_0(i), i = 1, \ldots, N$ would be the corresponding inlet

[6]The uniform partition is granted from the usage of the linspace command that MATLAB provides.

cross-sectional area, pressure and flow[7] and the respective outlet quantities in the Ascending Aorta (AAo).

Due to increased flow rates and consequently fluid velocities, that occured amidst the efforts of simulating an exercise environment, the solver wasn't able to converge to a correct solution and the CFL condition was not satisfied and thus, the simulation results of the exercising environments were inaccurate. In order to overcome this barrier and reduce the timestep, we additionally introduced a second-order time discretization scheme.

The θ-scheme inserted[8] in the incompressible Navier-Stokes equations is written as:

$$\frac{1}{\Delta t}(\mathbf{u}^{n+1} - \mathbf{u}^n) + \theta\left(-\nu\Delta\mathbf{u}^{n+1} + \mathbf{u}^{n+1}\cdot\nabla\mathbf{u}^{n+1}\right) + \nabla p = \mathbf{h}^{n+1}, \tag{3.28}$$

Where $\mathbf{h}^{n+1} := \theta\mathbf{f}^{(n+1)} + (1-\theta)\,\mathbf{f}^n - (1-\theta)\left(-\nu\Delta\mathbf{u}^n + \mathbf{u}^n\cdot\nabla\mathbf{u}^n\right).$

Remark: The correct selection of θ is not a straightforward procedure and must be done bearing in mind what time-stepping scheme is needed. In the case where $\theta = 0$, θ- scheme transforms to Explicit Euler, $\theta = \frac{1}{2}$ to Crank-Nicolson and $\theta = 1$ to Implicit Euler.

[7] Those inflow rates are the given vectors that were provided as correct and accurate approximations for Newton's method.

[8] The time discretization schemes are used in the third Windkessel equation which includes a time derivative.

CHAPTER 4

1D Results in the Abdominal Aortic model

The scope of this thesis is to create different computational models with the intention of simulating two states, a mild exercising, a moderate exercising state and comparing them with a resting state. The one-dimensional models that were introduced piece-by-piece in the previous subsections were developed in MATLAB (Mathworks INC.) code to reenact those two states, where physiological parameters such as the radiuses of the arterial segments, their elastances and their Windkessel parameters were modified in furtherance of simulating each state, following the available literature and specific guidelines/clinical protocols regarding the qualitative changes in blood flow and blood pressure measurements and their respective waveforms, that have been published in the last fourty years. In order to interpret the results that occured from the one-dimensional models and their respective simulations and in hopes of a deeper understanding, we need to introduce a few of the effects that exercising has uppon the cardiovascular system and in specific parts of it, such as the supraceliac and the infrarenal aortic segments.

4.1 Direct effects of exercise in the cardiovascular system

The positive effect of exercising in human health is a fact known to be existant for many decades. However, the reasons behind this fact and the bio-mechanisms that contribute to a healthier cardiovascular system are still unclear, yet to be determined and are continuously researched up to this day. A few possible explanations could be the constant hemodynamic stimuli de-

rived from wall shear stresses and transmural pressure[1] [30] that promotes functional and structural remodelling in the arterial walls and the increased cardiac output that results in an expansion of the size of the heart chambers and thus heart's enhanced ability to contract [32]. In addition, blood pressure plays an essential role in the assessment of arterial health as the mean arterial pressure (MAP) and the systolic blood pressure (SBP) increase during exercising while the diastolic blood pressure (DBP) value slightly perturbates and thus the arterial walls need to adapt accordingly to the increased load caused from physical activity. While the pressure wave propagates, the measured pulse pressure (PP) alters, depending on which site of the arterial tree the measurement is taken, namely, the distance from the heart.

According to the available literature derived from cross sectional studies, there is a strong correlation between blood pressure increments and aortic enlargement (increase in the cross-sectional area of the vessel) as a vascular response to exercising [52]. In more detail, the ascending aorta, the abdominal aorta and the common iliacs are the primary arterial segments that become enlarged as an adaptation to physical activity [52] during lower-limb exercising which will be our simulating activity.

The main focus of the one-dimensional model is set on the abdominal aorta and its main outlets: The celiac artery, the superior mesenteric, the renals, the abdominal aortic segments and lastly the common iliac arteries. In addition to vascular changes, due to increased blood flow during different levels of exercise, Young's Modulus is altered as well as specific compliance and proximal/distal resistance parameters (C, R_p, R_d respectively) in the Windkessel models in order to match the literature values of flow and pressure in the respective exercise intensities.

Nevertheless, the study of the direct effect of physical exercise has dual nature. Besides the health benefits, arterial hemodynamics consist a strong overall health indicator and a predictor of cardiovascular events such as the formation of atheromatic plaque or a probable creation/presence of an aneurysm in a specific part of an arterial segment. The waveform characteristics acquired from our one-dimensional hemodynamic model and the physiological properties of the model itself not only withhold information of paramount importance such as the alteration between SBP and DBP, peak systolic flow patterns in different exercise intensities but can be also utilized by clinical physicians as a cardiovascular risk assessment tool in order to evaluate patient-specific situations of whether a person is eligible to do recreational (or even competetive)

[1] Via the Law of Laplace which was mentioned earlier in Chapter 1

sports by submitting them to special MRI tomography scanners equipped with ergometer bikes (hence our interest is lower-body exercising) and echocardiographic criteria and thus, categorize them to low-risk and high-risk groups.

Lastly, regarding the specification of the exercise intensity, the two environments are distinguished into two different, elevated heart rate levels: The baseline resting state is 60 beats per minute (BPM), the mild intensity is 85 BPM and the moderate is 100 BPM. The specifications of those heart rates that we are using are derived from sources such as the guidelines of European Health Instutes and a deviation between the simulating exercise state and the exact heart rate is expected as various categorization protocols have been used throughout the years.

4.2 Results: Flow and Pressure waveforms in the 1D model

In this subsection, the main results of the simulations of the one-dimensional models are presented, discussed and compared with the available literature data. Figure (4.1) below depicts the workflow that was followed to achieve both qualitative and quantitative changes in flow, pressure and their respective waveforms.

A thorough analysis of the above diagram, regarding the step-by-step procedure of setting up the simulation:

- Due to lack of raw waveforms during physical activity in literature data, we were not able to use actual human waveforms in a real exercising environment. However, the waveform of resting state was extracted from PC-MRI medical images and with the aid of the available literature data [90] regarding the qualitative differences between waveform characteristics of those individual states, such as: the amplitude point of the waveforms during peak systole, a quantified temporal reduction of diastolic phase, the temporal shift of the dicrotic notch point, a reduction in the width of the waveform during the systolic phase and more, we were able to use the rest waveform as a "reference" waveform and extrapolate-generate normalized waveforms with the sought-after characteristics for each exercising case.

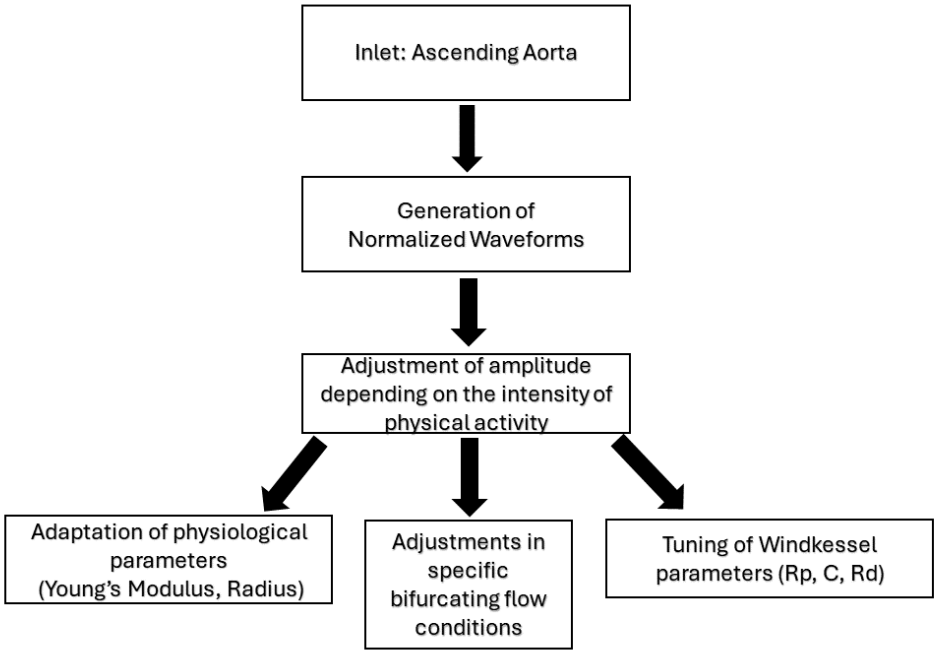

Figure 4.1: Workflow diagram of the one-dimensional simulation setup.

- Young's modulus modifications and the percentile increments of radiuses of specific arterial segments were obtained from previous studies [21, 53, 63, 78] as was mentioned earlier.

- During physical activity, the total abdominal aortic flow increases. However, the supply of blood in specific outlets such as the celiac artery, the renal arteries, the superior mesenteric artery (SMA) decreases, as mentioned and later shown in [83]. Thus, a modification in the flow conditions of those bifurcations in the arterial tree was mandatory.

- Lastly, regarding the tuning of the Windkessel parameters, we followed an iterative procedure in order to calculate the outlet pressures as shown in [94]. Specifically, for the total peripheral resistance:

$$R_{total} = \frac{\text{MAP}}{\bar{Q}_{inlet}}, \tag{4.1}$$

MAP $= \frac{1}{3}(P_s - P_d) + P_d$ is the mean arterial pressure where P_s, P_d are the peak systolic and diastolic pressure in a specific inlet of an arterial segment and $\bar{Q}$ is the mean flow rate at the given inlet.

For the specification of the proximal and distal resistances, we followed a generic rule-of-thumb approach [4, 87] in which $\frac{R_d}{R_p} \sim 10$ and

$$\frac{1}{R_{total}} = \sum_{i=2}^{N} \frac{1}{R_p^i + R_d^i}. \tag{4.2}$$

Where N are the total terminal branches of the arterial model, $i = 1$ matches the ascending aorta. Then, we modified them until we received pressures in normal ranges.

For the compliances:

$$C_{total} = \frac{Q_{max} - Q_{min}}{P_s - P_d} \Delta t. \tag{4.3}$$

Where Q_{max} and Q_{min} are the maximum and minimum inlet flow rates respectively, and Δt is the temporal difference between the achieved maximum and minimum flow rates.

The above process is repeated for each outlet and thus, a case-specific designation of each Windkessel parameter is achieved and integrated into the one-dimensional model.

Now, the flow waveforms that are used in the three cases as boundary conditions at the inlet of the ascending aorta are the following,

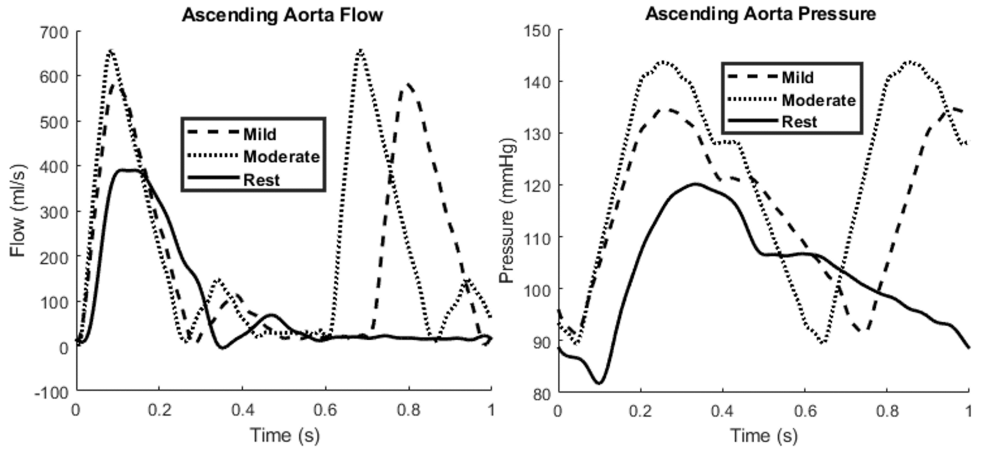

Figure 4.2: Ascending Aorta Inlet waveforms.

The flow and pressure waveforms of the mild and moderate cases respectively were multiplied by an amplitude factor L, which was selected so that the desirable systolic amplitudes, mean flow rates and pressure rates were achieved[2]. Rest case was simulated with a period of $T = 1s$, Mild with a period of $T = 0.7s$ and Moderate with a period of $T = 0.6s$.

The main results of the simulations, regarding the flow and pressure waveforms in the abdominal aorta and its outlets, that were derived from the workflow pipeline described above and implemented in MATLAB, are presented in Figure (4.3) and Figure (4.4). Each step of the workflow was constructed in such way that the derived results would reflect the direct effect of exercise, especially in the abdominal aorta and its outlet arteries.

[2]While the CFL condition was met.

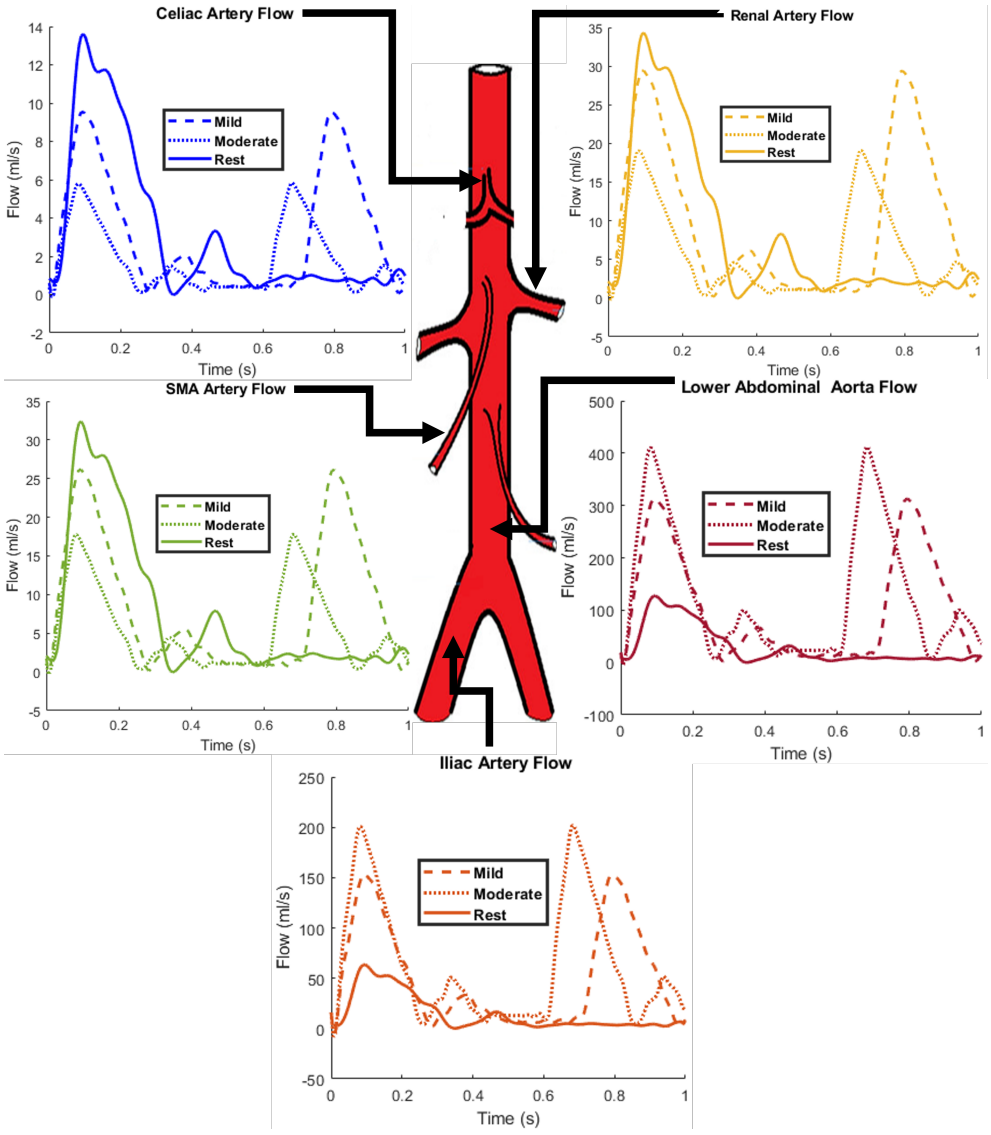

Figure 4.3: Abdominal Aorta Flow Results.

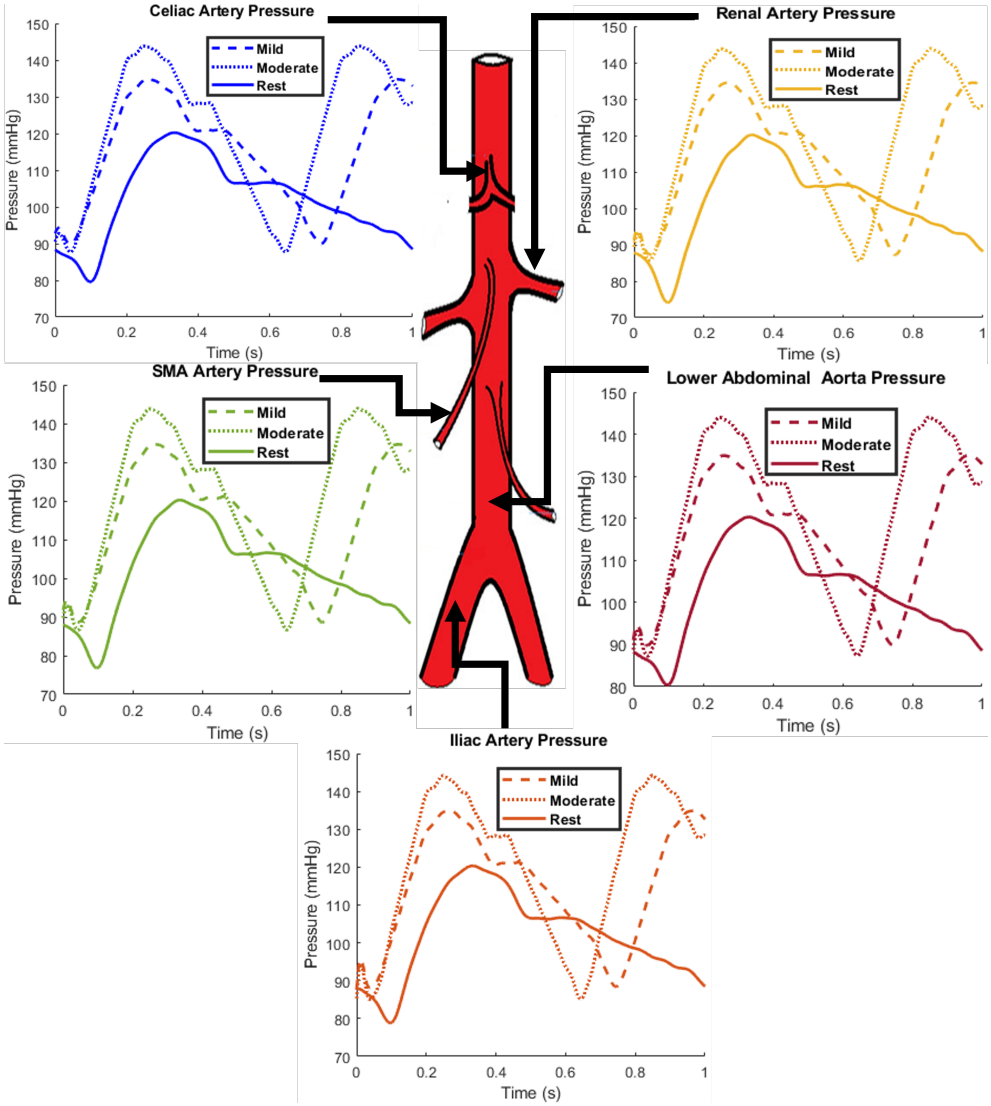

Figure 4.4: Abdominal Aorta Pressure Results.

Regarding the above results: Figure (4.3) and Figure (4.4) show that during the Rest case, retrograde flow[3] is present at the end of the systolic deceleration phase and lasts for a small time period. In both exercising states, the retrograde flow is mostly eliminated and is present in the very early stage of systolic acceleration. This can be attributed due to the intense dynamic of the cardiovascular system in the beginning of each cardiac cycle. Few *in-vivo* studies have shown that especially during low-intensity activities, retrograde flow increases as antegrade flow augments [29]. Our model does not predict this kind of behaviour during the mild state. However, respective *in-vivo* studies [34] claim to observe a diminish of retrograde flow during late systole when the intensity increments reached a minimum of 50% increase in heart rate, which is something that our model predicts [16]. It should be noted that in most setups of hemodynamic modelling, it is common for the inlet velocity waveforms to be extra-modified as the existence of retrograde flow tends to influence the robustness of the solver and its equivalent algorithm [41].

While the pressure wave, which originates from the left ventricle of the heart, propagates through the arterial tree and correspondingly through the abdominal aorta, we observe that SBP and its peak increases while it travels away from the heart. This fact is attributed to the physiology of the arterial system as it consists of numerous bifurcations and while the wave travels through the mother-daughter geometries, a part of it is reflected back from the peripheral vessels and is added to the main travelling wave [55]. As seen in Figure (4.4) this fact is preserved in both exercising cases. Nevertheless, recent studies proposed that the significant increase of systolic blood flow during exercise does not happen only due to wave reflection but mostly due to forward travelling waves and that the reflected waves are a minor contribution in the central blood pressure, even in the resting case [72]. Lastly, as shown in Table (4.1) MAP is also increasing while the intensity increases and also, in the Moderate case we observe that the DBP is lower than Mild's in every vessel. This behaviour is volitional while the pressure waveform was generated for the Moderate case in order to match the literature data which predicts a small drop in DBP while the intensity increases as a chain-reaction of the parasympathetic nervous system and as an aftermath of the vasodilation of the arteries [39].

A further analysis regarding the contribution of each forward and backward waves would fall into the field of pulse wave intensity/seperation analysis. The

[3]Retrograde flow is the reversal of the flow. It is defined as blood flowing backwards, in the opposition of its designated direction which is forward.

	Rest			Mild			Moderate		
	SBP	DBP	MAP	SBP	DBP	MAP	SBP	DBP	MAP
Artery									
AAo	120.13	81.71	94.52	134.72	91.38	105.82	143.66	89.44	107.52
UAA	120.29	80.43	93.72	134.87	90.15	105.05	143.98	87.73	106.48
CA	120.25	79.55	93.12	134.79	89.92	104.88	143.93	87.66	106.42
SMA	120.23	76.75	91.24	134.62	88.55	103.91	143.94	86.57	105.69
RA	120.19	74.06	89.44	134.52	87.17	102.95	143.93	85.60	105.04
LAA	120.33	80.33	93.66	134.89	89.81	104.85	144.10	87.21	106.17
CI	120.36	78.78	92.64	134.92	87.65	103.40	144.27	85.05	104.79

Table 4.1: Table of pressure values in the inlet and in the abdominal aorta. AAo: Ascending Aorta, UAA: Upper abdominal aorta, CA: Celiac Artery, SMA: Superior mesenteric artery, RA: Renal Artery, LAA: Lower Abdominal Aorta, CI: Common Iliac artery.

overall shape, peak amplitude, dicrotic notch point and other characteristics of the pressure waveform withhold information of immense value if one wants to evaluate the global hemodynamic situation of a person or a patient and determine its arterial distensibility status. In this thesis, the focus is mostly shifted on the quantitative and qualitative changes regarding blood flow and a more detailed analysis the results of physical activity on the pressure waveforms can be found in [54, 73].

The diastolic phase duration is decreased at both exercise levels and the dicrotic notch duration seems to decrease as well by a small percentage, in every abdominal aortic segment. In addition, the flow and pressure waveforms exhibit a time-lag between the maximum amplitude points of both waveforms which are shown in Figure (4.5) below. The depicted behaviour is exhibited in the rest of the segments of the arterial model.

Moreover, the modifications that were enforced uppon the inlet waveforms which originated by our own work were preserved throughout every respective waveform of flow and pressure in the arterial tree and accordingly, in the abdominal aorta and its branches. Thus. the tunings that each of the models underwent were successfully absorbed and integrated in the computational code.

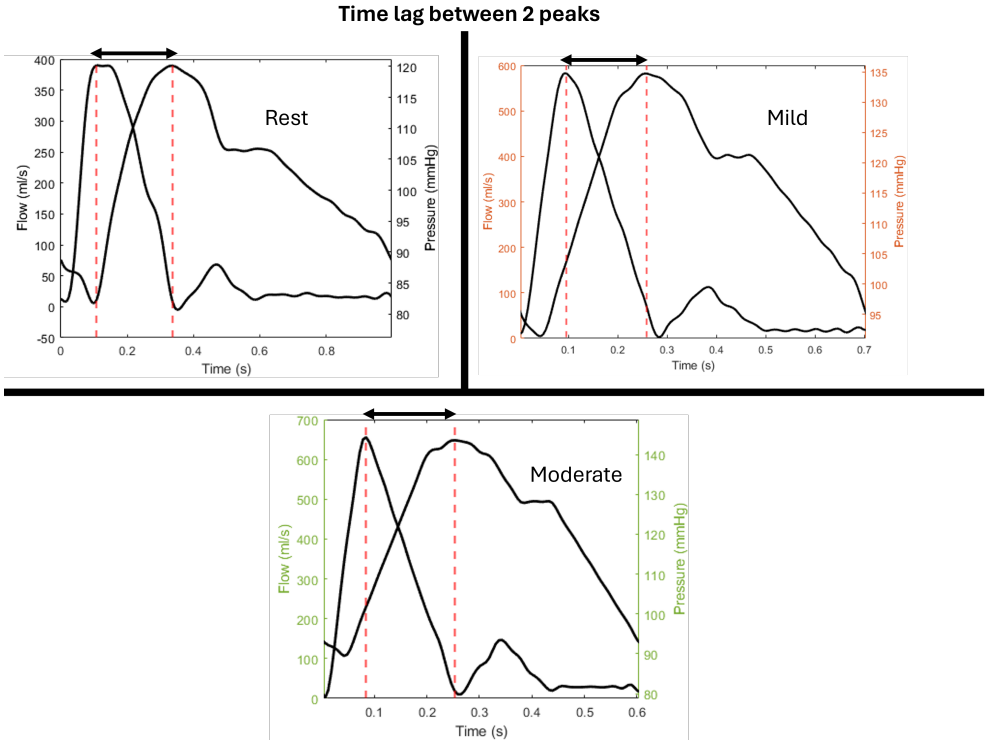

Figure 4.5: Comparison of the Time Lags between the three states in the Ascending Aorta. For the Rest case, Time Lag was estimated at ~ 0.22 seconds, at ~ 0.168 for the Mild case and at ~ 0.162 for the Moderate case.

Table 4.2 Mean Flow in the abdominal aorta (L/min)			
Artery	Rest	Mild	Moderate
Ascending Aorta	5.0115	6.2836	8.7255
Upper Abd.Aorta	4.6937	6.1166	8.1065
Celiac	0.3050	0.2048	0.1471
SMA	0.7218	0.4991	0.3859
Renal	0.7568	0.5099	0.3716
Lower Abd.Aorta	3.0388	6.1873	8.0755
Common Iliac	1.5664	3.5446	4.5511

In **Table 4.2**, we observe that during Rest, mean flow values are decreasing while travelling towards the abdominal aorta. However, in both Mild and Moderate cases, despite the fact that the inflow waveforms are way more dynamic and the inflow is substantially increased, we observe that the mean flow

values in the branches of the abdominal aorta are decreasing and the mean flow values from the Upper to the Lower abdominal aorta are increasing. Both of those phenomena are due to the construction of the one-dimensional computational model where such adjustments were made, according to Figure (4.3). This downward trend in the branching arteries of the abdominal aorta is the reason behind why mean flow values increase in the Upper-Lower Abd.Aorta.

In reality, an autoregulation mechanism[4] redistributes a significant % of descending aorta's blood flow in such way in order to match the vascular, muscular and metabolic needs and thus during lower-body exercising the blood that is extracted from branchial arteries, abdominal aorta branches e.t.c is decreased [83] and consequently filled with less blood which is driven towards the main segments of the abdominal aorta and then towards the legs. Thus, our model is able to reproduce the main quantitative and qualitative differences that exist between those three hemodynamic states and is in agreement with other similar studies [15, 27, 53, 79, 83].

The one-dimensional models that were created are the stepping stone for the three-dimensional simulations. Each step of the set-up of the simulation can be modified and recreated in such way so that a clinical physician can reenact a hemodynamic environment of a specific sport (in the case of Sports Science focus, e.g, a sport utilizing the upper limbs) or a medical expert can emulate a pathological vessel, a respective disease and its effect in a specific aortic or arterial segment. The majority of the physiological parameters that were used for the hemodynamic models were extracted from studies that were depicting an idealized aorta. An expansion of this setup idea and consequently, of this thesis would be the construction of a depositorium of flow and pressure waveforms which would be derived from actual CT scans, PC-MRIs, electrocardiograms or applanation tonometry tests and thus, the one-dimensional model would become patient-specific.

Thus, the results that occured from those simulations were used as guidelines, in terms of expected flow rate and pressure values, regarding the results that occured from the three-dimensional simulations. The following multiscale modelling utilizes the 1D-0D coupled mathematical models and couples them with with the 3D problem, which is introduced in the next chapter.

[4]That was integrated in our computational models that were developed in MATLAB.

CHAPTER 5

The three-dimensional model of the Lower abdominal aorta

The three-dimensional mathematical modelling of an arterial segment is considered as a state-of-the-art process in the field of hemodynamics. In order to understand the concepts revolving around vascular hemodynamics in a deeper sense and to investigate the effects of localized hemodynamic quantities such as wall shear stress (WSS), oscillatory shear index (OSI) e.t.c, the development and the utilization of computational techniques and software is required.

The mathematical formulation of the 3D problem consists of the three-dimensional, incompressible Navier-Stokes equations expressed as,

$$\bar{\nabla} \cdot \mathbf{u} = 0, \tag{5.1}$$

$$\frac{\partial \mathbf{u}}{\partial t} + \mathbf{u} \cdot \bar{\nabla}\mathbf{u} + \frac{1}{\rho}\bar{\nabla}p = \nu \Delta \mathbf{u} \tag{5.2}$$

Where Δ is the Laplacian operator, $\mathbf{u}$ is the velocity field, p is the pressure, ν is the kinematic viscosity and ρ is the density.

From the method of characteristic curves, it occurs that the above non-linear system of PDEs is classified as parabolic [88] and thus, the required conditions are: An initial condition, which will be linked with the velocity field and will be used at the inlet of the geometry and boundary conditions which will be linked with either the velocity field, the pressure or both, will be used at the outlets of the geometry.

The respective workflow diagram of the 3D simulations is the following:

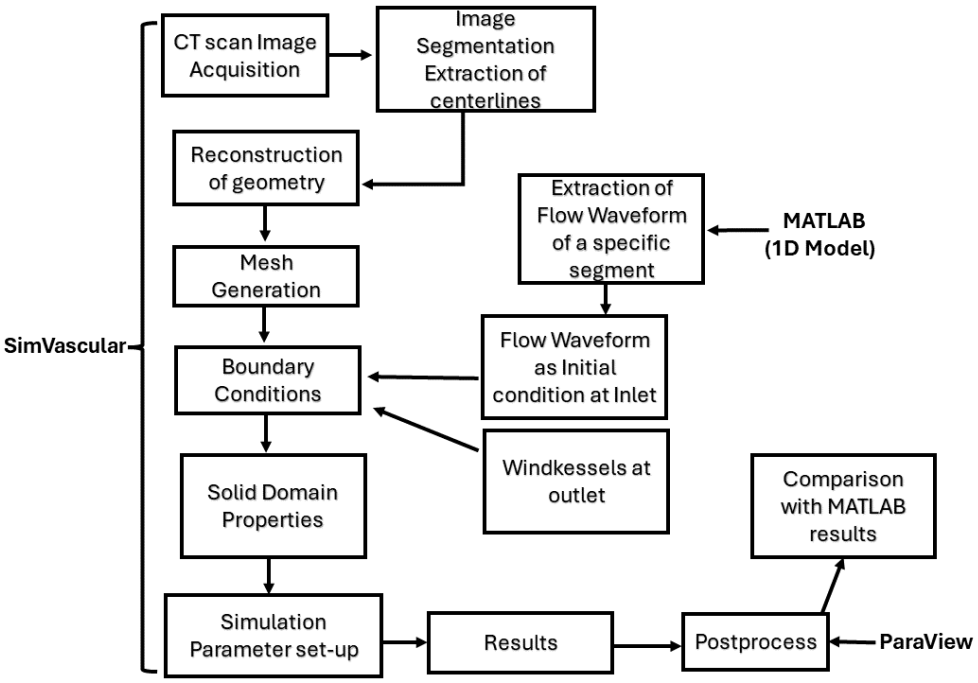

Figure 5.1: Workflow diagram of the three-dimensional simulation setup

Most of the numerical simulation steps were executed in the CFD software SimVascular [44, 86], which is a cutting-edge medical imaging software and is widely used for hemodynamic simulations. Our final patient-based, reconstructed from CT data, solid geometry model was the suprabirfucation part of the abdominal aorta including the common iliacs. Then, a mesh of 400.000 tetrahedrons (tetrahedral elements) was automatically generated by the Delaunay triangulation algorithm [76], which is part of the default meshing technique option in SimVascular [75, 84]. The simulations were performed for 4 cardiac cycles for every case. Regarding the inflow and outflow conditions and the steps depicted in Figure (5.1):

Boundary conditions

- At the inlet, we prescribed a flow waveform that was extracted from the 1D model, using a parabolic velocity profile for the cases of Rest, Mild and Moderate exercising and was used as an initial condition. The

holistic 1D-0D arterial model that was created in MATLAB equips us with flow waveforms at any given inlet of an arterial segment and thus enables us to simulate any segment we want, as long as access to CT scans or MRI images is possible.

- At each outlet, a Windkessel model was used where the R_p, C, R_d parameters were recalculated from the Equations (4.1 - 4.3) and not granted from the 1D model as in the 1D model, the total number of outlets of the arterial tree were more than the total number of outlets of the 3D geometry and thus a re-estimation of those parameters for the outlet boundary conditions of the 3D model was mandatory. However, the recalculation process remains the same as in the 1D because the inlet, maximum and minimum flows, systolic and diastolic pressures that were used for the calculations of the Windkessel parameters were derived from the 1D model.

- The solid physical domain (vessel walls) were modelled as rigid. Thus, a no-slip condition is enforced.

- As for the step of the parameter set-up, an appropriate time-step size was selected for the simulations, along with the selection of a threshhold of the error residuals. Regarding the discretization of the governing equations, a FEM approach is utilized and the linear solver used by SimVascular solves the obtained algebraic system directly [24, 25].

Most of the hemodynamic indices-parameters that were computed in our 3D simulations were velocity-related[1], such as WSS (and its distribution) which is considered as a primary parameter, its time-averaged value of respective period T for each case, namely TAWSS and other, secondary hemodynamic parameters that are based on WSS such as oscillatory shear index (OSI) and Residual Residence Time (RRT). Regarding the non-time averaged quantities, we studied the instanteneous velocity, pressure and WSS in specific points of the cardiac cycle: During Peak systole, End-systole, Mid-diastole and End-diastole. All the above indices were visualized in Paraview (Kitware, Inc.).

Wall shear stress is defined as the tangential stress on the wall which occurs due to friction generated from fluid flow on the wall's surface and is measured in $dynes/cm^2$. Due to the Newtonian nature of the blood that was assumed

[1]This is due to the availability of flow rate values which can be used to calculate the velocity as the cross-sectional area is known.

as part of the modelling process of blood flow, WSS is calculated by Newton's viscosity law

$$\boldsymbol{\tau}_w = -\mu \frac{\partial u}{\partial y}\Big|_w \tag{5.3}$$

The time-averaged wall shear stress is defined as

$$\mathbf{TAWSS} = \frac{1}{T}\int_0^T |\tau_w| dt \tag{5.4}$$

Where τ_w is the instantaneous stress shear stress vector calculated above and T is the period of a cardiac cycle.

WSS is characterized as primary hemodynamic index since it influences a plethora of biological factors that have a pivotal role in the development of arterial diseases, such as atherosclerosis. The distribution of WSS along the vessel wall can be used as a predictor of regions of atheromatic plaque formation as it favors particular locations of the vessel wall where WSS value is low and/or oscillatory. Thus, low WSS values in a wall's region is considered pro-atherogenic and high WSS values[2]is considered athero-protective [49, 96].

Oscillatory shear index (OSI) is an index used in order to quantify the temporal oscillations of WSS and measure the unidirectionality of WSS, meaning that it captures any deviations between WSS and TAWSS. OSI values are inversely correlated with WSS values, in the sense that at regions of low WSS high OSI values are expected and vice versa [7]. Thus, its definition depends on WSS and is calculated as

$$\mathbf{OSI} = \frac{1}{2}\left(1 - \frac{|\int_0^T WSS\, dt|}{\int_0^T |WSS|\, dt}\right) \tag{5.5}$$

The OSI index values range from 0 up to 0.5. The minimum value 0 corresponds to unidirectional wall shear stress during a period T of a cardiac cycle and the maximum value 0.5 corresponds to a flow that is purely oscillatory [91].

Relative residence time (RRT) is used to evaluate the residence time of fluid particles near a region of the vessel wall and is frequently utilized in studies of aneurysmatic geometries as endothelium regions that exhibit high

[2]Up to a certain threshold

RRT are more prone to atherosclerosis, aneurysm formation and thrombus development [71]. It provides an insight of a particle-wall interactions and is calculated via the TAWSS and the OSI as,

$$\mathbf{RRT} = \frac{1}{(1 - 2 \times OSI) \times TAWSS} \tag{5.6}$$

5.1 3D Results and hemodynamic indices

The main results of the 3D simulations were obtained in CGS units, which is the work-around units in bio-engineering problems and then inserted in ParaView for postprocessing and evaluation of the velocity field, pressure and of the hemodynamic indices and were compared. Each of the different cardiac cycle phases are pointed in Figure (5.2) below:

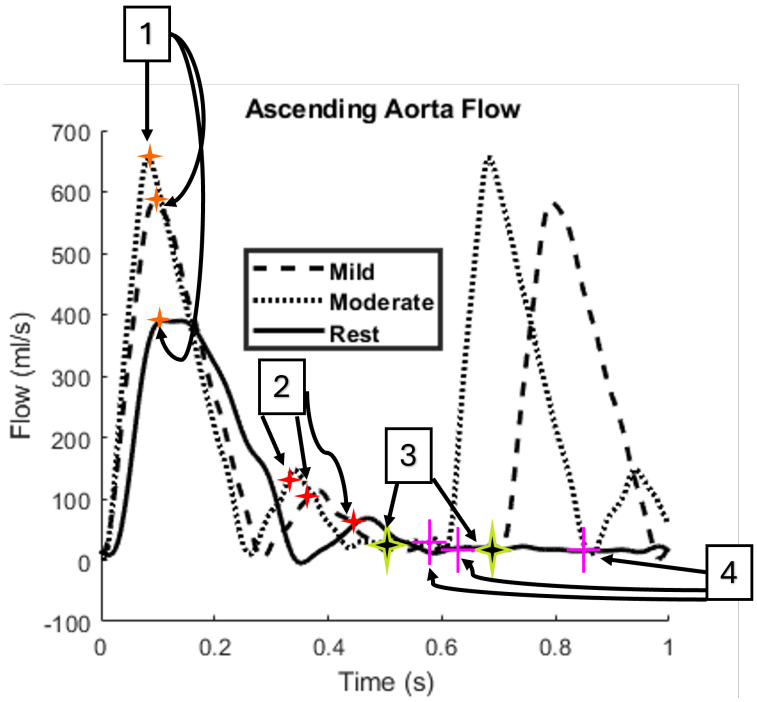

Figure 5.2: Depiction of different phases in a cardiac cycle.

Regarding the selection of each cardiac cycle phase, each one of them is a

point of reference for hemodynamic modelling and both primary and secondary hemodynamic parameters are frequently analyzed over those phases: Number one is the peak of the systolic phase, number two is towards the end of systolic phase, number three is the middle of diastolic phase and number four is the end of the diastolic phase. All the results from the 3D simulations were extracted from the fourth cardiac cycle with a view to neglect any dynamic behaviour that might be exhibited.

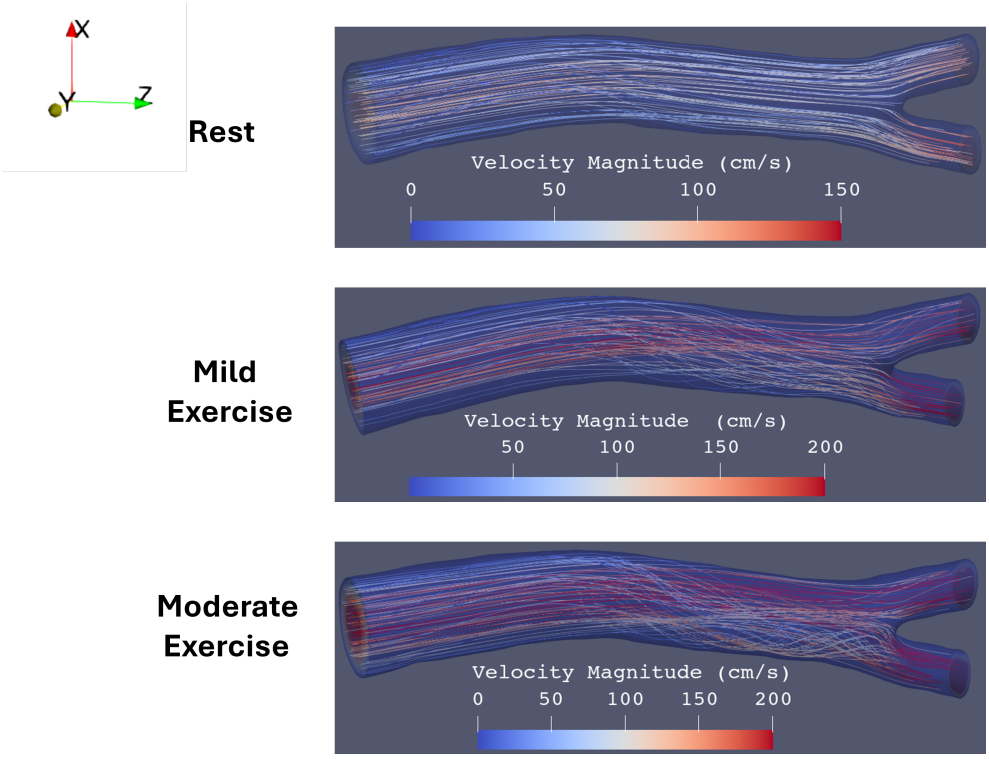

Figure 5.3: Visualization of the velocity streamlines during peak systolic phase.

In Figure (5.3), the alteration between the three states appears to have a major effect on the trajectory of the streamlines. During Rest, the streamlines followed a parallel course. However in both exercise levels, a mixing of the streamlines was visible which indicates: **1)** the intense hemodynamic events that take place in the infra-midpoint of the lower abdominal aorta and **2)** the possibility of the existence of transient flow even for a very small time period.

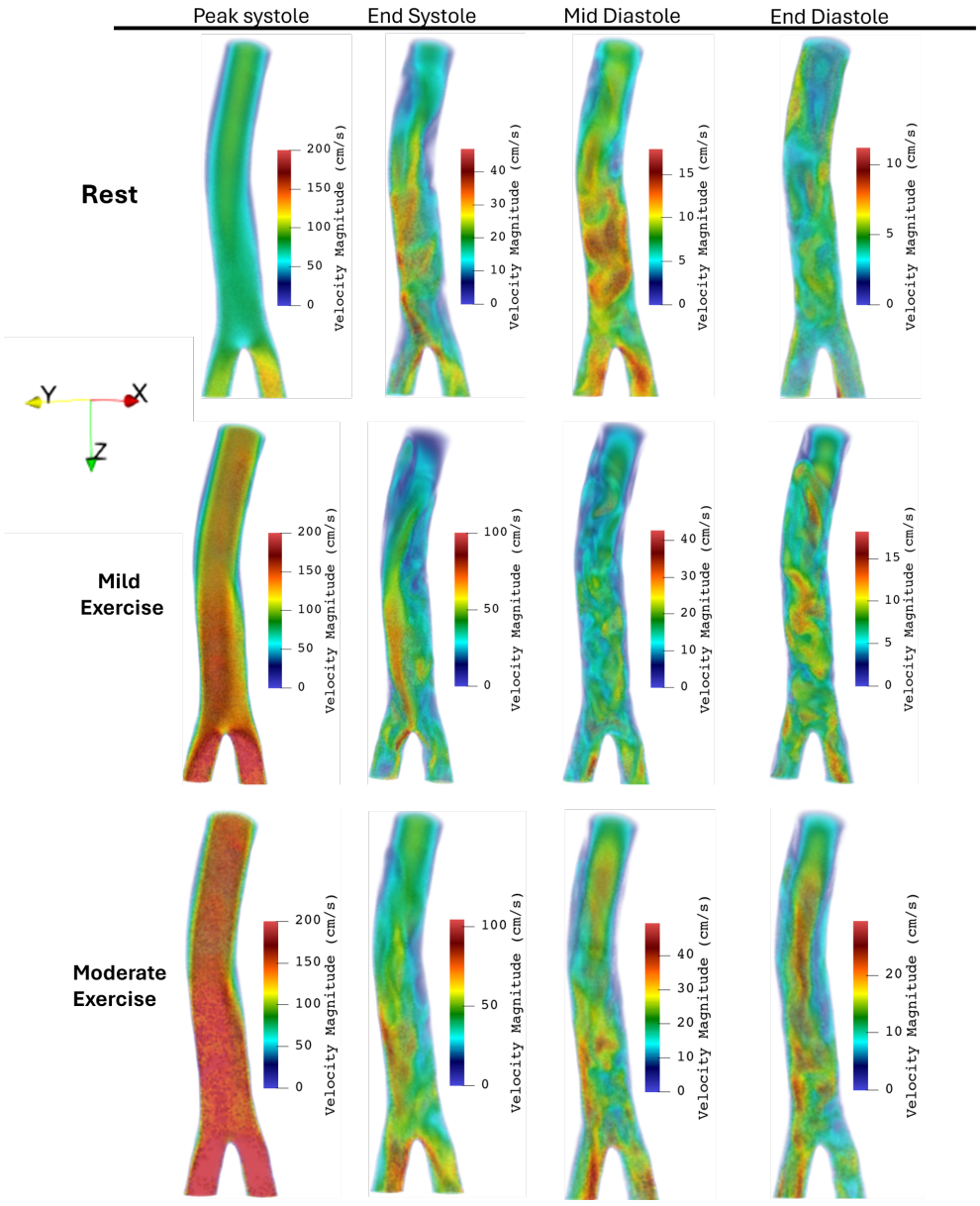

Figure 5.4: Visualization of the volume rendering of the magnitude of the velocity field at Rest, Mild and Moderate exercise at four different cardiac cycle phases.

Remark: Figure (5.4) visualizes the differences between the velocity fields in the three cases at four different cardiac cycle phases. "Peak systole" corresponds to the maximum flow rate in the cardiac cycle. "End systole" corresponds to a time point after the systolic deceleration and after the dicrotic notch, "Mid diastole" is the time interval between the End systole and the End diastole and lastly "End diastole" corresponds to the time point right before the end of the cardiac cycle. During Peak systole, the values of the velocity field in Moderate exercise surpassed the value of 200 cm/s in the greater part of the lower abdominal aorta while Rest case reached a maximum of 130 cm/s only at infrabifurcation. Mild exercise showed a big increase below the midpoint of the segment down to the iliacs. This gradual increase in the three different cases is expected due to the increased vascular, muscular and metabolic needs and thus, a greater flow rate is exhibited in the exercise cases which is translated to greater velocity values. However, a slight overestimation of the flow rates is expected as the vessel walls were not modelled as deformable.

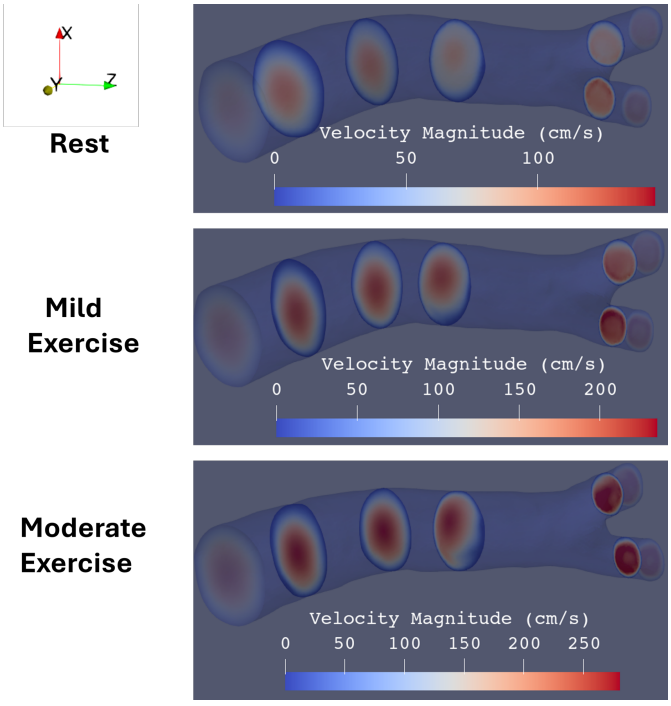

Figure 5.5: Contour slices on different parts of the aortic segment during Peak systole.

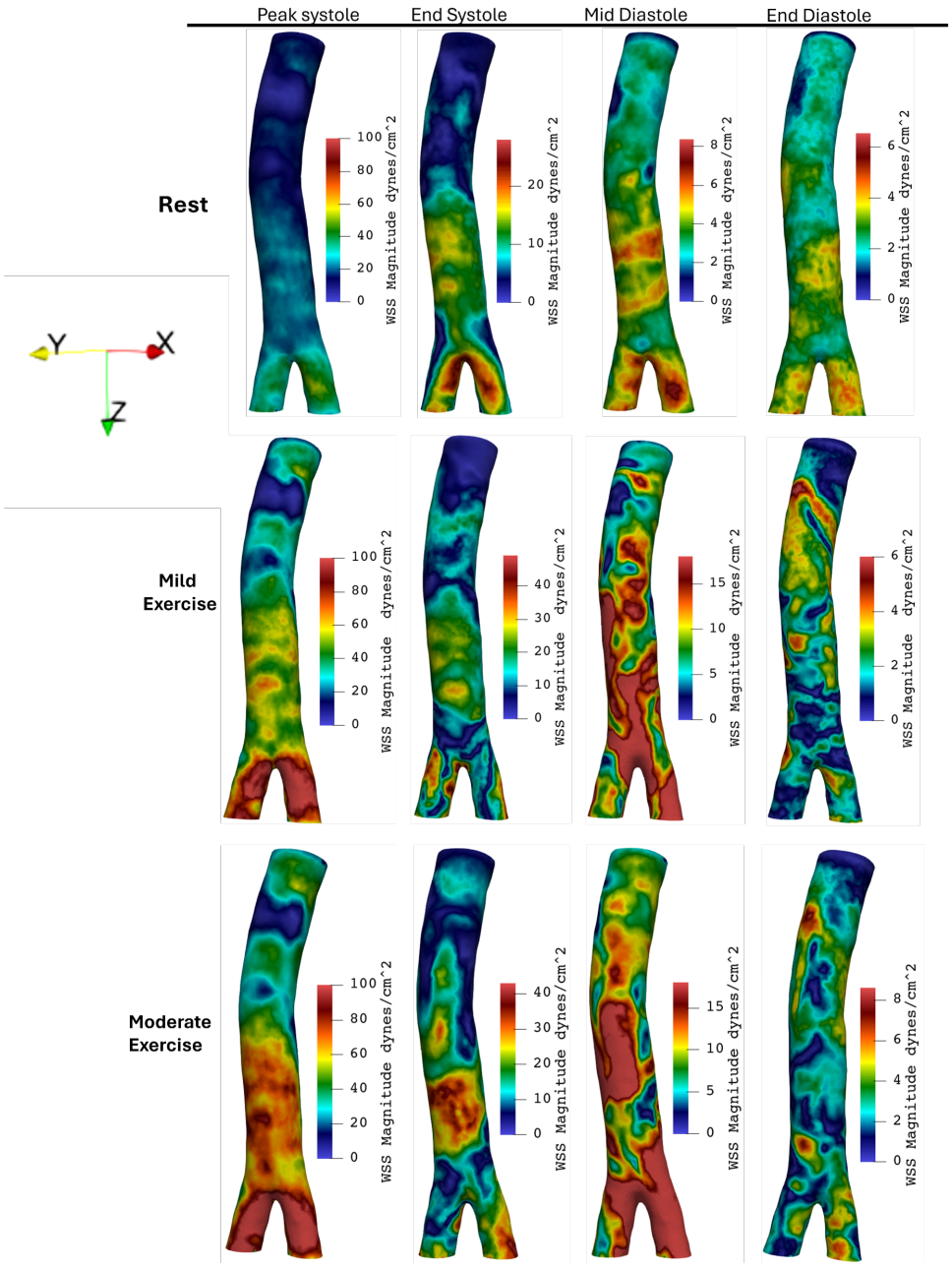

Figure 5.6: Wall shear stress comparison of Rest, Mild and Moderate exercise in four different cardiac cycle phases.

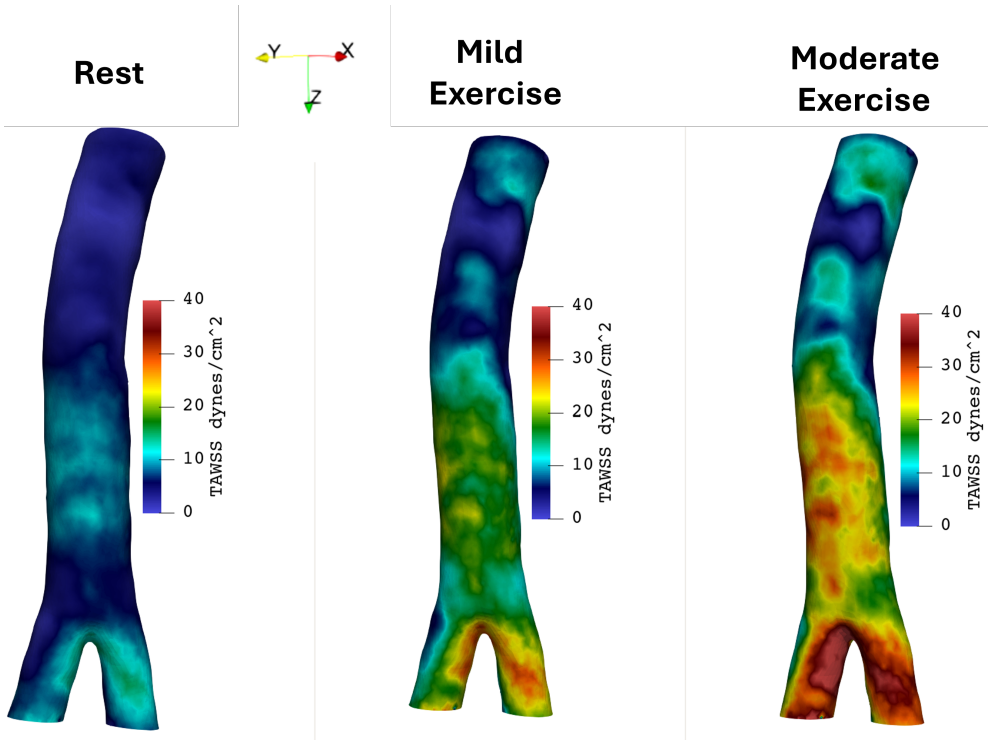

Figure 5.7: TAWSS comparison of Rest, Mild and Moderate exercise.

Direct exercise plays a pivotal role in arterial hemodynamics. According to various studies [81, 83, 91], the positive impact of physical activity is considered to occur from the elimination of adverse hemodynamic conditions such as the presence of low WSS. To further explore the local effect that different exercise levels have in the systemic arteries of the arterial tree and its correlation with the arisal of cardiovascular events, one has to deploy advanced computational methods in order to analyze the effect that hemodynamic indices have on the specific segment. In the arterial segment of the infrarenal abdominal aorta, the presence of atheromatic plaque is rather common and the occuring aortic hemodynamics are strongly impacted from the outflow conditions of the suprarenal vessels such as the renals, the celiac and the SMA arteries. Thus, the study of the exercise effect upon the adverse hemodynamic conditions is of paramount interest and is highly sought-after.

In Figure (5.4), a disturbed flow region appears towards "Mid systole" phase which is visible around the midpoint of the arterial segment and seems to be almost-removed in the Mild Exercise and totally removed in Modarate Exer-

cise. The third midpoint slice shown in Figure (5.5) reveals the presence of a complex hemodynamic flow drived towards suprabifurcation region of the segment. From the Figures (5.6)-(5.7) we observe that during Rest, WSS is below 10 $dynes/cm^2$ in the first half of the arterial segment and is categorized as low, then it increases to values between 20 and 30 $dynes/cm^2$ in the suprabifurcation position and receives a value of $\sim$ 45 $dynes/cm^2$ at the common iliac region.

The same behaviour is exhibited in the TAWSS where the gradual elimination of low WSS is visible from Rest to Mild and then Moderate Exercise is clear of low WSS values in the majority of segment's length. From a medicinal aspect, the increase in WSS and TAWSS in combination with the increased flow rate is linked to the production of athero-protective factors [83]. However, some of the aforementioned studies and the constructed models that simulate similar cases with ours seem to predict a more dominant behavior regarding the complete elimination of low WSS in the entirety of the infrarenal abdominal aorta. This difference could be attributed to a number of factors such as the origin of the inflow waveforms, different geometric properties of the three-dimensional problem and even the velocity profile.

The OSI index exhibits an inverse behavior in comparison to TAWSS. At specific regions in Figure (5.7) at both exercise levels, there exists a region of low wall shear stress below the inlet height of the lower abdominal aorta, which according to Figure (5.8) below is the region where OSI receives its maximum and maximal values. In addition to that it can be observed from Figure (5.9) that just below this region, there exists an elliptical-shaped region which receives a maximum OSI value during Rest and a minimum value during Moderate exercise and as seen in Figure (5.7), the inverse phenomenon is exhibited. The exact same result can be observed at the height of the right common iliac, towards the outer side of the artery.

Thus, the calculation of TAWSS and OSI showed a consistent, inversed behavior in our simulations. High TAWSS regions were low OSI regions and vice versa. The hypothesis that gradual increase in exercise intensities eliminates low wall shear stress is verified in our simulations and our multiple-scale models were able to recreate qualitative and quantitative results similar to the ones in the available literature data [15, 83].

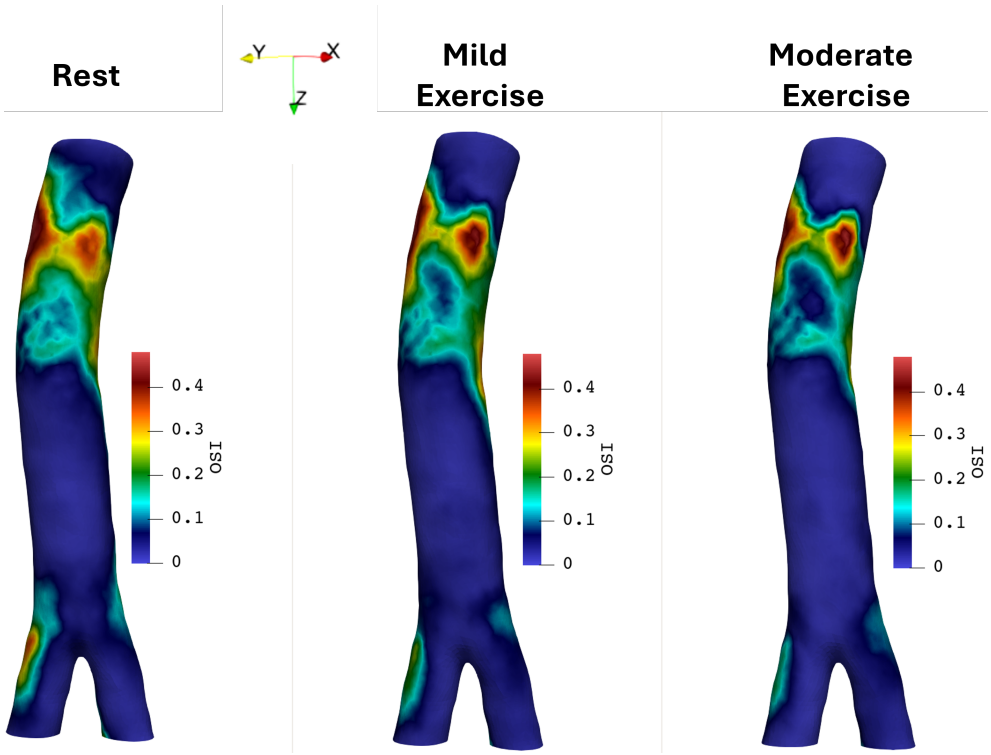

Figure 5.8: OSI index comparison of Rest, Mild and Moderate exercise.

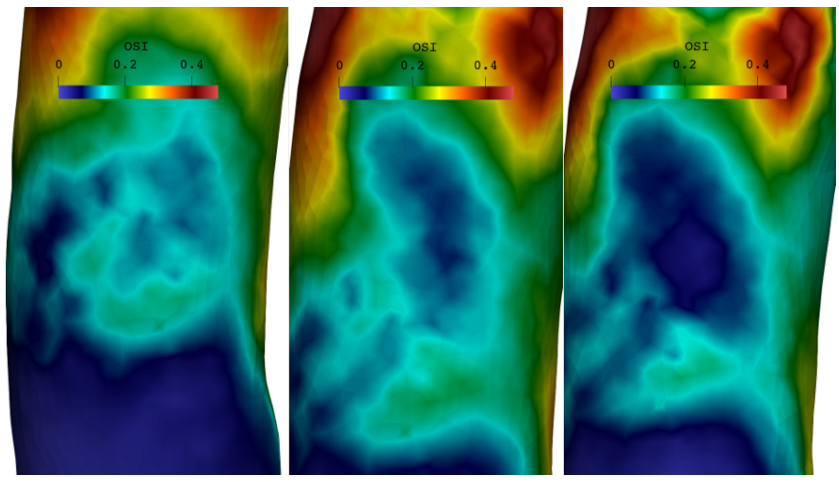

Figure 5.9: Different OSI value regions below the aortic inlet.

As shown in Figure (5.10) below, RRT exhibits the same kind of behavior with OSI regarding its distribution acting on the upper part of the infrarenal abdominal aorta as a gradual decrease is observed from Mild to Moderate exercise levels and as an hemodynamic index, it includes the effect of OSI and consequently of TAWSS.

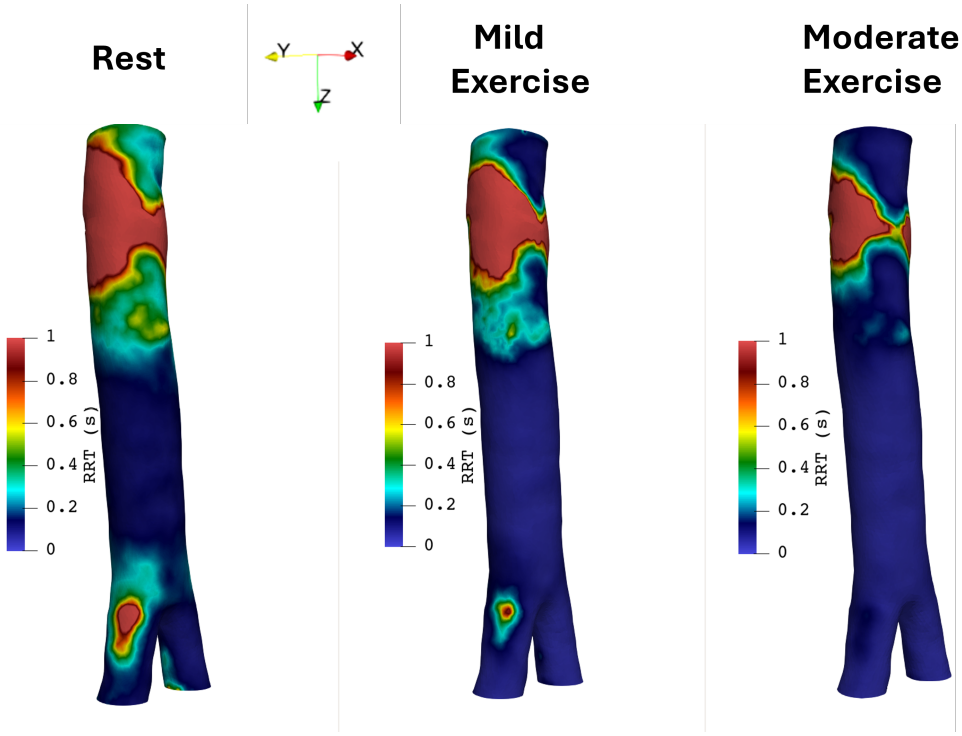

Figure 5.10: RRT index comparison of Rest, Mild and Moderate exercise.

However, in healthy arterial segments such as the one we use in our simulations, RRT index has not been studied sufficiently. In addition, it is rarely calculated in studies of integrated environments of exercise, such as the ones we simulate and thus, there is limited available literature data to compare our results with [82].

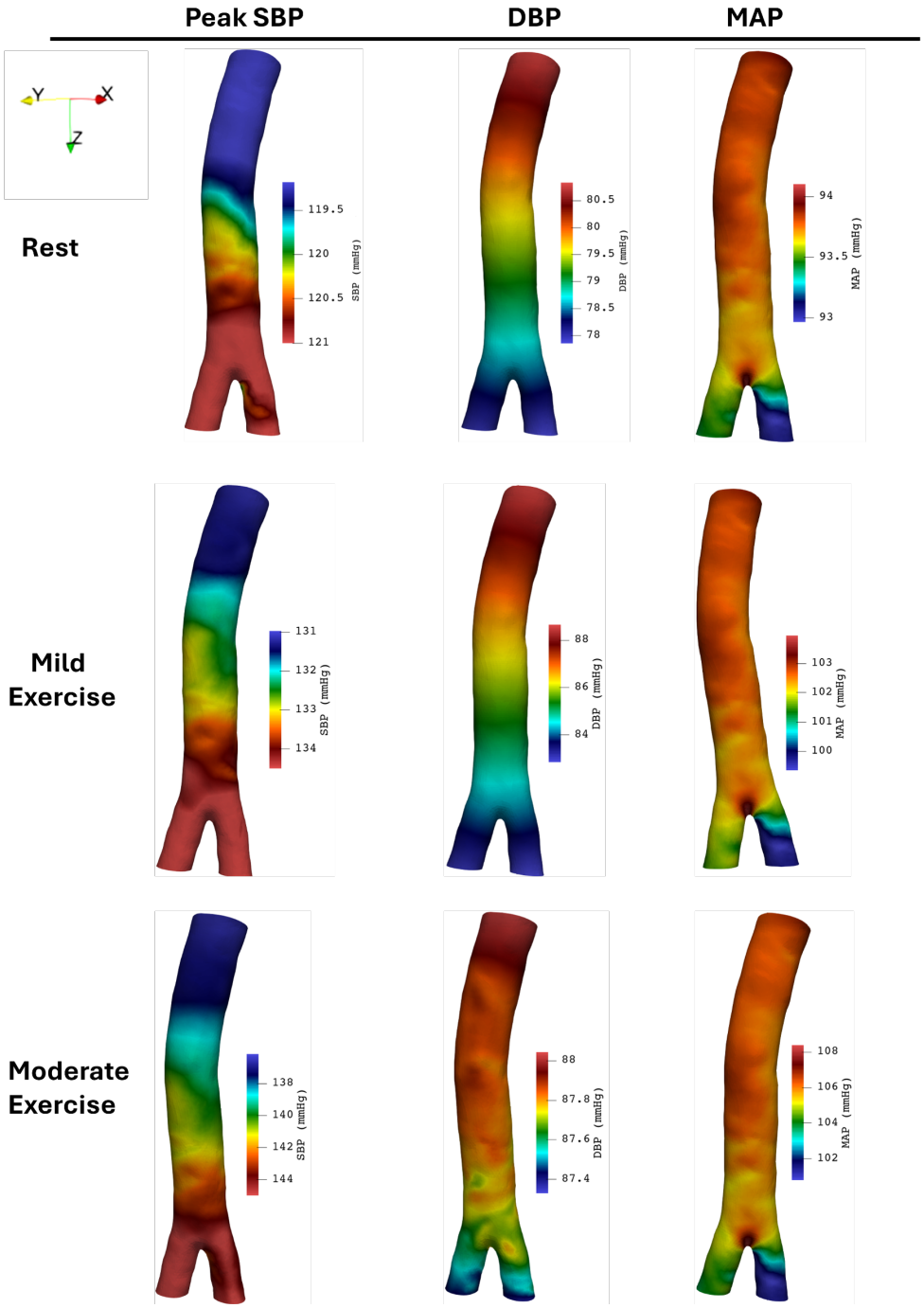

Figure 5.11: Distribution of Peak SBP, DBP and MAP pressures in the infrarenal abdominal aorta.

Lastly, regarding the distribution of the pressure along the infrarenal segment: Two different cardiac phases were taken into consideration in the simulation , the peak systolic blood pressure and diastolic blood pressure. The MAP pressure was calculated from the same formula that was introduced in the previous chapter. For each case, a re-estimation of the outlet conditions was mandatory as the lower abdominal and common iliac radiuses were modified and the respective flow rates and thus the Windkessel parameters had to be re-estimated. Despite the fact that in the re-estimation procedure, the results from the one-dimensional model were used as guidelines, the derived results from the three-dimensional simulations were more detailed in regards of the distribution of pressure, especially towards the suprabifurcation region and a small deviation from the results of the Table (4.1) is expected.

The peak systolic blood pressure follows a reverse trend[3] regarding the values it receives as the arterial pulse wave increases while travelling towards the iliacs. In the Rest case it reaches a maximum of $\sim$ 120 mmHg in the common iliac while Mild and Moderate exercise reach a maximum of 134 and 144 mmHg respectively. The diastolic and mean arterial pressures respectively descended in a predictable fashion from the inlet down towards the iliacs. However the descends in both Rest and Mild Exercise cases in the diastolic blood pressure were greater than those suggested in Table (4.1). This might be attributed to the fact that the inlet flow is way too dynamic and implicit, coupled momentum-pressure solver that SimVascular uses deploys a pressure drop towards the end of the diastolic phase for convergence purposes.

Lastly, two profound observations can be done regarding the MAP: While evaluating it, it can be observed that in the bifurcation area where the flow splits into the iliacs, a local pressure increase occurs. This can be credited to either a possible fault that occured during the reconstruction of 3D geometry or due to the fact that the pressure condition that was enforced in the one-dimensional model is not actually met in the three-dimensional model when evaluating the MAP. Either way, this phenomenon does not seem to affect the rest of the evaluated results but only the MAP case. The second observation is the extra pressure drop that can be observed in the left iliac, a fact that could be attributed the difference of the radiuses between the two common iliac arteries.

Overall, we observe that the one-dimensional pressure results from our simulations, as shown in Table (4.1) and the thre-dimensional results shown in

[3]During the Peak systolic phase in pressure, the corresponding flow waveform is at the deceleration of the systolic phase, as shown in Figure (4.5) in the previous chapter.

Figure (5.11) are in agreement and in tune overall, which showcases the consistency of the modelling techniques and the configuration that was used to extract the boundary conditions that were used in both 1D and 3D simulations.

5.2 Limitations of the 1D and 3D models in the thesis

Regarding the construction of the **1D** models, the biggest limitation that we faced was the absence of raw flow and pressure waveforms in the literature data (hence the approach we followed). The acquisition of waveforms derived from PC-MRI could play a pivotal role in the comparisons between computed, simulation results and measured, clinical results and also, those waveforms could be extrapolated and used as a foundation for patient-specific modelling. Another limitation that was met was the configuration of an idealized abdominal aorta geometry, as the geometric characteristics such as the radiuses[4], the elastance modulus e.t.c were derived from previous studies that had hypothesized an ideal geometry as well. A further acquisition of patient-specific details about the arterial segments could result in a more precise simulation with more accurate results and less deviation from the clinical literature data.

A parabolic velocity profile is a common approach among hemodynamic modelling. However, a plug profile or a Womersley profile would be able to capture the complex hemodynamic phenomena in a more detailed way. In addition, the tuning of the Windkessel parameters was depended on the evaluation of the flow rate and the SBP, DBP and MAP, of which calculations heavily relied on the waveforms and on specific formulas provided from literature. Nevertheless, the tuning of the Windkessel models in both 1D and 3D models is not a straightforward task and needs a patient-specific approach to yield similar measured-calculated results.

During the construction of the models we hypothesized a laminar flow throughout the arterial segment. As shown in Figure (5.3), a gradual increase of the intensity in physical activity resulted in the development of a more complex flow during the peak systolic phase which seems to become transient or even turbulent. Furthermore, throughout the thesis blood had been simulated as a Newtonian fluid which, despite the fact that it is a commonly met consesus

[4]The radiuses were kept constant throughout the segments. A "correction" of this hypothesis would be to include different radius values at each inlet and outlet of the model.

in hemodynamic modelling, is not accurate as blood exhibits non-Newtonian behavior.

Regarding the **3D** simulations, an absence of boundary layer had been hypothesized, for simplicity purposes. The vessel walls were modelled as rigid, non-deformable due to absence of physiological parameter details such as the actual thickness of the wall. Aorta consists of three different layers. In our simulations, we considered that only one of those layers were present (the endothelium). Thus, a future extension could be the modelling of a deformable wall in either a constant or variable fashion to simulate the aortic luminal motion and the integration of more than one layers inside the vessel with their respective boundary layers. Those steps would convert the problem to a fluid-structure interaction (FSI) case. Lastly, a region-specific refinement of the constructed mesh especially at regions where the index of WSS is low could provide detailed insight of the developing hemodynamics.

5.3 A glimpse of a future step: Effect of exercise in AAA

The primary goal of this thesis was to simulate the effect of exercise in the physiology of a healthy human. However, due to the continuous rise of cardiovascular diseases globally, the study of the effect of exercise in diseased vessels such as in aneurysmatic geometries using CFD techniques has become a necessity. In order to understand the underlying hemodynamic phenomena that take place in those geometries and figure out if, when and under what conditions an exercise level could be beneficial to a person suffering from e.g an AAA, the estimation of primary and secondary hemodynamic parameters could be beneficial and provide a coincise yet important point of view regarding the course of the disease. Thus, a future extension of the pipeline workflow that was followed through the course of this thesis, regarding the multiscale mathematical models that were developed, is the utilization of this workflow in order to study a pathological case such as the presence of an aneurysm in the abdominal aorta (AAA). In this section, we briefly introduce what is the definition of an aneurysm and examine the AAA case in combination with Mild and Moderate exercise under the wall condition of rigidity, which in general consists a simplistic approach while studying AAAs and an FSI approach is more common.

An aortic aneurysm typically refers to the enlargement of a specific segment

of the aorta which leads to the formation of a bulge-like structure. In particular, the vessel wall is unable to tolerate the expansile force of each systolic contraction and as a result, expands [5]. This enlargement occurs due to gradual weakening of the arterial wall which is owed to **1)**Pathological changes in the anatomy of the wall itself and **2)**Effect of hemodynamic conditions on the wall. In general, the pathogenesis of an aneurysm is considered multifactorial, as overall quality of life, health-harming habits such as smoking, age, family health history, race and various other factors contribute to its formation.

Abdominal aortic aneurysm (AAA) refers to the presence of an aneurysm in the lower part of the aorta and comprises the vast majority of aortic aneurysms, as the most common locations of aneurysm formation are the infrarenal abdominal aortic regions [48, 69]. The enlargement of the AAA can be either observed as a stable increase of the diameter of the vessel or as a rapid enlargement in an unspecified period of time. A common criterion for identifying even a small AAA is when its diameter exceeds 3 cm or when vessel's diameter is permanently increased by 150% in comparison to an adjacent diameter of the same arterial segment [74].

The following figure is an infrarenal abdominal aortic aneurysm including the common iliac arteries and was acquired from CT scans using the imaging software Mimics (Materialise inc.).

Figure 5.12: Depiction of a AAA. Derived from a reconstructed geometry.

As was mentioned earlier, various studies have hypothesized that a key parameter to the formation and growth of an aneurysm is low WSS. However, it still remains unclear what the direct effects of exercise (and its gradual increments, in terms of intensity) are on the hemodynamic conditions that exist either in the whole arterial segment or in the bulge region of the aneurysm. The generic guidelines, originating from both European and American health institutes [58], that are provided to people suffering from a AAA tend to become outdated and thus, a re-establishment of those guidelines is mandatory in order to validate the benefits of exercising in the cardiovascular health and in the slowing of arterial diseases. Nevertheless, this re-establishment can be re-enforced with both clinical data results **and** the results that occur from CFD simulations.

In order to examine the effects of exercise on the hemodynamic indices in our AAA geometry, we repeated the same procedure and followed the same workflow that was earlier described in Figure (5.1) in this chapter. All of the simulations were perfomed for four cardiac cycles again, for every case and the last cardiac cycle was used to compute TAWSS, RRT and the velocity fields. According to the available literature data, lower limb exercising slows down the progression of a AAA as it diminishes adverse hemodynamic effects, such as low wall shear stress and exhibits an increase of TAWSS, especially around the region of the aneurysm [22, 45].

As expected, in Figure (5.13) we observed that the region of the aneurysm displays low TAWSS values, between 2 - 3.5 $dynes/cm^2$. However, the gradual increase of physical activity showed a significant increase of TAWSS for each case. During Mild Exercise, low TAWSS regions were sufficiently diminished and during Moderate Exercise, TAWSS reached up to three-times the Rest case values of TAWSS and almost every low TAWSS region was eliminated. The simulation results are consistent and in agreement with the suggested literature data above and correctly predicted the qualitative hemodynamic changes in a AAA and the direct effect of exercise on it. In addition, a further increase of TAWSS was observed in the aliquot parts of the inlets of the segments, which can be an athero-protective action towards an additional, future aneurysm formation in that area.

The same behavior was exhibited in the common iliac arteries, where the TAWSS was over 50 $dynes/cm^2$ during Mild Exercise and over 70 $dynes/cm^2$ during Moderate Exercise. However, excessive augmentations in TAWSS can have a negative impact on the health of artery wall and might foreshadow an underlying health issue.

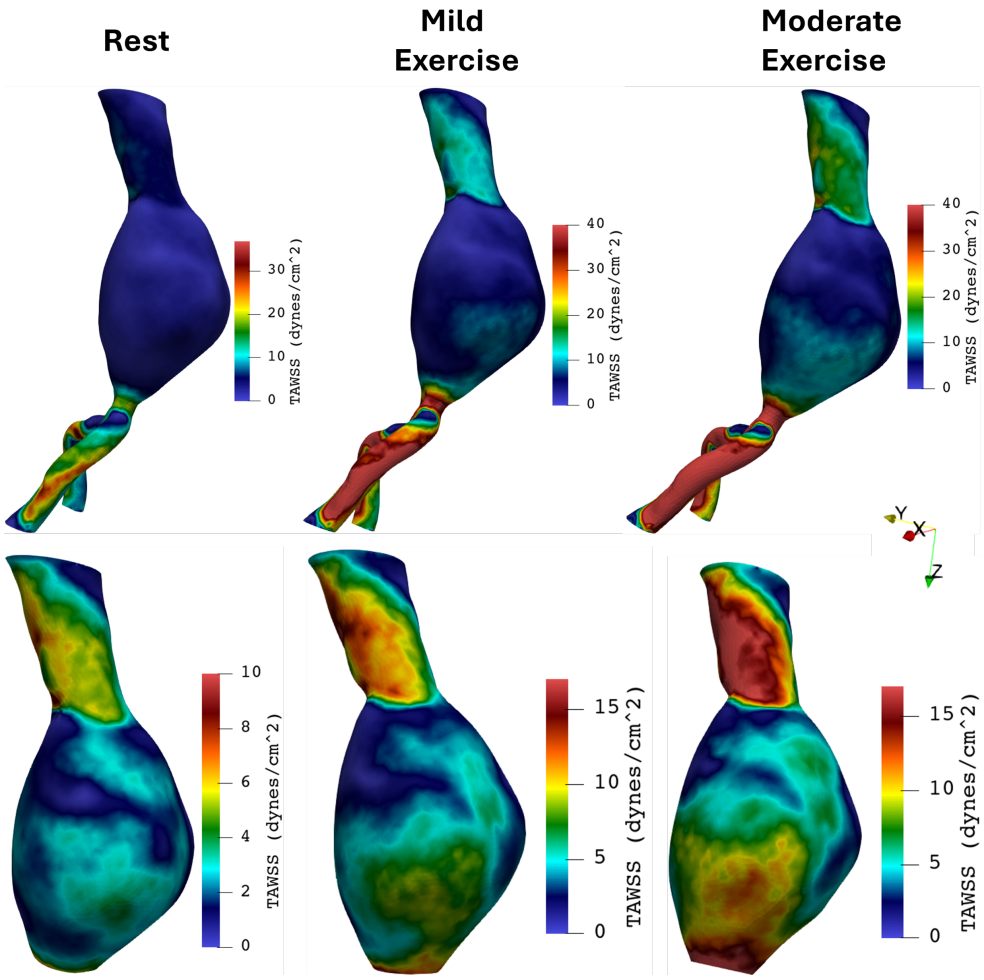

Figure 5.13: First row: TAWSS comparison of Rest, Mild and Moderate exercise in the whole AAA. Second row: TAWSS at the inlet and the region of the aneurysm.

The computations of TAWSS and RRT in Figure (5.13) and Figure (5.14) respectively, revealed that during the Rest case a favorable environment towards atherogenesis was created as the RRT index received high values at the majority of the aneurysm while the lowest TAWSS values were observed in the regions of maximum RRT values. In contrast to Figure (5.10), the healthy segment only showed a particular region of RRT presence while Figure (5.14) showed that during Rest, the whole aneurysm is under adverse hemodynamic

conditions. Thus, in the majority of the aneurysm, the residence time of fluid that stayed in the aneurysm area for a prolonged period of time during the Rest case was increased in comparison to both exercise states.

During both exercise states and especially in Moderate exercise, it was observed that half of the aneurysmatic region had been cleared off residual particles. Nevertheless, even during Mild Exercise a significant reduction in RRT was observed and thus, both exercise intensities seemed to showcase particle clearance in an enhanced way, in half of the aneurysm.

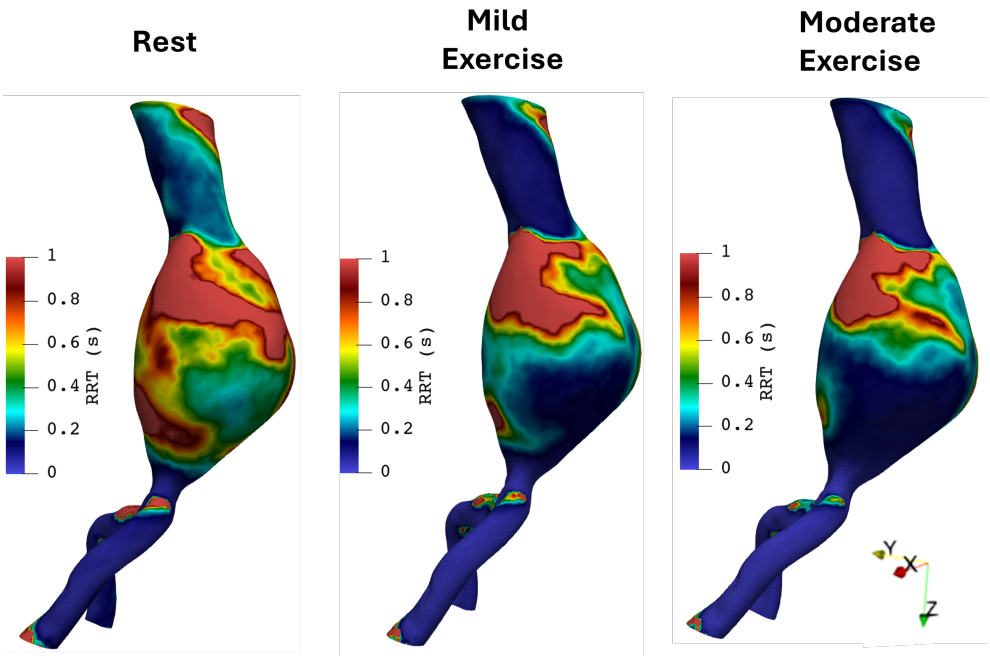

Figure 5.14: RRT index comparison of Rest, Mild and Moderate exercise.

As shown in Figure (5.15), a jet-like flow is exhibited. Even at peak systole, there are regions of low flow rate and points of flow stagnation, especially at Rest case where numerous regions of the aneurysm present stagnation points[5]. However, it can be observed that these areas are getting eliminated with the gradual increase of physical activity due to augmented flow magnitudes and increments of wall shear stress. Those constricted regions of stagnant flow have been correlated with the development of a thrombosis [11].

[5]The stagnation points are the regions towards the center left and right of the aneurysm, pseudocoloured as deep blue.

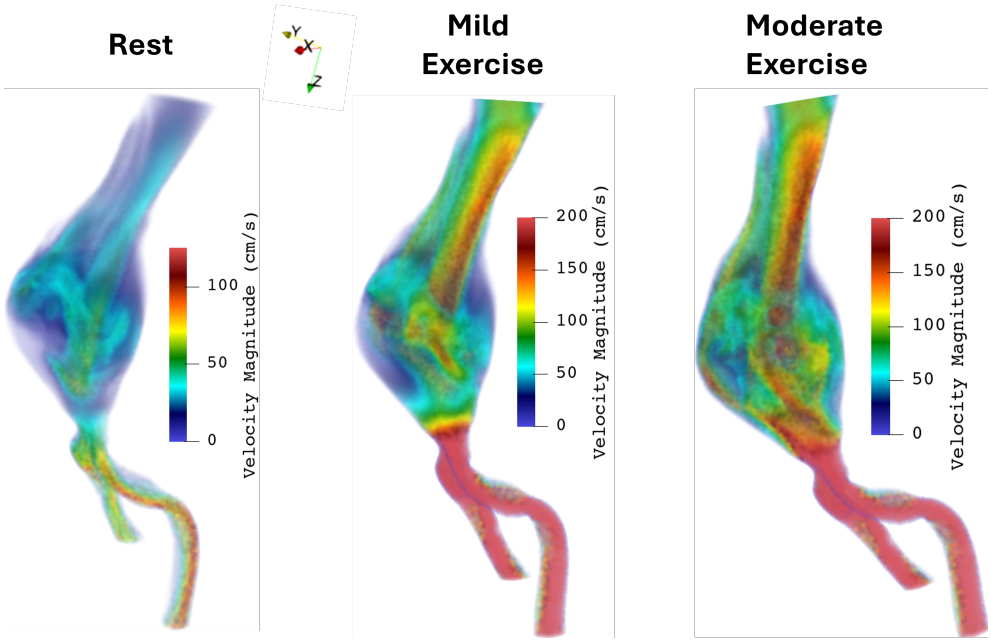

Figure 5.15: Visualization of the volume rendering of the magnitude of the velocity field at Rest, Mild and Moderate exercise during the Peak of the systolic phase.

Thus, we tested and then confirmed the hypothesis that exercise plays a pivotal, positive role in the hemodynamic conditions of both healthy **and** diseased vessels and can also play a protective role regarding the further growth and development of a AAA.

5.4 Conclusions

The process of modelling blood flow under various states is a complex task, encounters numerous challenges and preoccupies the interest of many scientific fields such as mathematics, bio-engineering, medicine and more. Due to the technonogical advancements and breakthroughs that are continuously occuring, CFD has gained significant ground regarding its utilization in studying such problems. The development and the coupling of multiscale mathematical models enables scientists to come up with new strategies in order to face the challenges that the blood flow process exhibits. The costly, invasive methods

that are used from clinical physicians to assess the health status of a person can be partially replaced with detailed simulations that can reenact either simple or more complex hemodynamic states, such as the effect of exercise in major systemic arteries with stunning accuracy. Thus, the future of the medical progress in studying cases such as exercising or the effects of a disease on an arterial segment, lies within the enhancement of such multiscale models, a fact that is confirmed from the ever-increasingly studies that are conducted in a cross-scientific fashion.

The zero-dimensional, Windkessel models were coupled with both one-dimensional and three-dimensional models and were used as a blackbox at the outlets of specific arteries in order to model the compliance-capacitance of the smaller arteries of the arterial tree down in vasculature. The respective parameters of Windkessel models were calculated from specific formulas in an iterative way.

The one-dimensional mathematical modelling that was employed as an information originator of the flow and pressure waveforms, flow rate values, various pressure values (SBP, DBP, MAP) needed a-priori only a handful of basic physiological parameters in order to reproduce physiologically accurate results in the major systemic arteries. Through the one-dimensional modelling we were able to isolate a specific part of the arterial tree and study its primary hemodynamic parameters. The 1D models were able to capture phenomena such as the pressure drop that is exhibited in both mean and diastolic blood pressure and the inverse behavior of pressure during the peak of the systolic phase. Via proper tuning that the 1D models underwent in the bifurcating regions of the arterial tree, they were able to predict the change of the flow ratio that exists in specific outflow arteries of the abdominal aorta between the Resting state and in simulating the Mild and Moderate exercise states.

The three-dimensional models were created step by step, starting from the 3D geometry reconstruction from CT images. Then, the 3D simulation parameters were tuned and a mathematical multiscale approach was deployed: The generated flow and pressure waveforms that were derived from the 1D models were used as inflow boundary conditions of the Lower Abdominal arterial segment while the 0D, Windkessel models and their parameters were adjusted accordingly and placed at the terminal points of the segment. From those simulations we acquired information regarding the velocity field and the pressure distribution. Both exercise environments that were simulated reproduced results that are in agreement with similar numerical simulations in the available literature and validated the hypothesis that gradual increase of exercise elim-

inates adverse hemodynamic conditions that are exhibited in that particular segment of the abdominal aorta. Finally, another multiscale approach was deployed in an aneurysmatic geometry where secondary hemodynamic indices such as TAWSS and RRT were calculated and showcased the positive effect of exercise.

Bibliography

[1] Milton Abramowitz and Irene A Stegun. *Handbook of Mathematical Functions*. Courier Corporation, Apr. 2012.

[2] Milton Abramowitz and Irene A Stegun. *Handbook of mathematical functions, with formulas, graphs, and mathematical tables,* New York, Dover Publications, 1965.

[3] Jordi Alastruey et al. "Lumped parameter outflow models for 1-D blood flow simulations: Effect on pulse waves and parameter estimation". In: *Communications in Computational Physics* 4 (2008), pp. 317–336.

[4] Jordi Alastruey et al. "Physical determining factors of the arterial pulse waveform: theoretical analysis and calculation using the 1-D formulation". In: *Journal of engineering mathematics* 77 (Sept. 2012), pp. 19–37. DOI: 10.1007/s10665-012-9555-z.

[5] Jordi Alastruey et al. "Pulse wave propagation in a model human arterial network: Assessment of 1-D visco-elastic simulations against in vitro measurements". In: *Journal of Biomechanics* 44 (Aug. 2011), pp. 2250–2258. DOI: 10.1016/j.jbiomech.2011.05.041.

[6] Maria Teresa de Almeida Jansen Catanho, Mridu Sinha, and Varsha Vijayan. "Model of Aortic Blood Flow Using the Windkessel Eect". In: 2012.

[7] Md. Al-Amin Sheikh, Anis Suhaila Shuib, and Mohd Hardie Hidayat Mohyi. "A Review of Hemodynamic Parameters in Cerebral Aneurysm". In: *Interdisciplinary Neurosurgery* (Mar. 2020), p. 100716. DOI: 10.1016/j.inat.2020.100716.

[8] John David Anderson. *Computational Fluid Dynamics*. International Marine, Feb. 1995.

[9] H B Atabek. "Wave Propagation through a Viscous Fluid Contained in a Tethered, Initially Stressed, Orthotropic Elastic Tube". In: *Biophysical Journal* 8 (May 1968), pp. 626–649. DOI: 10.1016/s0006-3495(68)86512-9.

[10] Henry S. Badeer. "HEMODYNAMICS FOR MEDICAL STUDENTS". In: *Advances in Physiology Education* 25 (Mar. 2001), pp. 44–52. DOI: 10.1152/advances.2001.25.1.44.

[11] D. Bluestein et al. "Steady Flow in an Aneurysm Model: Correlation Between Fluid Dynamics and Blood Platelet Deposition". In: *Journal of Biomechanical Engineering* 118 (Aug. 1996), pp. 280–286. DOI: 10.1115/1.2796008.

[12] Roberto Burattini and Silvia Natalucci. "Complex and frequency-dependent compliance of viscoelastic windkessel resolves contradictions in elastic windkessels". In: *Medical Engineering Physics* 20 (Oct. 1998), pp. 502–514. DOI: 10.1016/s1350-4533(98)00055-1.

[13] Sunčica Čanić and Eun Heui Kim. "Mathematical analysis of the quasilinear effects in a hyperbolic model blood flow through compliant axisymmetric vessels". In: 26 (Jan. 2003), pp. 1161–1186. DOI: 10.1002/mma.407.

[14] Marianne Catanho, Mridu Sinha, and Varsha Vijayan. *BENG 221 - Mathematical Methods in Bioengineering Model of Aortic Blood Flow Using the Windkessel Eect Model of Aortic Blood Flow Using the Windkessel Model Catanho, Sinha, Vijayan*. 2012.

[15] C Cheng. "Abdominal aortic hemodynamic conditions in healthy subjects aged 50–70 at rest and during lower limb exercise: in vivo quantification using MRI". In: *Atherosclerosis* 168 (June 2003), pp. 323–331. DOI: 10.1016/s0021-9150(03)00099-6.

[16] Christopher P Cheng et al. "Blood flow conditions in the proximal pulmonary arteries and vena cavae: healthy children during upright cycling exercise". In: *American journal of physiology. Heart and circulatory physiology* 287 (Aug. 2004), H921–H926. DOI: 10.1152/ajpheart.00022.2004.

[17] Grigorios Chrimatopoulos, Efstratios E Tzirtzilakis, and Michalis A Xenos. "Magnetohydrodynamic and Ferrohydrodynamic Fluid Flow Using the Finite Volume Method". In: *Fluids* 9 (Dec. 2023), pp. 5–5. DOI: 10.3390/fluids9010005.

[18] Sejong Chun, Jonghan Jin, and Wan-Ho Cho. "Construction of the prediction model between pressure and flow rate for pulsating flows based on the Greenfield-Fry model concerning wave dispersion". In: *Experiments in Fluids* 58 (Apr. 2017). DOI: 10.1007/s00348-017-2327-9.

[19] R. Courant, K. Friedrichs, and H. Lewy. "On the Partial Difference Equations of Mathematical Physics". In: *IBM Journal of Research and Development* 11 (Mar. 1967), pp. 215–234. DOI: 10.1147/rd.112.0215.

[20] Barry James Cox and James Murray Hill. "Flow through a circular tube with a permeable Navier slip boundary". In: *Nanoscale research letters* 6 (May 2011). DOI: 10.1186/1556-276x-6-389.

[21] Frank A. Dinenno et al. "Regular endurance exercise induces expansive arterial remodelling in the trained limbs of healthy men". In: *The Journal of Physiology* 534 (July 2001), pp. 287–295. DOI: 10.1111/j.1469-7793.2001.00287.x.

[22] Monica M. Dua and Ronald L. Dalman. "Hemodynamic Influences on abdominal aortic aneurysm disease: Application of biomechanics to aneurysm pathophysiology". In: *Vascular Pharmacology* 53 (July 2010), pp. 11–21. DOI: 10.1016/j.vph.2010.03.004.

[23] Ali Ebrahimi. "Mechanical Properties of Normal and Diseased Cerebrovascular System". In: *Journal of vascular and interventional neurology* 2 (Apr. 2009), pp. 155–62.

[24] Mahdi Esmaily-Moghadam, Yuri Bazilevs, and Alison L Marsden. "A bi-partitioned iterative algorithm for solving linear systems arising from incompressible flow problems". In: *Computer Methods in Applied Mechanics and Engineering* 286 (Apr. 2015), pp. 40–62. DOI: 10.1016/j.cma.2014.11.033.

[25] Mahdi Esmaily-Moghadam, Yuri Bazilevs, and Alison L. Marsden. "A new preconditioning technique for implicitly coupled multidomain simulations with applications to hemodynamics". In: *Computational Mechanics* 52 (May 2013), pp. 1141–1152. DOI: 10.1007/s00466-013-0868-1.

[26] Elisa Fevola et al. "A Vector Fitting Approach for the Automated Estimation of Lumped Boundary Conditions of 1D Circulation Models". In: *Cardiovascular Engineering and Technology* 14 (June 2023), pp. 505–525. DOI: 10.1007/s13239-023-00669-z.

[27] Luca Formaggia, Daniele Lamponi, and Alfio Quarteroni. "One-dimensional models for blood flow in arteries". In: *Journal of Engineering Mathematics* 47 (Dec. 2003), pp. 251–276. DOI: 10.1023/b:engi.0000007980.01347.29.

[28] Y C Fung and B W Zweifach. "Microcirculation: Mechanics of Blood Flow in Capillaries". In: *Annual Review of Fluid Mechanics* 3 (Jan. 1971), pp. 189–210. DOI: 10.1146/annurev.fl.03.010171.001201.

[29] Joaquin U Gonzales et al. "Role of retrograde flow in the shear stimulus associated with exercise blood flow". In: *Clinical physiology and functional imaging* 28 (Aug. 2008), pp. 318–325. DOI: 10.1111/j.1475-097x.2008.00812.x.

[30] Daniel J. Green et al. "Vascular Adaptation to Exercise in Humans: Role of Hemodynamic Stimuli". In: *Physiological Reviews* 97 (Apr. 2017), pp. 495–528. DOI: 10.1152/physrev.00014.2016.

[31] J. F. Hale, D. A. McDonald, and J. R. Womersley. "Velocity profiles of oscillating arterial flow, with some calculations of viscous drag and the Reynolds number". In: *The Journal of Physiology* 128 (June 1955), pp. 629–640. DOI: 10.1113/jphysiol.1955.sp005330.

[32] Ylva Hellsten and Michael Nyberg. "Cardiovascular Adaptations to Exercise Training". In: *Comprehensive Physiology* 6 (Dec. 2015), pp. 1–32. DOI: 10.1002/cphy.c140080.

[33] Irving P Herman and Springer Science+Business Media. *Physics of the human body*. Springer, Cop, 2016.

[34] V.E. Hjortdal et al. "Effects of Exercise and Respiration on Blood Flow in Total Cavopulmonary Connection". In: *Circulation* 108 (Sept. 2003), pp. 1227–1231. DOI: 10.1161/01.cir.0000087406.27922.6b.

[35] Peter R. Hoskins, Patricia V. Lawford, and Barry J. Doyle, eds. *Cardiovascular Biomechanics*. Springer International Publishing, 2017. DOI: 10.1007/978-3-319-46407-7.

[36] Paul A. Iaizzo. *Handbook of Cardiac Anatomy, Physiology, and Devices*. Ed. by Paul A. Iaizzo. Springer International Publishing, 2015. DOI: 10.1007/978-3-319-19464-6.

[37] Andrea Natale Impiombato et al. "A Simple Transient Poiseuille-Based Approach to Mimic the Womersley Function and to Model Pulsatile Blood Flow". In: *Dynamics* 1 (Sept. 2021), pp. 9–17. DOI: 10.3390/dynamics1010002.

[38] Lucian Mihai Itu et al. "A parameter estimation framework for patient-specific hemodynamic computations". In: *Journal of Computational Physics* 281 (Jan. 2015), pp. 316–333. DOI: 10.1016/j.jcp.2014.10.034.

[39] George A. Kelley and Kristi Sharpe Kelley. "Progressive Resistance Exercise and Resting Blood Pressure". In: *Hypertension* 35 (Mar. 2000), pp. 838–843. DOI: 10.1161/01.hyp.35.3.838.

[40] A K Khalid, Z S Othman, and CT M N M Shafee. "A review of mathematical modelling of blood flow in human circulatory system". In: *Journal of Physics: Conference Series* 1988 (July 2021), p. 012010. DOI: 10.1088/1742-6596/1988/1/012010.

[41] H. J. Kim et al. "On Coupling a Lumped Parameter Heart Model and a Three-Dimensional Finite Element Aorta Model". In: *Annals of Biomedical Engineering* 37 (July 2009), pp. 2153–2169. DOI: 10.1007/s10439-009-9760-8.

[42] Richard E Klabunde. *Cardiovascular Physiology Concepts*. Lippincott Williams Wilkins, Dec. 2020.

[43] T W Körner. *Fourier Analysis*. Cambridge University Press, June 2022.

[44] Hongzhi Lan et al. "A Re-Engineered Software Interface and Workflow for the Open-Source SimVascular Cardiovascular Modeling Package". In: *Journal of biomechanical engineering* 140 (Feb. 2018). DOI: 10.1115/1.4038751.

[45] Andrea S. Les et al. "Quantification of Hemodynamics in Abdominal Aortic Aneurysms During Rest and Exercise Using Magnetic Resonance Imaging and Computational Fluid Dynamics". In: *Annals of biomedical engineering* 38 (Apr. 2010), pp. 1288–1313. DOI: 10.1007/s10439-010-9949-x.

[46] J Rodney Levick. *An introduction to cardiovascular physiology*. Arnold, 2003.

[47] Damiano Lombardi. "Inverse problems in 1D hemodynamics on systemic networks: A sequential approach". In: *International Journal for Numerical Methods in Biomedical Engineering* 30 (Sept. 2013), pp. 160–179. DOI: 10.1002/cnm.2596.

[48] Hong Lu and Alan Daugherty. "Aortic Aneurysms". In: *Arteriosclerosis, Thrombosis, and Vascular Biology* 37 (June 2017). DOI: 10.1161/atvbaha.117.309578.

[49] Adel M. Malek. "Hemodynamic Shear Stress and Its Role in Atherosclerosis". In: *JAMA* 282 (Dec. 1999), p. 2035. DOI: 10.1001/jama.282.21.2035.

[50] Kuntinee Maneeratana. "Development of the finite volume method for non-linear structural applications". In: (Jan. 2000).

[51] Alison L. Marsden and Mahdi Esmaily-Moghadam. "Multiscale Modeling of Cardiovascular Flows for Clinical Decision Support". In: *Applied Mechanics Reviews* 67 (Apr. 2015), p. 030804. DOI: 10.1115/1.4029909.

[52] Emanuele Monda et al. "Thoracic Aortic Dilation: Implications for Physical Activity and Sport Participation". In: *Diagnostics* 12 (June 2022), p. 1392. DOI: 10.3390/diagnostics12061392.

[53] J. E. Moore et al. "Pulsatile Flow Visualization in the Abdominal Aorta Under Differing Physiologic Conditions: Implications for Increased Susceptibility to Atherosclerosis". In: *Journal of Biomechanical Engineering* 114 (Aug. 1992), pp. 391–397. DOI: 10.1115/1.2891400.

[54] J P Murgo et al. "Effects of exercise on aortic input impedance and pressure wave forms in normal humans." In: *Circulation Research* 48 (Mar. 1981), pp. 334–343. DOI: 10.1161/01.res.48.3.334.

[55] Jonathan P. Mynard et al. "Measurement, Analysis and Interpretation of Pressure/Flow Waves in Blood Vessels". In: *Frontiers in Physiology* 11 (Aug. 2020). DOI: 10.3389/fphys.2020.01085.

[56] Elie Nader et al. "Blood Rheology: Key Parameters, Impact on Blood Flow, Role in Sickle Cell Disease and Effects of Exercise". In: *Frontiers in Physiology* 10 (Oct. 2019). DOI: 10.3389/fphys.2019.01329.

[57] Rod Nave. *HyperPhysics Concepts*. Gsu.edu, 2017. URL: http://hyperphysics.phy-astr.gsu.edu.

[58] Miriam E Nelson et al. "Physical Activity and Public Health in Older Adults". In: *Circulation* 116 (Aug. 2007), pp. 1094–1105. DOI: 10.1161/circulationaha.107.185650.

[59] Mette S Olufsen. "5. Modeling Flow and Pressure in the Systemic Arteries". In: *Society for Industrial and Applied Mathematics eBooks* (Jan. 2004), pp. 91–136. DOI: 10.1137/1.9780898718287.ch5.

[60] Ali Ostadfar. "Fluid Mechanics and Biofluids Principles". In: *Biofluid Mechanics* (2016), pp. 1–60. DOI: 10.1016/b978-0-12-802408-9.00001-6.

[61] Johnny T Ottesen, Mette S Olufsen, and Jesper K Larsen. *Applied Mathematical Models in Human Physiology*. SIAM, Jan. 2004.

[62] K. H. Parker and C. J. H. Jones. "Forward and Backward Running Waves in the Arteries: Analysis Using the Method of Characteristics". In: *Journal of Biomechanical Engineering* 112 (Aug. 1990), pp. 322–326. DOI: 10.1115/1.2891191.

[63] E.M Pedersen et al. "Quantitative abdominal aortic flow measurements at controlled levels of ergometer exercise". In: *Magnetic Resonance Imaging* 17 (May 1999), pp. 489–494. DOI: 10.1016/s0730-725x(98)00209-4.

[64] Erik Morre Pedersen et al. "Development of Velocity Profiles and Retrograde Flow in the Porcine Abdominal Aorta under Different Haemodynamic Conditions". In: *Scandinavian Cardiovascular Journal* 33 (Jan. 1999), pp. 206–214. DOI: 10.1080/14017439950141632.

[65] T J Pedley. *The Fluid Mechanics of Large Blood Vessels*. Cambridge University Press, Apr. 1980. DOI: 10.1017/cbo9780511896996.

[66] Benoît Pier and Peter J. Schmid. "Linear and nonlinear dynamics of pulsatile channel flow". In: *Journal of Fluid Mechanics* 815 (Feb. 2017), pp. 435–480. DOI: 10.1017/jfm.2017.58.

[67] A. Quarteroni, A. Manzoni, and C. Vergara. "The cardiovascular system: Mathematical modelling, numerical algorithms and clinical applications". In: *Acta Numerica* 26 (May 2017), pp. 365–590. DOI: 10.1017/s0962492917000046.

[68] Alfio Quarteroni, Riccardo Sacco, and Fausto Saleri. *Numerical Mathematics*. 2nd. Springer, Jan. 2007. DOI: 10.1007/b98885.

[69] Anastasios Raptis et al. "Comparison of physiological and post-endovascular aneurysm repair infrarenal blood flow". In: *Computer Methods in Biomechanics and Biomedical Engineering* 20 (Aug. 2016), pp. 242–249. DOI: 10.1080/10255842.2016.1215437.

[70] Michal Sajkowski. *Courant Number in CFD*. SimFlow, Apr. 2023. URL: https://sim-flow.com/courant-number-in-cfd/.

[71] Huseyin Enes Salman et al. "Biomechanical Investigation of Disturbed Hemodynamics-Induced Tissue Degeneration in Abdominal Aortic Aneurysms Using Computational and Experimental Techniques". In: *Frontiers in Bioengineering and Biotechnology* 7 (May 2019). DOI: 10.3389/fbioe.2019.00111.

[72] Martin G. Schultz et al. "Exercise Central (Aortic) Blood Pressure Is Predominantly Driven by Forward Traveling Waves, Not Wave Reflection". In: *Hypertension* 62 (July 2013), pp. 175–182. DOI: 10.1161/hypertensionaha.111.00584.

[73] J. E. Sharman et al. "The effect of exercise on large artery haemodynamics in healthy young men". In: *European Journal of Clinical Investigation* 35 (Dec. 2005), pp. 738–744. DOI: 10.1111/j.1365-2362.2005.01578.x.

[74] Palma M. Shaw, John Loree, and Ryan C. Gibbons. *Abdominal Aortic Aneurysm (AAA)*. PubMed, 2020. URL: https://www.ncbi.nlm.nih.gov/books/NBK470237/.

[75] Mark S. Shephard and Marcel K. Georges. "Automatic three-dimensional mesh generation by the finite octree technique". In: *International Journal for Numerical Methods in Engineering* 32 (Sept. 1991), pp. 709–749. DOI: 10.1002/nme.1620320406.

[76] Jonathan Richard Shewchuk. "Delaunay refinement algorithms for triangular mesh generation". In: *Computational Geometry* 22 (May 2002), pp. 21–74. DOI: 10.1016/s0925-7721(01)00047-5.

[77] Yubing Shi, Patricia Lawford, and Rodney Hose. "Review of Zero-D and 1-D Models of Blood Flow in the Cardiovascular System". In: *BioMedical Engineering OnLine* 10 (2011), p. 33. DOI: 10.1186/1475-925x-10-33.

[78] Georgina K. Stebbings et al. "Resting Arterial Diameter and Blood Flow Changes With Resistance Training and Detraining in Healthy Young Individuals". In: *Journal of Athletic Training* 48 (Mar. 2013), pp. 209–219. DOI: 10.4085/1062-6050-48.1.17.

[79] Brooke N. Steele, Mette S. Olufsen, and Charles A. Taylor. "Fractal network model for simulating abdominal and lower extremity blood flow during resting and exercise conditions". In: *Computer Methods in Biomechanics and Biomedical Engineering* 10 (Feb. 2007), pp. 39–51. DOI: 10.1080/10255840601068638.

[80] N. Stergiopulos, D.F. Young, and T.R. Rogge. "Computer simulation of arterial flow with applications to arterial and aortic stenoses". In: *Journal of Biomechanics* 25 (Dec. 1992), pp. 1477–1488. DOI: 10.1016/0021-9290(92)90060-e.

[81] Ga-Young Suh et al. "Hemodynamic Changes Quantified in Abdominal Aortic Aneurysms with Increasing Exercise Intensity Using MR Exercise Imaging and Image-Based Computational Fluid Dynamics". In: *Annals of biomedical engineering* 39 (Apr. 2011), pp. 2186–2202. DOI: 10.1007/s10439-011-0313-6.

[82] Anqiang Sun et al. "Does Lower Limb Exercise Worsen Renal Artery Hemodynamics in Patients with Abdominal Aortic Aneurysm?" In: *PLOS ONE* 10 (May 2015). Ed. by Rudolf Kirchmair, e0125121. DOI: 10.1371/journal.pone.0125121.

[83] Charles A Taylor, Thomas J.R. Hughes, and Christopher K Zarins. "Effect of exercise on hemodynamic conditions in the abdominal aorta". In: *Journal of Vascular Surgery* 29 (June 1999), pp. 1077–1089. DOI: 10.1016/s0741-5214(99)70249-1.

[84] Charles A. Taylor, Thomas J. R. Hughes, and Christopher K. Zarins. "Finite element modeling of blood flow in arteries". In: *Computer Methods in Applied Mechanics and Engineering* 158 (May 1998), pp. 155–196. DOI: 10.1016/S0045-7825(98)80008-X.

[85] Gerald Teschl. *Ordinary differential equations and dynamical systems*. American Mathematical Society, 2012.

[86] Adam Updegrove et al. "SimVascular: An Open Source Pipeline for Cardiovascular Simulation". In: *Annals of Biomedical Engineering* 45 (Dec. 2016), pp. 525–541. DOI: 10.1007/s10439-016-1762-8.

[87] I.E. Vignon-Clementel et al. "Outflow boundary conditions for 3D simulations of non-periodic blood flow and pressure fields in deformable arteries". In: *Computer Methods in Biomechanics and Biomedical Engineering* 13 (Oct. 2010), pp. 625–640. DOI: 10.1080/10255840903413565.

[88] Wolf von Wahl. *The Equations of Navier-Stokes and Abstract Parabolic Equations*. Vieweg+teubner Verlag, 1985, p. 264.

[89] Lee Waite and Jerry Michael Fine. *Applied biofluid mechanics*. Mcgraw-Hill, 2007.

[90] Anran Wang et al. "Quantification of radial arterial pulse characteristics change during exercise and recovery". In: *The Journal of Physiological Sciences* 68 (Dec. 2016), pp. 113–120. DOI: 10.1007/s12576-016-0515-7.

[91] Peter D. Weinberg. "Haemodynamic Wall Shear Stress, Endothelial Permeability and Atherosclerosis—A Triad of Controversy". In: *Frontiers in Bioengineering and Biotechnology* 10 (Mar. 2022). DOI: 10.3389/fbioe.2022.836680.

[92] Nico Westerhof, Jan-Willem Lankhaar, and Berend E. Westerhof. "The arterial Windkessel". In: *Medical Biological Engineering Computing* 47 (June 2008), pp. 131–141. DOI: 10.1007/s11517-008-0359-2.

[93] J. R. Womersley. "Method for the calculation of velocity, rate of flow and viscous drag in arteries when the pressure gradient is known". In: *The Journal of Physiology* 127 (Mar. 1955), pp. 553–563. DOI: 10.1113/jphysiol.1955.sp005276.

[94] Nan Xiao, Jordi Alastruey, and C. Alberto Figueroa. "A systematic comparison between 1-D and 3-D hemodynamics in compliant arterial models". In: *International Journal for Numerical Methods in Biomedical Engineering* 30 (Sept. 2013), pp. 204–231. DOI: 10.1002/cnm.2598.

[95] Liang Zhong et al. "Application of Patient-Specific Computational Fluid Dynamics in Coronary and Intra-Cardiac Flow Simulations: Challenges and Opportunities". In: *Frontiers in Physiology* 9 (June 2018). DOI: 10.3389/fphys.2018.00742.

[96] Manli Zhou et al. "Wall shear stress and its role in atherosclerosis". In: 10 (Apr. 2023). DOI: 10.3389/fcvm.2023.1083547.